Cristiano Filipe Brás de Sousa

Biochemical and Biophysical characterization of tau aggregates derived from different research models

Dissertação de Mestrado em Biologia Celular e Molecular com Especialização em Neurobiologia, orientada pelo Doutor Kristof Van Kolen (Janssen Pharmaceutica) e pelo Professor Doutor Carlos Duarte (Universidade de Coimbra) e apresentada ao Departamento de Ciências da Vida da Universidade de Coimbra

Junho 2018

UNIVERSIDADE DE COIMBRA

The work presented in this thesis resulted from a partnership between the University of Coimbra and Janssen Pharmaceutica NV, Beerse I. All experimental activities were performed at Janssen Pharmaceutica NV, Beerse I, a Johnson & Johnson pharmaceutical research and development facility in Beerse, Belgium.

All data presented in this thesis is strictly confidential

Beerse, 2018

Acknowledgements

Dankjewel! To Kristof Van Kolen, my supervisor, who made this thesis possible. It has been a great year and it was a pleasure to work with you. All the knowledge, science discussions, lab guidance and advices that you gave me were very important and will be present in all my future scientific career! Thank you for introducing me to science!

To Dr. Marc Mercken, thank you for accepting me in your group and allowing this project to come true. Also for the knowledge transmitted, it was very important to learn how to discuss science.

I would like to thank all the group members for the practical knowledge transmitted throughout this year, specially to Lore Delbroek and Bruno Vasconcelos. Also to Marc Vandermeeren that not only helped in the lab but also shared a lot of funny moments.

For all the students and the great moments shared who contributed to the knowledge of Belgian culture (beers). Thank you Ana Raquel, Dina, Sara and Teresa for being part of the Iberic group.

It was also great to have the huge Janssen's Portuguese community that made me feel as if it was Portugal and gave support not only in the lab but also in the off-work "meetings". Specially Rafaela, Tiago, Francisco, Miguel, Alberto and Andreia.

A special thanks to André Marreiro that helped me even before I arrived in Janssen and during this entire year gave a crucial support in my project sharing ideas, teaching techniques, discussing data and during the writing of my thesis, helping to get over all the difficulties of the most stressful moments. Also for contributing to the great time outside the lab and totally non-work-related discussions.

I would like to thank the teachers of the first year of the Masters, in particular Emilia Duarte, Ana Luísa Carvalho and Carlos Duarte that were able to arouse even more my interest in the fascinating world neurobiology research.

It was also very important to keep contact with my Portuguese friends that even thousands of kilometres away were able to be always present. Those that will be present in my life for long time.

Quero também agradecer à minha familia, aos meus pais e ao meu irmão que tornaram possível todo o meu percurso não só académico como pessoal. São o apoio importante para eu continuar a perseguir os meus objetivos. Obrigado!

Abstract

Passive immunization with an anti-tau monoclonal antibody to block seeding by extracellular tau aggregates is currently explored as a disease-modifying strategy for the treatment of Alzheimer's disease (AD) and other tauopathies. As tau aggregates responsible for the spatio-temporal sequences of seeding events underlying disease progression are poorly defined, it is not yet clear which epitope is preferred for obtaining optimal therapeutic efficacy. The Janssen tau antibody collection has been generated by immunizations with different tau species: aggregated- and non-aggregated tau and human *post-mortem* AD brain-derived tau fibrils. Evaluation of these antibodies in cellular- and in vivo seeding assays revealed clear differences in maximal efficacy suggesting different epitope exposure in both type of fibrils. Limited proteolysis experiments supported the hypothesis that some epitopes are more exposed than others in the tau seeds. In addition, sonication of tau fibrils, to improve seeding potency, not only caused a shift in size distribution of the tau seeds but also exposed more epitopes close to the microtubule binding domain. In particular for antibodies binding close to this domain, efficacy seems to depend on the structural properties of fibrils purified from tau Tg mice- and *post-mortem* human AD brain.

Data in this thesis provided mechanistic insight on the improved seeding capacity of recombinant and *in vivo* generated tau seeds after sonication. On top of this, a number of epitopes that are differentially exposed in tau fibrils derived from human AD brain and tau transgenic mice could be identified. More research is needed to verify whether these differences are also seen in other tauopathies as suggested by the conformational templating hypothesis.

Keywords: Alzheimer's disease; Tau; immunotherapy; Aggregate characterization.

Resumo

Imunoterapia com anticorpos monoclonais contra tau para o bloqueio da capacidade de aggregação de aggregados de tau extracelulares está atualmente a ser explorado como uma estratégia de tratamento para a doença de Alzheimer e outras patologias da proteina Tau.

Devido ao baixo conhecimento sobre os agregados de tau responsáveis pelos eventos de agregação, não é possível identificar com certeza qual o melhor epítopo para obter a melhor estratégia terapêutica. A biblioteca de anticorpos produzidos na Janssen foi gerada com alvo a differentes espécies de tau: monómeros e agregados de tau humana recombinantes e também agregados extraídos de cérebros *post-mortem* humanos de pacientes com doença de Alzheimer. A caracterização destes antiorpos em testes de agregação celulares e em modelos animais mostrou claras diferenças na capacidade de inibição de agregação, sugerindo diferenças na exposição dos epítopos nos vários tipos de agregados. Testes de proteólise limitada de agregados de tau fundamentaram a hipótese de que alguns epítopos estão diferencialmente expostos nos agregados provenientes de diferentes fontes. Para complementar, sonicação de aggregados de tau provocaram um aumento da sua capacidade de induzir agregação mas também uma alteração do seu tamanho e aumento da exposeção de alguns epítopos, especialmente próximo do domínio de ligação aos microtúbulos. Particularmente, anticorpos que se ligam próximo a este domínio mostraram que a sua efícacia é dependente das propríedades estruturais dos agregados de tau extraídos de modelos transgénicos ou de cérebros humanos *post-mortem* com doença de Alzheimer.

Os resultados apresentados nesta tese providenciam novo conhecimento sobre o efeito da sonicação na capacidade de agregação de agregados de tau producidos com proteína recombinante ou isolados de modelos animais. Além disso, sugere que vários epítopos estão diferencialmente expostos nos agregados de tau provenientes de modelos animais ou de cérebros humanos de pacientes com doença de Alzheimer. A continuação deste estudo poderá elucidar se estas diferenças podem ser superados pela teoria dos modelos de conformação.

Palavras-chave: Doença de Alzheimer; Tau; imunoterapia; Caracterização de agregados.

Abbreviations

Aβ – Amyloid β

ACE-III – Addenbrooke's Cognitive Examination III

AD – Alzheimer's Disease

APOE – Apolipoprotein E

APP – Amyloid precursor protein

BACE1 – β-site APP-cleaving enzyme 1

CSF – Cerebrospinal Fluid

ELISA – Enzyme-linked immunosorbent assay

EM – Electron microscopy

fAD – Familial Alzheimer's disease

FAT – Fast axonal transport (FAT)

FRET - Fluorescence Resonance Energy Transfer

FTD – Frontotemporal Dementia

FTDP-17 – Frontotemporal Dementia with Parkinsonism linked to chromosome 17

GTO – Granular insoluble Tau oligomers

GWAS – Genome-wide association studies

ISF – Interstitial fluid

MAP – Microtubule-associated protein

MRI - Magnetic resonance imaging

MSD – MesoScale Discovery

MTBD – Microtubule-binding domain

MT – Microtubule

NFT – Neurofibrillary tangle

PAD – Phosphatase activation domain

PET – Positron emission tomography

PHF – Paired helical filament

PRD – Proline-Rich Domain

sAD – Sporadic Alzheimer's disease

WHO – Word Health Organization

WT – Wild-type

Index

1. Introduction

1.1. Dementia

Dementia is described as a chronic and progressive syndrome that results from neuropathological conditions in the brain. It affects cognitive function, impairing functions such as memory, thinking, language, learning and judgment. Dementia also has impact in daily tasks, affecting emotional control, social behaviour and motivation (1). Among others, Alzheimer's disease (AD), vascular dementia, dementia with Lewy bodies and frontotemporal dementia (FTD) are the most common diseases with Alzheimer's contributing with 60-80% of the cases (2,3).

According to the World Health Organization (WHO), in 2015 there were more than 47 million people worldwide affected by dementia and projections point to an increase to 78 million in 2030 and 145 million in 2050, causing voluptuous costs to the patients and governments, of about US$ 1 200 000 million (4).

Although being one of the most expensive diseases combining health and social care, dementia research funding is still lower than other diseases with lower governmental bills (5). In figure 1, this is illustrated taking UK as example.

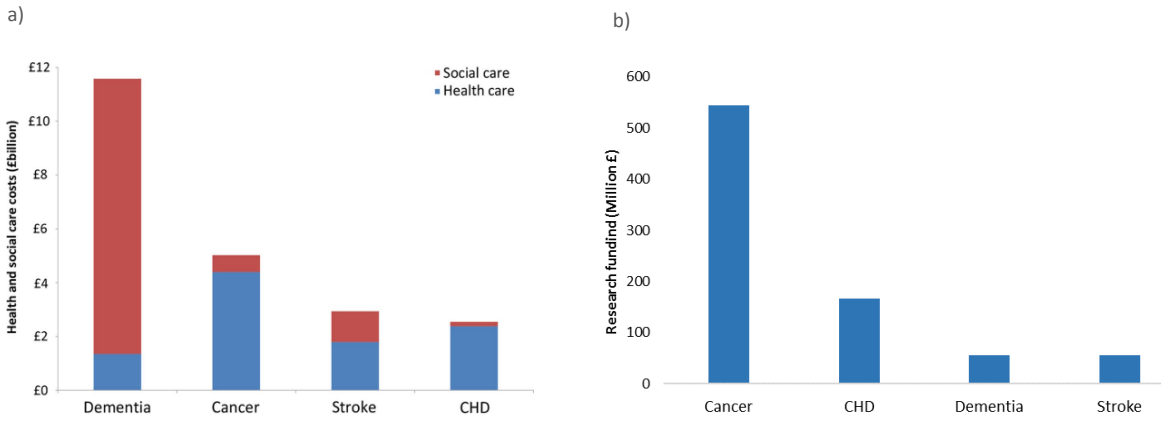

Figure 1 - Comparison of annual costs to research funding in UK.

Annual cost of health and social care (a) compared to research funding b) in UK in 2012 (CHD – coronary heart disease). Adapted from Luengo-Fernandez *et al* 2015 (5).

1.2. Alzheimer's Disease

Alzheimer's is one of the most common neurological diseases worldwide. It was first described by Alois Alzheimer in 1901 after observing a 51 years old woman, Auguste Deter, with alterations in behaviour, daily routines and personality, who died after 4.5 year with severe symptoms of mental disability. In 1907, Alzheimer described another patient with similar symptoms (6). With the in depth pathological investigation from the two patients, Alois Alzheimer wrote in 1911 a report (7) where he described what years later would be called Alzheimer's disease (8).

The neuropathological hallmarks of AD are the extracellular neuritic plaques of amyloid-β (Aβ) and intracellular neurofibrillary tangles of hyperphosphorylated tau protein (9). At the clinical level, this disease is characterized by loss of memory with impaired ability to recall recent events, deterioration of intellectual skills and progressing changes in behaviour. In the later stages of the disease loss of control in motor and body functions is also observed (10). The clinical examination can be performed by using the Addenbrooke's Cognitive Examination III (ACE-III), which scores multiple factors, such as attention, memory, vocabulary fluency, language and visuospatial skills. This test is scored from 0 to 100, where someone with a score of 100 will have no cognitive impairment (11). Risk factors for AD can be poor education, low mental activity, smoking, depression and traumatic head injury, anticipating the onset of the disease (10).

By magnetic resonance imaging (MRI) it is observed that the brain of patients with AD shows loss of volume, mostly in hippocampal volume and grey matter density. This loss correlates with other AD biomarkers such as Aβ42 and Tau levels in the cerebrospinal fluid (CSF) (12). Tau pathology spreads throughout the brain by an apparent systematic spatio-temporal pattern. This is best described by dividing the affected areas according to their "Braak stages" I-VI (13) as shown in Fig. 2. It is now known that the pathology might start not in the transentorhinal layer as thought before but in the locus coeruleus, where AT8-positive soluble pre-tangles are found that will gradually became insoluble and create the neurofibrillary tangles (NFTs) (14). After that, the pathology spreads through synaptically connected regions from the locus coeruleus to the transentorhinal layers (stages I-II). It then starts to affect the limbic areas (stages III-IV) and finally the pathology reaches the isocortical areas (stages V-IV) with consequent destruction of the isocortical association areas (13).

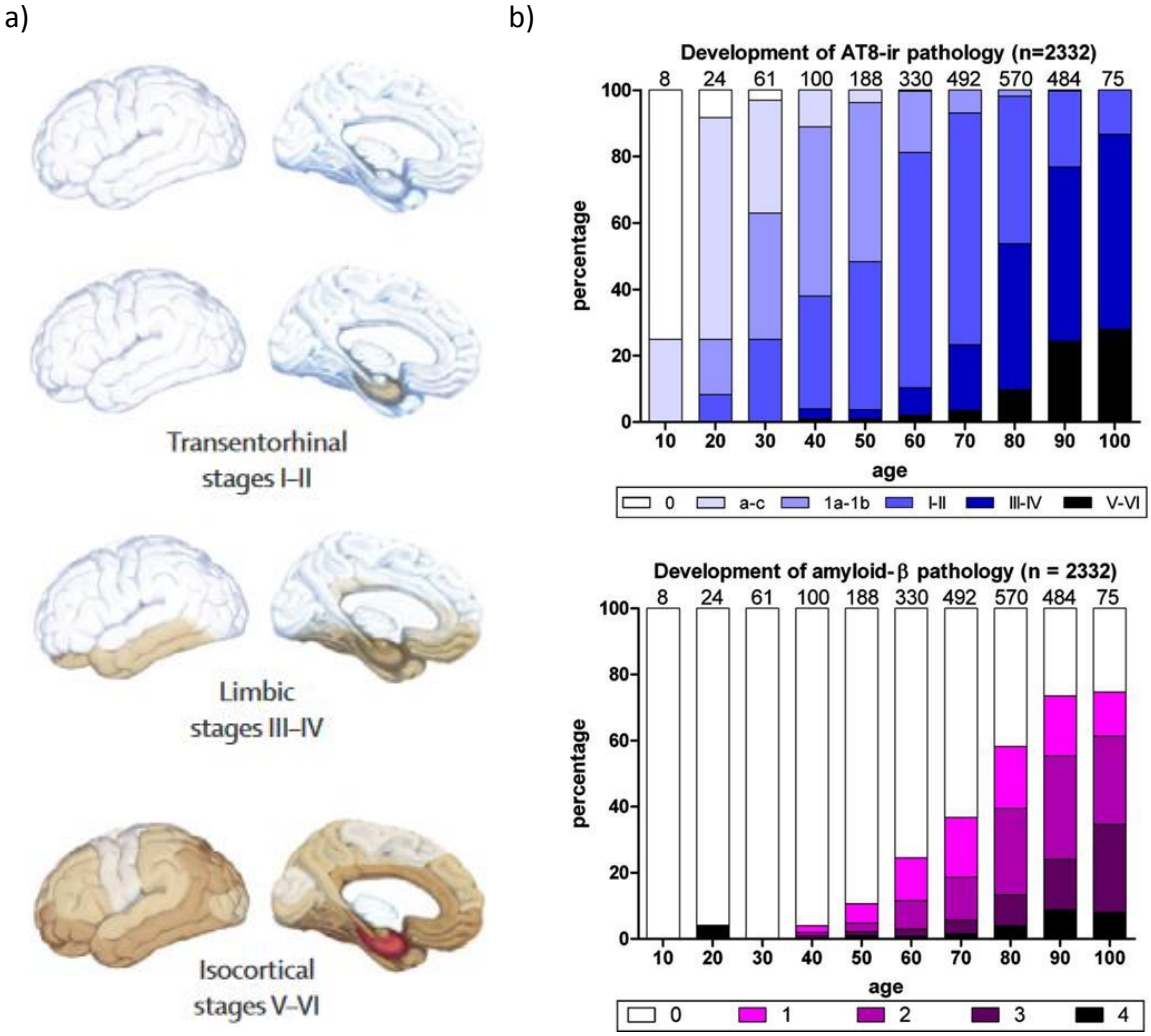

Figure 2 - Braak staging can be identified in brains from young post-mortem individuals.

Brain areas affected by pathology are identified by Braak staging (a). This can be observed in *post-mortem* brains from young individuals and correlates with aging (b). Adapted from Villemagne *et al* 2015 (15) and Braak *et al.* 2011 (14).

Braak staging can be applied in people under 30-year-old that show no cognitive alteration but already shown Aβ plaques, fibrillary tangles of Tau and abnormally phosphorylated Tau (14). These also show that many years before the onset of AD, there are already some pathological changes in the brain.

AD can be divided in familial Alzheimer's disease (fAD) and sporadic Alzheimer's disease (sAD). These two types of AD do not differ in clinical features (16,17). The most common form is sAD and occurs essentially due to a complex environmental-genetics interaction (18). fAD only counts for

~5% of AD cases and is caused by genetic inherited autosomal dominant mutations in amyloid precursor protein (APP) and presenilin genes(19).

1.3. APP cleavage – Aβ production

The production of Aβ occurs by a cascade of APP cleavages that can happen in one two manners, the amyloidogenic pathway and non-amyloidogenic pathway. The amyloidogenic pathway is characterized by two cleavages. β-secretase and ɣ-secretase. The last cleavage, which is made by ɣ-secretase, (composed by presenilin1 (PS1), presenilin2 (PS2), nicastrin, anterior pharynx-defective-1 and presenilin enhancer-2), occurs in the intramembrane domain of APP (20,21) (Fig. 3). From amyloidogenic pathway of APP cleavage, multiple products arise, among them Aβ (22). The amino acid length depends on the place that ɣ-secretase cleaves the product of β-secretase cleavage. This complex does not have a strictly precise place to cleave (23), resulting in a peptide that varies from 36 to 43 aminoacids. The most abundant are $A\beta_{40}$ (~80-90%) and $A\beta_{42}$ (~5-10%) (24). These ratios can be modified by presenilin and APP mutations, significantly increasing Aβ42-Aβ40 ratio, a hallmark of AD (25).

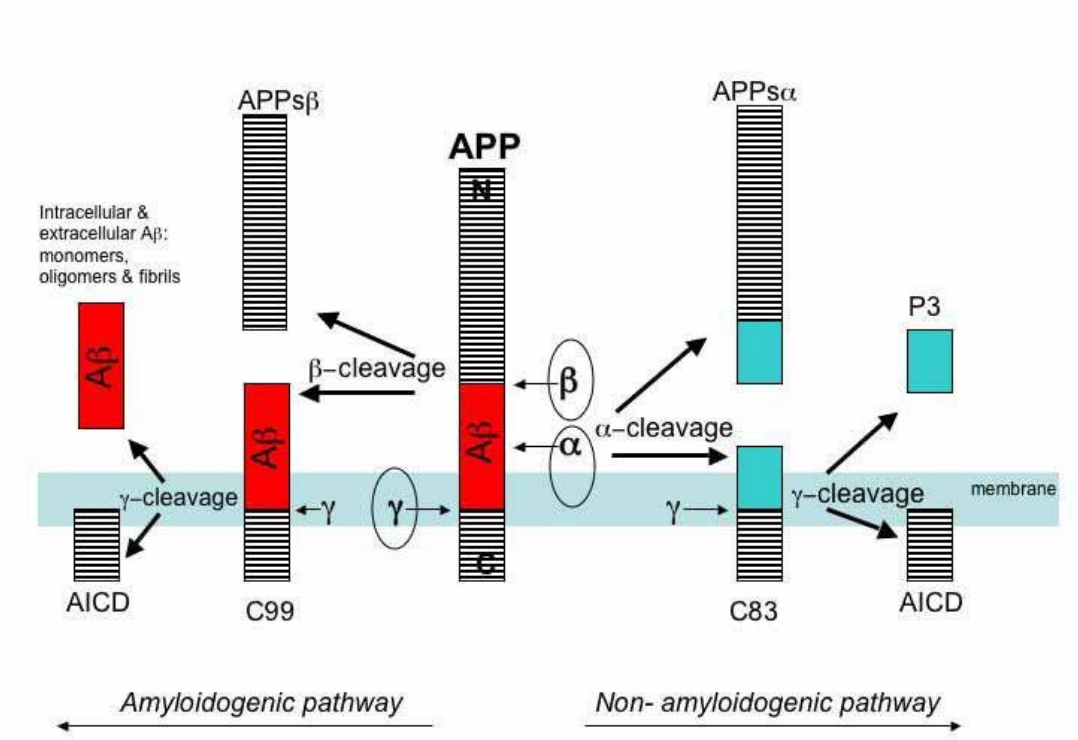

Figure 3 - Representation of amyloid precursor protein (APP) cleavage

APP has two cleavage pathways depending on the complexes involved. α-secretase in the non-amyloidogenic pathway or β-secretase followed by ɣ-secretase in the amyloidogenic pathway. From Cole *et al* 2007 (23).

1.4. Mutations

fAD can occur with mutations in genes such as presenilin1 and presenilin2 in chromosome 1 and APP in chromosome 21, leading the APP to the amyloidogenic way.

Among the mutations that causes Alzheimer's, a recent study (26) showed that in 18 patients with mutation, 10 of them were "*de novo*" mutations not inherited from the healthy parents.

Mutations in presenilin1, presenilin2 and APP cause increase of Aβ42 and decrease of Aβ40, creating a change in Aβ42/40 ratio and inducing pathogenicity through changes in the catalytic subunit (27). These mutations affect the catalytic, impairing its function (28). These mutations which lead to Aβ aggregates cause not only a decrease in long-term potentiation (29) but also synaptic depression by disrupting glutamate reuptake, inducing long-term depression (30) impairing cognitive functions such as learning and memory.

In sAD, although not linked to genetic mutations, genome wide-association studies (GWAS), pointed to several loci associated to risk factors such as apolipoprotein E (APOE), CD2AP, CD33, EPHA1, ABCA7, EPHA1, CD33 and CD2AP (31,32). Those risk factors, although not sufficient neither necessary to the occurrence of AD, they are linked to the anticipation of the age-of-onset of sAD (33). Many other loci have been identified as potentially risk factors or protective factors but the real importance of those loci remain to be studied (34). Among all risk factors presented, the higher contributor for sAD are APOE polymorphisms. ApoE is a major transport protein involved in lipid homeostasis by controlling lipid transport from a cell to another (35). APOEε4 polymorphic allele is known as the major risk factor for sAD. Heterozygotics for this allele have a 3-fold increase and homozygotics a 15-fold increase risk to develop sAD (33). This polymorphism is highly associated with the progression of mild cognitive impairment to AD (36).

BACE-1 is the enzyme responsible for the β-cleavage and has all the functional properties of the β-secretase complex. This means that BACE-1 cleavage is an important step in Aβ production (37). Mutations in APP can be responsible to make APP a better substrate for β-cleavage, increasing the efficiency of BACE-1, and therefore increased Aβ production. For example, the denominated Swedish mutation, a double mutation right after the BACE-1 cleavage site (LysMet → AsnLeu) significantly increases BACE-1 processing and Aβ production (38). On the other hand it has been found that there is another APP mutation that is linked to a decreased processing by BACE-1 *in vitro* leading to lower amyloid burden in and protects elderly people against Alzheimer's disease and cognitive decline, constituting a protective factor for AD (39).

1.5. Aβ oligomerization

Since one of the hallmarks of AD is the presence of neuritic plaques of Aβ, it is important to study their production. Mutations involved in fAD such as presenilin and APP induce an increased production of $A\beta_{42}$ resulting from the amyloidogenic proteolytic pathway (Fig. 3), working as a gain of function in $A\beta_{42}$ production (25). Those fAD mutations affect the rate of APP proteolysis, precisely enhancing ɣ-secretase activity (40-42). $A\beta_{42}$ is more prone to create oligomers than $A\beta_{40}$ (29) and consequently, with the increase of $A\beta_{42}$ there are more oligomerization of Aβ and fibrils production (43) that is observed in patients with AD. *In vitro* studies showed that fibrils decrease

cell viability 40-fold more that monomeric peptides and 10-fold more than fibrils (44), being involved in neuronal loss. These findings indicate that oligomers are more neurotoxic than fibrils (45). Although, these oligomers and fibrils can be found in healthy people, with no cognitive alterations (46), suggesting a good biomarker and a therapeutic to prevent the triggering of the disease. It can be observed between 25 and 15 years before the expected age of onset (47). Aβ peptides have been claimed to interact with fibrinogen and factor XII that are involved in blood clotting and increase their clotting capacity and create abnormal clots, persistent fibrin deposition and generation of proinflammatory molecules, damaging neurons and possibly contributing to the worsening of cognitive function in AD patients (48). There are also research results showing that Aβ oligomers can spread in a prion-like manner where aggregation starts in one cell with an abnormal β-structure enriched protein oligomer and can spread to other cells, inducing misfolding of proteins and creating oligomers, protofibrils and amyloid fibrils, for example, Aβ plaques (49). There is however no significant evidence that this prion-like propagation of AD can occur from one person to another, even in the context of hemotherapy (50). These prions can transmit different strains according to how the prion originated and can be distinguished in *in vivo* experiments (51). This prion-like transmission opens the possibility of developing immunotherapies to prevent the spreading of oligomers, but the fact that different types of oligomers exist makes that the therapy should be adapted for each case. One of the sources of Aβ deposits recently found is the *dura mater* and although these Aβ seed are present in AD brains, this study suggested that those seeds are not enough to reproduce the full clinical observation in AD patients (52). Aβ oligomers also seem to have not only a prion-like propagation but also other etiologies. For example, it has been found that in the pituitary-gland, in patients that received growth hormone treatment, there is observable Aβ seeding in the absence of the abnormal prionic protein (53). There still yet some questions to be answered such as why different characteristics such as conformation and size of aggregating proteins influence their pathogenic capacity.

1.6. Tau

Tau is a microtubule-associated protein essentially expressed in the axons and has the function of stabilizing the microtubules facilitating the transport inside the neuron between the soma and the distant parts as the synapses and it is encoded by the gene *MAPT* (54) located in the 17q21.3 locus

(55). It can also be found in somatodendritic compartment of neurons and oligodendrocytes (56). Besides the binding with microtubules, Tau also binds to APOE, especially APOE ε3 and ε4 (57). Tau can be divided in four regions, the N-terminal projection, regulating microtubule spacing and interacting with the cellular membrane, a proline-rich domain (PRD) where multiple phosphorylation sites exist, the microtubule binding domain (MTBD) which will unbind from microtubules when phosphorylation occurs, and a C-terminal region (58-60). Tau has 6 splicing variants, depending on the number of amino terminal inserts, 0N, 1N or 2N, and how many microtubule-binding domains are present, 3R or 4R, resulting in the 6 isoforms, 2N4R, 2N3R, 1N4R, 1N3R, 0N4R and 0N3R. This is due to alternative splicing of exons 2, 3 and 10 (61-63), as described in Fig. 4. In humans, the most expressed isoforms are the 1N4R and 1N3R (64). In other species such as mouse, rat or guinea pig, the C-terminal changes are conserved where the three-repeats isoforms are present essentially in the foetus or neonate and the four-repeat isoforms increase with the development and are present in the adult's brains (65). This change may be responsible for the synaptic plasticity alterations since the number of microtubule-binding domains control their dynamic instability. The 4R Tau has one more microtubule-binding domain than the 3R that increase the microtubule stability being more efficient to promote microtubule assembly. That way, the 3R Tau is important to allow the microtubules to suffer more changes that are needed during the development (66). However, the changes in the N-terminal are different depending on the species. In adult rats, the 1N and 2R are dominant while in mice 0N is the dominant isoform but the effect of these changes remains to be elucidated (65). Changes in Tau alternative splicing, phosphorylation and increased or decreased interaction with tubulin may contribute to the appearance of diseases named Tauopathies (67). For example, the phosphorylation in Serine 262 decreases Tau's interaction with microtubules and is highly associated with Alzheimer's Disease (59,68) and strategies to reduce this phosphorylation are already being studied (69).

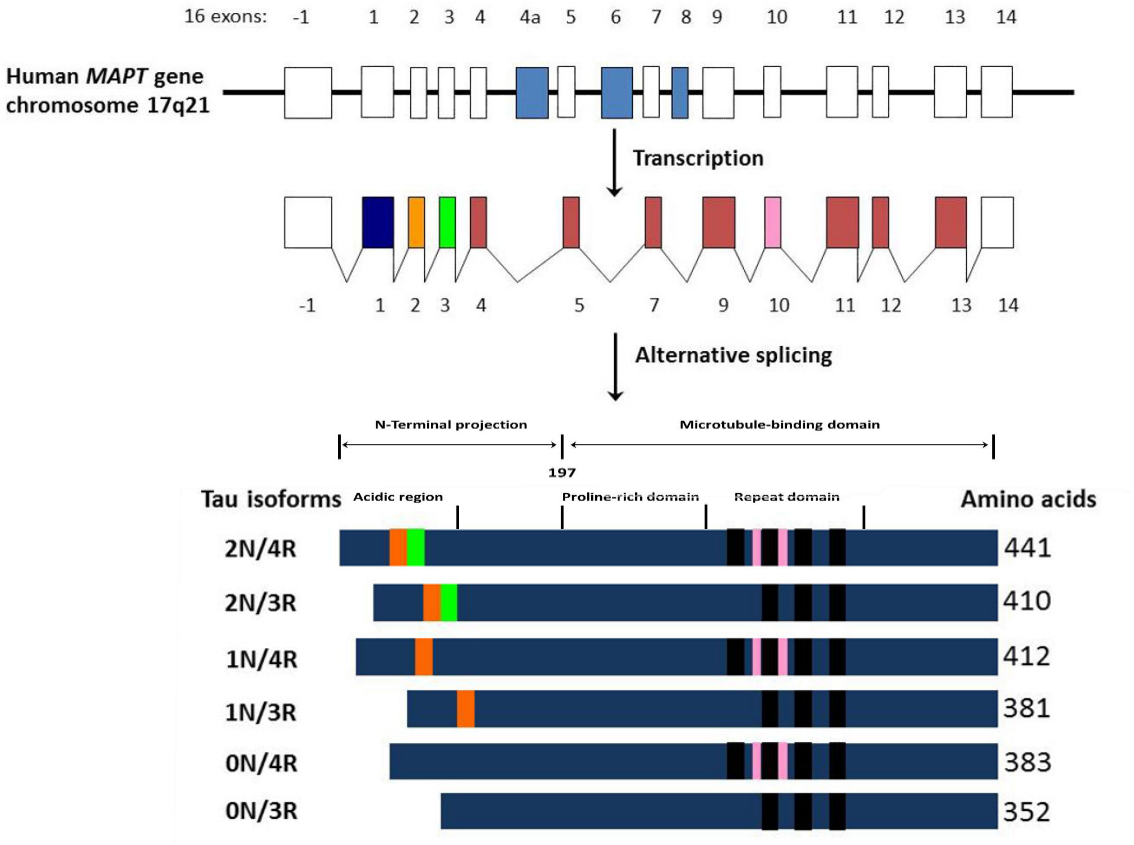

Figure 4 - Human Tau isoforms depend on the alternative splicing.

***MAPT* gene is located at 17q21.3 locus. The alternative splicing of exons 2, 3 and 10 originate different amino acids length Tau. Exon 2 and 3 are present in the N-terminal and are responsible for the N-terminal inserts that can be 0, 1 or 2. The exon 10 splicing changes the microtubule binding domain repeats that can be 3 or 4, depending on the presence or absence of the exon 10. It origins 6 Tau isoforms. Adapted from Luna-Muñoz *et al* 2013 (70).**

Phosphorylation is the most studied post-translational modification studied in Tau protein. It can occur in three types of amino acids: serine (S), tyrosine (Y) and threonine (T). In Tau protein there are 85 putative phosphorylation sites (71). Especially the phosphorylation in Serine 262, that as mentioned before, decreases Tau interaction with microtubules, inducing Tau conformational changes that impair its biological function (59). The same phosphorylation has been suggested to decrease Tau binding to APOEε4 (57). This means that Tau phosphorylation modulates Tau function, disrupting its binding to microtubules and other proteins and consequently inducing its aggregation (71). Tau phosphorylation is regulated by the balanced activity of kinases and phosphatases as shown in Fig. 5. The kinases involved in Tau phosphorylation are divided in 3 groups: tyrosine protein kinases, proline-directed protein kinases (PDPK) and protein kinases non-PDPK (72) and some phosphatases are PP2A, PP2B, PP1, PP2, STEP and all of them are known to be involved in AD (73).

The unbalanced phosphorylation/dephosphorylation equilibrium leads to Tau aggregation. Tau protein stabilizes the

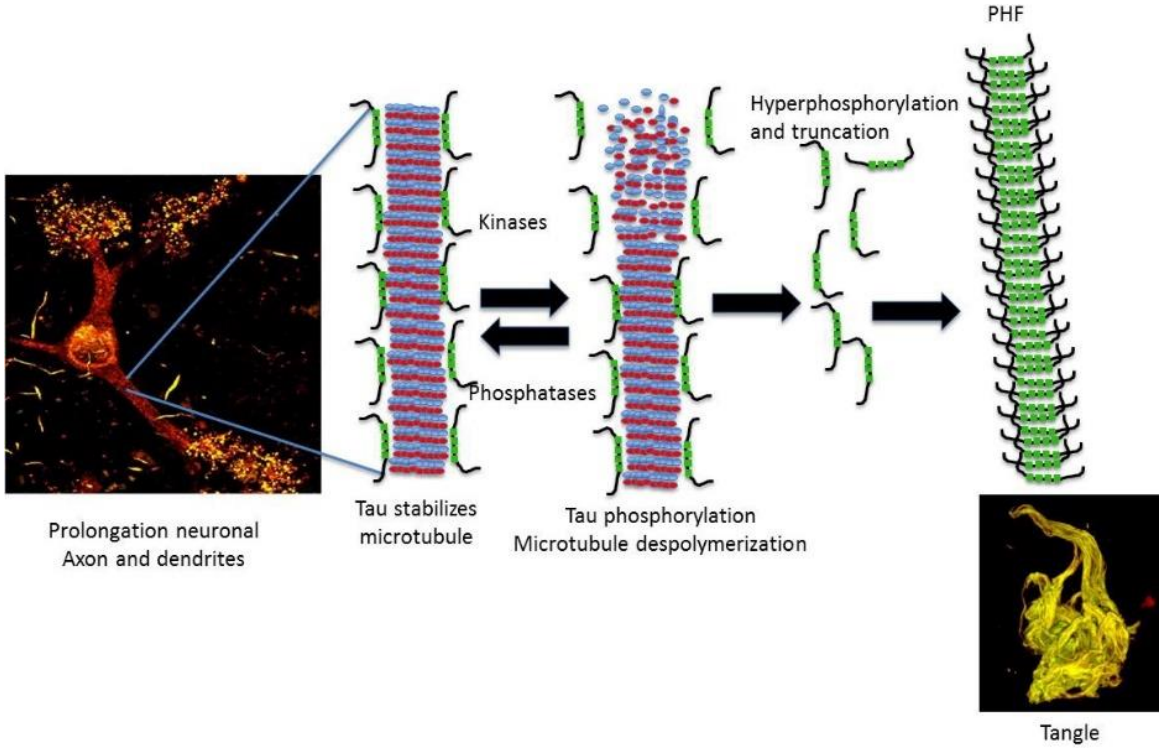

Figure 5 – Hyperphosphorylation of tau leads to loss-of-function and pathologic aggregation

microtubule while Tau phosphorylation leads to microtubule-affinity loss and consequent microtubule depolymerisation. Hyperphosphorylation also increases Tau-Tau binding affinity, producing aggregates. From Luna-Muñoz *et al* 2013 (70).

The unbalanced phosphorylation/dephosphorylation equilibrium creates a hyperphosphorylated form Tau, an hallmark of AD and can be corrected by using selective kinase inhibitors (72) or by increasing phosphatase activity (74). On the other hand, hyperphosphorylation of aggregated tau can be a result of the increased stability of the phosphorylated residues in the aggregate, resulting in protection from phosphatases (75).

1.7. Extracellular Tau

Although Tau being an intracellular protein, it can be found in extracellular environment, for example in interstitial fluid (ISF) (76) and in the CSF. The release of Tau to the extracellular matrix was firstly thought to be a consequence of neuronal death but other studies suggest that it can occur in different ways such as exosomes (77), constitutively in an unconventionally mechanism as naked protein (78) and in other membrane vesicles (79). Increased neuronal activity also leads to

the increase of extracellular Tau, shown in healthy cortical neurons, where an increase of synaptic transmission through AMPA receptor activation leads to release of higher amounts of Tau (80,81). Although little is known about the mechanisms involved in Tau release, quantification of extracellular Tau content in CSF and ISF has been suggested to be a biomarker for preclinical diagnosis of AD (82).

Extracellular Tau, depending on the species, can be responsible or not for the spreading of Tau toxicity. Studies suggest that extracellular Tau originated from neuronal death increased their toxicity to the neighbouring neurons but when extracellular Tau is derived from the overexpression of Tau, secreted Tau does not result in increased toxicity (79). It has also been reported that CSF Tau levels increase with age but this occurs in healthy individuals, which suggests that not all the CSF Tau is toxic (83).

Extracellular protein also shows an ability to get into other cells by different mechanisms. Monomeric protein can enter via muscarinic receptor-mediated endocytosis (84), soluble Tau oligomers by bulk endocytosis (85) or even larger Tau aggregates by macropinocytosis (82).

1.8. Tauopathies

Tauopathies are known as a subtype of neurodegenerative diseases characterized by the deposition of misfolded Tau in brain tissues. Examples of such diseases are Alzheimer's disease, progressive supranuclear palsy, dementia with Lewy bodies, Pick's disease, and some fronto-temporal dementias (FTD) (86). Recently, Huntington's disease is being introduced in these subtype of neurodegenerative disorders since the patients show Tau aggregates in various brain structures, different cognitive dysfunction depending on the Tau haplotype and also because different Tau splicing, phosphorylation, oligomerization and subcellular distribution influenced by the mutant huntingtin protein (87).

Since Tau is highly soluble and the *in vitro* solubility is much higher than the intracellular concentration, recruitment of Tau into aggregates is counterintuitive (88,89). There are two short motifs that are thought to be responsible for the initiation of aggregation. These hexapeptide

motifs are present at the microtubule binding domains, in two of the repeats. They have high propensity to form β-sheet structures that are needed to initiate Tau aggregation. In fact, the motifs are responsible for the rearrangement of Tau into fibrils composed by two tightly interdigitated β-sheets (90). Aggregation starts from monomeric Tau protein that can aggregate into dimers, small soluble oligomers, granular insoluble Tau oligomers (GTO), paired helical filaments (PHF) and neurofibrillary tangles (NFT) as shown in Fig. 6.

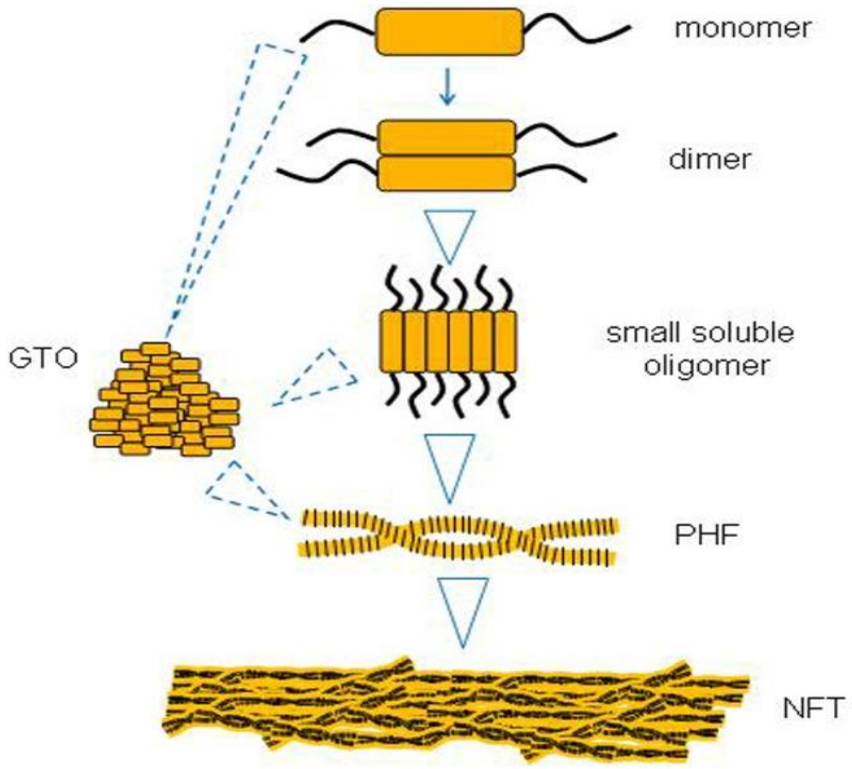

Figure 6 - Progression of Tau aggregation.

Tau aggregates are originated from the monomeric soluble Tau, aggregating into dimers, small oligomers, insoluble granular Tau oligomers (GTO), paired helical filaments (PHF) and neurofibrillary tangles (NFT). From Cowan *et al* 2013 (91).

The toxicity of Tau is dependent on the state of oligomerization. In several studies, it was observed that oligomers have impact in the fast axonal transport (FAT) at physiological levels but only the retrograde transport, mediated by dyneins. Soluble monomeric Tau, even 10 times more concentrated than the physiological level, did not affect none of the FAT. This effect was due to an interaction of oligomeric Tau that has an exposed sequence in the N-terminus called phosphatase activation domain (PAD) that activates a signalling cascade and inhibits the FAT. Soluble monomeric Tau, given the fact that the conformation changes when the protein aggregates, do

not have the PAD exposed and do not have the same effect in the FAT (92). These studies have been important to show the impact that the protein conformation have on its toxicity. Also, contrarily to what was thought before, studies showed that NFT are not the ones directly related to neuronal loss and synaptic dysfunction but instead, they work as a protective mechanism to cell, decreasing the oligomeric (and toxic) concentration of Tau in cells (93).

There is still disagreement about the true toxic Tau species. NFTs were thought to be the toxic Tau species since they were found and could correlate with the dementia severity and neuronal death but some data is now supporting that NFTs could be a defence mechanism since they can sequester other smaller toxic aggregates and delay neuronal death (94). Also, there are evidence supporting that NFTs are not sufficient neither necessary to induce dementia nor neuronal death (91,95). PHFs were also thought to be the toxic specie since their presence in cells was related with neuronal loss but again further investigation shown that by inducing *in vivo* hyperphosphorylated Tau to aggregate into PHF, the neuronal toxicity decreased by decreasing their ability to sequester other microtubule-binding proteins (96). With the findings supporting that the fibrils were not the toxic species, the next specie thought to be toxic was the GTO. The hypothesis arrived only because of the increased presence of GTO with the AD progression but then in *Drosophila* models it has been shown that the presence of GTO does not lead to neuronal toxicity and it could even protect neurons from the hyperphosphorylated protein toxicity (97). There is remaining the soluble species of Tau, the monomeric and oligomeric Tau protein. Although monomeric, there are several different Tau species depending for example on the phosphorylation combinations and also the six splice variants and the small aggregates can differ on their sizer and also phosphorylation. Even knowing these differences, must of the research does not differentiate the effects of different species, only taking in account the monomeric or small oligomeric Tau. It could bring discrepancies in the results presented because depending on the phosphorylation or size variations, Tau protein can have or not toxic effects (91). For example, extracellular injection of monomeric Tau in cell cultures promotes the increase of intracellular calcium trough muscarinic receptors that leads to neuronal death (98). Also, in Tau transgenic mice, the soluble Tau impaired hippocampal function (95). The organelle trafficking is also impaired in mice overexpressing monomeric Tau and it leads to an erroneous mitochondrial distribution but when the soluble Tau overexpression is suppressed, those mice could recover and mitochondria distribution becomes normal (99). There are several other studies supporting that soluble small Tau oligomers, such as dimers, impair the fast axonal

transport (100), trimers can lead to synaptic and neuronal loss impairing memory (101), creating a well-accepted hypothesis that the soluble monomeric and small oligomeric Tau is responsible for the toxicity (91,93). Although, not all soluble Tau species appear to be toxic since many soluble Tau species are present in heathy individuals. Also, using two different mouse models expressing two different Tau forma differing on their propensity to create β-structure they had different tendency to aggregate and were named as pro-aggregant and anti-aggregant. The anti-aggregant model does not exhibited Alzheimer's disease typical changes such as aggregation, hyperphosphorylation, cognition impairments and synaptic and neuronal loss but the pro-aggregant showed those features. It indicates that the β-sheet structure and the aggregation are key factors to produce the phenotype. Also, after inhibiting the expression of pro-aggregant Tau, mice could recover from the behavioural, learning and memory deficits. This could support that specific type of soluble Tau could not induce pathology (102) but again, although soluble Tau species, they have specific characteristics that might be responsible for the variations.

Amongst all Tau species mentioned, the most accepted species that are thought to be causing toxicity are the soluble monomeric and small oligomeric Tau. Although, there are some research to be performed so that it is possible to distinguish which soluble species are responsible for Tau toxicity and which are not.

Strong evidence suggests that depending on the Tau isoform, the pathology may differ. Using three transgenic mice strains with the same genetic basis, when mice expressed human 2N4R Tau, there was motor impairment and axonopathy with axonal dilatations even without the presence of aggregates. This pathology occurs because of the clogging of the axons by the excessive Tau binding to the microtubules since 4R Tau has more affinity to the microtubules. On the other hand, when other strain expressed human 4R2N Tau but with P301L mutation, there was no axonopathy but aggregates where present and mice developed high levels of NFTs. This might happen because mutated Tau has less affinity to bind the microtubules. Supporting the same hypothesis, the third strain only expressed human 4R2N Tau at the same level as the murine isoform is usually expressed without the expression of any mouse Tau isoform. That way, Tau expression is lower and it produce less axonopathy because there is less Tau over-binding to the microtubules yet severer than in the strain expressing mutated Tau. This suggested that overexpression of Tau may be pathologic because it leads to overstabilization of microtubules and consequent axonopathy, being important

to have this in account when using overexpressing strain, even in the absence of aggregates (103). But mice expressing P301L mutation had precocious death because of the strong Tau aggregation observed. Counterintuitively since hyperphosphorylation is associated with Tau pathology, in Tau P301L transgenic mouse strain, the increased phosphorylation by GSK3β (a kinase associated with Tau phosphorylation) increased life expectancy of this mouse strain. This happened because although generally accepted that the hyperphosphorylation leads to decreased microtubule binding affinity, the alteration is dependent on the phosphorylation site. Specifically, GSK3β phosphorylates S396 that increase Tua-microtubule binding affinity and consequently decreases aggregation (104). The same has already been found with other specific phosphorylation sites (105). It is important to be aware that the paradigm that phosphorylation decreases Tau-microtubule bind affinity is actually dependent on the phosphorylation site and the phosphorylation may have the opposite effect, increasing microtubule binding affinity.

Importantly, Tau aggregates can be obtained from different sources and recent research suggested that by isolating PHFs from human-AD brains, after sonication, the aggregates could induce Tau seeding in WT mice expressing physiological levels of Tau, in contrast to synthetic fibrils that are only able to promote seeding in mice overexpressing Tau. The seeds generated from AD-brain derived seeds shown unique conformational characteristics potentially demonstrating differences in seeding potency and seeds characteristics in models expressing physiological levels of Tau (106).

1.9. Tau seeding and spreading

One of the biological functions of Tau is microtubule stabilisation. Kinase and phosphatase activity unbalances leads to hyperphosphorylated Tau that has a 20-fold decrease in tau-tubulin binding affinity. This will lead to more free Tau in the cell (107). Tau phosphorylation may be detected by using a panel of antibodies that bind to specific epitopes of Tau phosphorylation/dephosphorylation. Abnormal phosphorylation can start in young individuals, even under thirty, without clinical manifestation for years (14,108). Some studies claim that the base of Tau seeding was identified as a C-terminal truncated fragment of the repeat domain that could start the aggregation (109) and it could convert normal soluble protein into aggregated oligomers and fibrils (107). The mechanism of initiation is likely due to the progressive loss of

endosomal-lysosomal processing of neuronal proteins during patient's life, especially mitochondrial membrane proteins. Mutations in APP and presenilin are likely responsible for the anticipation of this loss-of-function of endosomal-lysosomal but not directly create initiation complex (107). Also, the charge neutralization may be responsible to trigger Tau aggregation. For example, heparin can be used to accelerate aggregation of recombinant Tau proteins. *In vivo*, some acidic cofactors may be responsible for to initiate the nucleation, for example nucleic acids (89). Another important factor for aggregation is the β-structure propensity characterised by hexapeptide motifs in two of the repeat regions of the microtubule binding domain. This β-structure is present in the core of PHFs (110).

According to the spreading hypothesis, tau aggregates are transported through the cytosol and reach the synapse, damaging the synaptic terminal, and through different mechanisms are released to the extracellular matrix and can enter the neighbouring neurons, initiating the same seeding cascade and spreading the toxicity (107). It was indeed found that Tau pathology is more evident in neurons with synaptic connections rather than those in spatial proximity after seeding. This was demonstrated by unilateral injection of Tau aggregates in the brain of Tau transgenic mice models and observation of presence of aggregates in the contralateral part of the injection through synaptic connected neurons (111). Tau seeding has also been observed *in vitro* by a FRET-based flow cytometry biosensor cellular assay. This seeding can be observed before histological detection of Tau aggregates. This way, it proposes a strong biomarker for early diagnosis of Tau seeding and consequent tauopathies (112).

The entrance of Tau seeds in the cell may occur in different ways such as by inducing cell membrane stress and pore-formation, endocytosis, micropinocytosis, and non-traditional free protein secretion, not enclosed by a membrane (113).

Braak stages suggest the spreading of Tau pathology through a sequence of structures that are gradually affected in a stereotypic and predictable manner. It also allows to detect the severity of the pathology depending on the areas affected (13,14). The aggregate pathology starts in a region without clinical manifestations but spreads to synaptic connected neurons and can propagate and spread in a prion-like manner. These aggregates also maintain their spreading ability when isolated in one mouse and injected into another and even if isolated from human brains who had tauopathies. Injecting brain extracts from tauopathies patients in transgenic mice expressing

human wild-type Tau resulted in Tau aggregation and spreading to connected brain regions (114,115).

The spreading of Tau pathology, as Aβ plaques, can be measured by Braak staging, using for example tau positron emission tomography (PET) agent [^{18}F]AV -1451 to obtain the area affected (13,116). There are many preclinical and clinical imaging results supporting the spreading ability of Tau seeds (117) but there still low sensitivity in this diagnosis method, not allowing to identify the early stages of Tau pathology which has to be defined *post-mortem* (118).

1.10. Amyloid-β and Tau aggregation

Tau aggregation can be found early in ageing, even before Aβ plaque deposition (14). There are Tauopathies that do not have the presence of Aβ aggregates, for example FTD, where it was found that Tau aggregates increase $A\beta_{42}$ production but do not reach a level that induces Aβ deposition (119). In AD, the presence of Tau aggregates seems to be accelerated after Aβ deposition reaches a threshold, having a synergistic effect (120,121). This is known as the amyloid cascade hypothesis (122). Several studies have been showing the same process (123) and it was found that when crossing two transgenic mouse models overexpressing mutated human APP and human wild-type Tau, an acceleration in cognitive impairment, reduction of dendritic spines and Tau aggregation is observed when compared to single transgenic mice expressing only the APP mutation or the human Tau (124). On the other hand, crossing a human APP transgenic mouse to a tau knockout mouse leads to an offspring less affected by behavioural deficits when comparing to when Tau is expressed (125). This supports the amyloid cascade hypothesis, but there are still several aspects to be understood, such as the mechanism underlying the Aβ-dependent Tau pathology acceleration, the increased neurotoxicity when combined both intracellular and extracellular aggregate stress by Tau and Aβ aggregates and the involvement of Aβ aggregates in Tau phosphorylation that may lead to increased aggregation. The hyperphosphorylation of Tau may occur by the activation of certain kinases by Aβ aggregates that increase the kinase activity and promotes a misbalanced phosphorylation/dephosphorylation ratio (126), as schematized in Fig. 7.

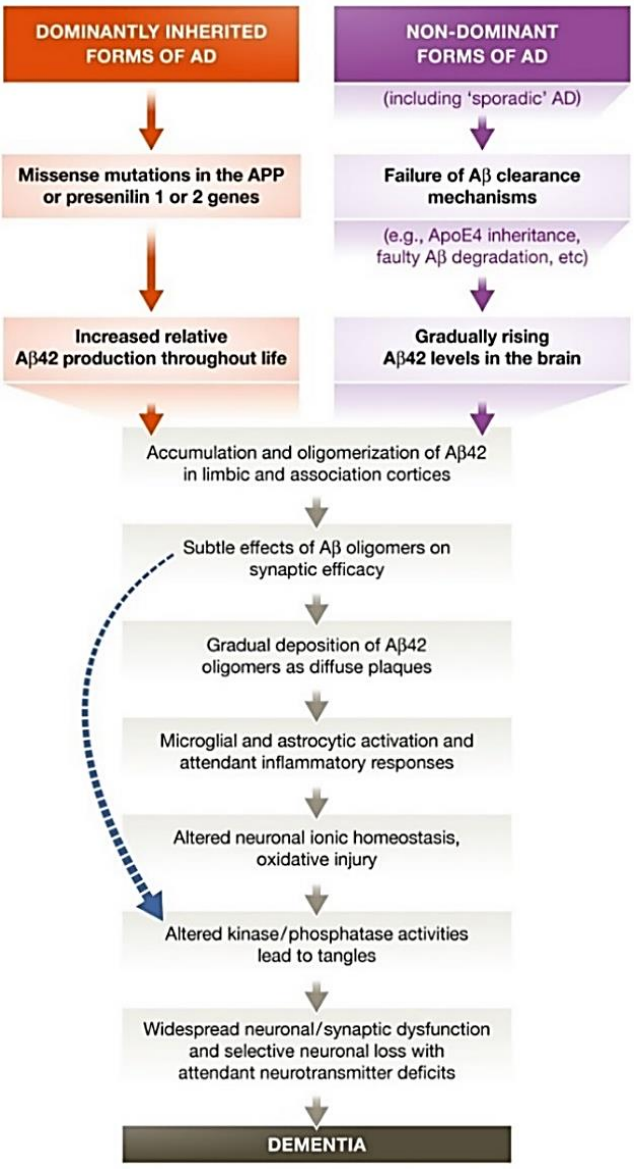

Figure 7 - Amyloid cascade hypothesis

AD progression from the mutations in fAD and the failure mechanisms during life that triggers the pathology to the impact of Aβ pathology in the increase of Tau pathology. From Selkoe *et al* 2016 (28).

Recent studies also suggest that the combined injection of Aβ and Tau seeds promotes higher Tau aggregation in neurons in culture. Also, the injection of Aβ seeds in mouse models accelerates the Tau pathology and increases the spreading of Tau aggregates by Aβ-induced Tau cross-seeding and strongly catalysing pre-existing Tau aggregation (127). In fact, this is such an important hypothesis that it is a potential treatment target to prevent the AD onset by disrupting the progression of Aβ pathology to prevent the acceleration of Tau pathology (123). The reverse has also been found after comparing the neuronal death and neurite degeneration in neurons derived from wild-type mice and neurons cultured from Tau knockout mice. After being treated with fibrillar Aβ, WT cells

had neuronal degeneration but in Tau-knockout mice cells, neuronal degeneration has not been observed. This suggests that Tau also plays an important role in Aβ induced neurodegeneration (128). Although the mechanisms are yet poorly understood, this data suggests that Aβ pathology accelerates Tau pathology in AD and triggers Tau aggregation by hyperphosphorylation but also that by a feedback loop, Tau enhances Aβ toxicity, increasing the toxicity observed in AD patients (129).

1.11. Research models for Tau seeding and spreading

The research in AD is mainly performed in mouse models but it is not possible yet to study the complete biochemical and behavioural changes combined in one mouse model. Until now, the study of AD is achieved by using transgenic mice that mimics some characteristics of the AD hallmarks. With this objective, mouse models that expresses with AD mutations such as APP, PS1 and PS2 genes mutations have been developed, creating mice that develop Aβ pathology. For example, the APP23 mouse line has human amyloid protein overexpression with the Swedish mutation (K670N and M671L). It creates a model with observable amyloidosis progression with PET as well as neurites and synapses degeneration. This model has also been widely used because hyperphosphorylated Tau is also present, supporting the amyloid cascade hypothesis (130,131). Several other mouse models of Aβ pathology allows to study Tau pathology because in the sightings of senile plaque of amyloid β, these mice develop NFTs. For example, the injection of Aβ42 fibrils in P301L mutant Tau transgenic mice, a mouse model overexpressing aggregation prone mutant Tau, creates a 5-fold increase of NFTs production (132). Other study showed that combined injection of Aβ and Tau seeds produces an increased Tau seeding and spreading in P301S mice (127). All these findings allow the study of Aβ-induced Tau pathology (133).

Other important model to study Tau pathology propagation has been proposed and it uses inducible overexpression of human Tau with P301L mutation. It only expresses human pathological Tau in the entorhinal cortex where it has been identified that the Tau pathology starts but in this model, even without the expression of pathological Tau in other brain areas, the pathology had the same pattern of spreading. It proposed that human pathological Tau aggregates originated in

the entorhinal cortex could induce aggregation of endogenous mouse Tau (134), while also spreading trans-synaptically across connected brain areas (135).

To study Tau aggregation and the effect of therapeutic candidates targeting spreading and clinical features of Tau pathology, several transgenic mouse models are being used. One model expresses for example pro-aggregant full-length human Tau (hTau40/ΔK280) or a truncated Tau repeat domain (Tau(RD)/ΔK280) and it leads to a pre-tangle pathology, and a massive formation of NFTs and neuronal loss, respectively. With the same models, it is also possible to switch-off the expression of the pro-aggregant Tau protein, allowing synaptic and memory impairment recovery, supporting the possibility that by removing amyloidogenic Tau, Tau pathology can be reversed (136). The spreading of Tau pathology can also be studied by crossing a transgenic mouse expressing mutated Tau (for example P301S mutation) that exhibits Tau aggregation, and a transgenic line overexpressing human WT Tau, for example ALZ17, that does not show any Tau filaments. From this crossing, a mouse model with increased Tau aggregation is obtained, showing that there is a synergetic effect between both Tau species (114). This is important because it allows the study and comparison of different tauopathies. The same authors of this study also found that by injecting Tau seeds derived from different human tauopathies-brains creates a distinct pattern of Tau seeding in this the ALZ17 mouse. This suggested that different Tau seeds might be responsible for the distinct clinical phenotypes of tauopathies and in injection models they are conformational templates for the aggregates generated. The same study showed that using human-derived seeds allows the study of Tau aggregation in WT mice, inducing more aggregation than when seeds derived from transgenic mice are used (115). In this and many other *in vivo* and *in vitro* studies (85,137,138), sonication of tau aggregates is used. Although, the effect of this procedure in the biochemical, biophysical and functional characteristics of the aggregates is not well understood yet except that it produces smaller size aggregates.

Tau seeds were, until recently, mostly synthetized by recombinant Tau, without the N/C- termini and only with one isoform of Tau, for example K18 with 4R Tau. These synthetic fibrils could only induce aggregation in transgenic mice overexpressing Tau. In WT mice expressing physiological levels of Tau, there were no observable Tau aggregation induction. A recent study showed that by isolating and purifying Tau seeds derived from human AD-brains, it is possible to induce Tau aggregation in WT mice. This allows to study Tau aggregation without the influence of

overexpressing Tau and to study the distinct aggregation potency between synthetic Tau fibrils and human AD-brains derived fibrils (106). As the Tau seeds described in the Guo et al., 2016 manuscript are also derived from a sarkosyl insoluble preparation from post-mortem AD brain it remains to be determined what discriminates this preparation from a regular PHF preparation (139).

Even with the improvement of the research models to study tauopathies, it was shown by Fitzpatrick and colleagues (140) with Cryo-electron microscopy (EM) that the structural differences observed between human AD-brain PHF and straight filaments such as the ones extracted from Tg tau mouse models can impact the exposure of antibody epitopes. It was observed that some regions were differently protected in the core of the PHF and straight filaments. Other study presented by Taniguchi-Watanabe and colleagues (141) showed that the core of the aggregates from different tauopathies are different. In this case, a limited digestion of the tau aggregates with trypsin showed that the proteolytic resistant core is different depending on the tauopathy. These findings suggest that although the mouse models to study tauopathies are improving, differences in the structure of the aggregates could change the exposure of antibody epitopes. Also, depending on the tauopathy, the aggregates can have different conformations and the regions that belong to the core of the aggregate, and consequently protected, can be different. This can prevent the binding of antibodies to their epitopes and therefore impair their immunotherapeutic effect. Even though injection models with conformational templating of aggregates can generate aggregates structurally similar to the ones present in the pathologic human brains (115), biochemical characterization of those aggregates was not performed yet.

To understand the biochemical and structural differences of aggregates from different models and tauopathies is highly important to comprehend how reliable are the results from the pre-clinical studies and predict the effect in humans. This could elucidate whether the same antibody is able to target more than one Tauopathy.

1.12. Aim of the research project

To fulfil this lack of knowledge on the field, the aim of this work is to characterize tau aggregates from research models such as P301S and P301L tau Tg mice, *in vitro* aggregated tau, and *post-mortem* human AD-brain PHF regarding their biochemical, biophysical and functional features, clarify the effect of the widely used sonication procedure in those characteristics and also evaluate how the conformation templating in the injection models can change the biochemical characteristics of the generated aggregates.

2. Methods and Materials

2.2. *In vitro* K18-P301L aggregation

K18 fibrils were prepared as described previously (138). Briefly, myc-tagged K18-P301L tau (Tebu Bio) (2 mg/mL) was incubated in the presence of 133 µM Heparin in 100 mM NH_4COO^- at 37 °C under gentle agitation. After 5 days, samples were centrifuged for 1 hour (h) (184 000 x g; TLA 100 rotor, Beckman) and supernatant was kept for analysis of remaining monomeric K18. The pellet was washed twice in 1 mL Dulbecco's Phosphate Buffered Saline (PBS) (Sigma-Aldrich cat #D8537) and finally resuspended in 400 µL PBS to obtain 5 mg/mL K18 fibrils which were directly aliquoted and frozen (-80 °C) or frozen after a sonication step (Branson probe sonicator, amplitude 15%, total sonication time was 2 min in pulses of 2 seconds).

2.3. Sarkosyl extraction from mouse brain

Tissue was weighed and homogenized in 6 volumes of buffer H (10 mM Tris, 800 mM NaCl, 1 mM EGTA and 10% sucrose/ pH 7.4). The homogenate was centrifuged at 34 000 x g (rotor TLA 100.2, Beckman Coulter) for 20 min at 4 °C. The supernatant was collected, an aliquot was kept as total homogenate and 1% N-lauroylsarcosine was added to the remaining fraction. After incubation at 37 °C for 90 min under gentle agitation the solutions were centrifuged at 180 000 x g (TLA 100 rotor, Beckman) for 1.5 h at 20 °C. The supernatants were kept as sarkosyl-soluble fraction, whereas the pellet containing the sarkosyl-insoluble material was resuspended in PBS, aliquoted and frozen at -80 °C. P301L brainstem sarkosyl insoluble fraction was resuspended in the same volume of the homogenate used for the extraction whereas P301S spinal cord sarkosyl insoluble fraction was resuspended in 66 times less volume than the homogenate used for the extraction, ending with a concentrated prep.

2.4. Human AD-brain PHF extraction

Frontal cortex brain tissue was homogenized in 6 volumes of cold buffer H (10 mM Tris, 800 mM NaCl, 1 mM EGTA and 10% sucrose/ pH 7.4) using a glass/Teflon Potter tissue homogenizer (IKA Works, Inc; Staufen, Germany) at 1.000 rpm.

The same volume of buffer H and homogenized tissue was added (final weight/volume ratio of 12 times) and extract was centrifuged at 27.000 x g for 20 min. The pellet was discarded and the supernatant was adjusted to a final concentration of 1% (w/v) N-lauroylsarcosine and incubated with rotation for 1.5h at 37°C. Subsequently the extract was centrifuged at 184000 x g for 90 min at 20°C. The pellet was carefully washed in PBS and resuspended in 66 times less volume of PBS, aliquoted and frozen at -80°C. Adapted from Greenberg et al. 1990 (139)

2.5. Direct ELISA

Nunc MaxiSorp™ high protein-binding capacity 96 well ELISA plates were coated either with PT76 or anti-MYC antibody (both produced at Janssen PRD) diluted in coating buffer (10mM Tris, 10mM NaCl pH 8.5; 50µL per well) at the concentration of 1 µg/mL and left overnight at 4°C. Plates were washed 5 times with 200µl of PBS/0.5%Tween-20 in an automatic washer (AquaMax 4000 Microplate Washer, Molecular devices), overcoated with 75µL of blocking solution (0.1% Casein in PBS) (Themo Scientific cat# 37528) per well and left for at least 1 h at room temperature (RT). After blocking, plates were washed again. Calibrator and unknown samples were diluted in blocking buffer and 50 µL were added to the assay plate. After an overnight incubation at 4°C, plates were again washed and 50µL per well of HRPO-labelled PT76 antibody in blocking buffer was added. Another wash was made and detection was performed with TMB Peroxidase EIA Substrate kit (BioRad) according to the manufacturers' instructions. After 5 minutes an equal volume of 2M H_2SO_4 was added to stop the enzymatic reaction. Detection was performed in Perkin Elmer EnVision® 2102 Multilabel Reader at OD_{450nm}. Binding curves were generated using GraphPad Prism7.0 software.

2.6. Western blotting

To run SDS-PAGE under reducing conditions, the samples were diluted in NuPAGE™ LDS Sample Buffer 1X (Thermo Scientific) and NuPAGE™ Sample Reducing Agent 1X (Thermo Scientific) and loaded on 4-12% Criterion™ XT Bis-Tris protein gel (BioRad cat# 3450124) in MOPS SDS running buffer 1X (Thermo Scientific, cat# NP0001-02) at 90V in the stacking gel and 130V during the

separation gel. After the separation, the gel was blotted on a nitrocellulose membrane (Trans-Blot® Turbo™ Midi Nitrocellulose Transfer Packs #1704159, BioRad). Under non-reducing conditions, the samples were diluted in NativePAGE™ Sample Buffer 1X (cat# BN2003 Thermo Scientific) and NativePAGE™ 5% G-250 Sample Additive (cat# BN2004 Thermo Scientific) and loaded in NativePAGE™ 3-12% Bis-Tris Protein Gels (cat# BN1001BOX Thermo Scientific) with NativePAGE™ Running Buffer 1X (Thermo Scientific, cat# BN2001) in the anode chamber and with 0.1X NativePAGE™ Cathode Additive (Thermo Scientific, cat# BN2002) in running buffer in the cathode chamber. Empty wells were loaded with sample buffer. The running was performed at constant 150V. After the separation, the gel was incubated 20 min in Tris/Glycine/SDS transfer buffer 1X (10x Tris/Glycine/SDS cat#1610732 BioRad) and blotted on a PVDF membrane (Trans-Blot® Turbo™ Midi PVDF Transfer Packs cat# 1704157 BioRad). After the transfer, the blot was destained in 100% methanol to remove excess of Coomassie, that was present during the run, and rinsed twice in MilliQ water. In both reducing and non-reducing conditions, membranes were blocked with TBS-T containing 5% Non-fat dry milk (Blotto NFDM, Santa Cruz biotechnology cat# SC-2325) for 1h and incubated with non-labelled primary antibody solutions (overnight at 4°C) and detected by HRP-labelled anti mouse antibodies or with HRP-labelled anti-tau antibodies at the concentration of 1 µg/mL during 2h at RT with gentle agitation. In both cases detection was done with ECL West Dura (Thermo Scientific).

For fluorescent detection of Western blots in reducing conditions, the steps were similar with exception of the blocking step which was performed with 5% BSA in TBS-T instead of 5% NFDM. The membranes were incubated with a non-labelled primary mouse anti-tau antibody and detected with Pierce™ Gt anti-Ms IgG (H+L) SuperClonal™ secondary antibody Alexa Fluor® 555 conjugate (Thermo Scientific) for 2h at RT, protected from light. The membrane was washed with TBS-T 3 times for 5 minutes and rinsed 3 times with TBS without Tween-20 to prevent fluorescence from the detergent.

Chemiluminescence and fluorescence imaging was performed with Amersham Imager 600 (GE Healthcare Life Sciences).

2.7. CFP/YFP FRET cell-based assays

HEK293-FRET CFP/YFP cells kindly provided by the group of Prof. Marc Diamond (142), were maintained as an adherent culture with cell culture medium Gibco™ DMEM supplemented with 10% Fetal Bovine Serum (BioWest, cat# S-1810), 1% Penicillin Streptomycin (Sigma-Aldrich), 1X GlutaMAX™ (Thermo Scientific cat# 35050061) and sodium pyruvate (Thermo Scientific cat# 11360070) at 37 °C, 5% CO_2 and controlled humidity. At 80% confluency, cells were splitted twice a week by trypsinization, centrifugation at 1000 x g (Centrifuge 5810, Eppendorf), resuspension in cell culture medium and plating at a density of $1x10^6$ cells/flask (Fisher Scientific, cat# 10-126-13).

To run a functional seeding assay, HEK293-FRET CFP/YFP cells were plated into a 96 well poly-D-lysine coated (Greiner Bio-One, cat# 655946) at a density of 2500 cells per well in a volume of 130 µL of cell culture medium and kept overnight in the incubator. On the second day, the standard curves and samples were diluted in PBS and co-incubated with the cells. Total volume of each well was adjusted to 150 µL with PBS. After 7 days of incubation, the cells were washed once with PBS and trypsinized with 50 µL for 5 min and transferred to a polypropylene 384 well-plate (Thermo Scientific, cat# CLS3657) containing 30 µL of Hank's Balanced Salt Solution (Sigma-Aldrich cat# H8264). FRET analysis was performed with BD FACSCanto™ II (Becton Dickinson, New Jersey, USA) as described in Marreiro et al (manuscript in preparation).

2.8. Biosensor cells imaging

HEK293-FRET biosensor cells were plated at the density of 25250 cells per well in a 96 well poly-D-lysine coated (Greiner Bio-One, cat# 655946) and with Lipofectamine™ 2000 transfection reagent (Thermo Scientific, cat# 11668019) were transfected with 12.5 ng of sonicated aggregated K18 per well. After 48h of incubation at 37 °C, 5% CO_2 and controlled humidity. Before the imaging the plasma membranes were stained with CellMask™ Deep Red (Thermo Scientific, cat# C10046) and Hoechst 33342 (Thermo Scientific, cat# H1399) both at the final dilution of 1/15000 in the medium already present in the cells in culture. After 10 minutes of incubation the cells were imaged in the Opera Phenix™ High Content Screening System (PerkinElmer) in confocal mode, with 40x water NA 1.1 objective and according to manufacture instructions.

2.9. Sucrose gradient separation

A discontinuous sucrose gradient was prepared by applying 1ml of PBS containing 60% sucrose, followed by 2ml layers of 50%, 40%, 30% and 20%, covered by a 1ml layer with 10% sucrose in a Thinwall Polypropylene Tube (Beckman Coulter, cat# 331374). Sample was diluted in a total volume of 500µL of PBS without sucrose and added on top of the gradient. This was followed by centrifugation for 16 h at 200.000 x g and 4 °C, rotor SW 40 Ti and ultracentrifuge Optima XL-100K (Beckman Coulter). After the run, 19 fractions of approximately 500µL were collected from the bottom to the top of the sucrose gradient with a peristaltic pump (Gilson MINIPULS® 3) using a glass capillary. The pellet of the ultracentrifugation was resuspended in 500 µL. The fractions were aliquoted and frozen at -80 °C.

2.10. Biochemical analysis MesoScale Discovery (MSD)

Coating antibodies were diluted in PBS (1µg/ml) and aliquoted into MSD plates (30 µL per well) (L15XA, MSD, Rockville, MD, USA), and incubated overnight at 4°C. After washing 5 times with 200µl of PBS/0.5%Tween-20, the plates were blocked with 0.1% casein in PBS for 2 h and washed again 5 times with 200µl of PBS/0.5%Tween-20 in an automatic washer (AquaMax 4000 Microplate Washer, Molecular devices). After adding samples and standards (both diluted in 0.1% casein in PBS), the plates were incubated overnight at 4°C. Subsequently, the plates were washed 5 times with 200µl of PBS/0.5%Tween-20 and 25 µL of SULFO-TAG™ conjugated detection antibody diluted in 0.1% casein in PBS was added and incubated for 2 h at RT while shaking at 600rpm. After a final wash 5 times with 200µl of PBS/0.5%Tween-20, 150µl of 2 X buffer T (MSD) was added, and plates were read with MESO SECTOR S 600 (MSD). Signals were divided by the background of each plate. Background corresponds to the signal of the wells incubated with casein 0.1% instead of sample. Statistical analysis was performed with GraphPad Prism7.0 software (GraphPad Software, La Jolla California, USA).

2.11. Limited proteolysis of tau seeds

Limited proteolysis analysis of human PHF samples and P301S Tg mouse sarkosyl insoluble fractions was performed as previously described with minor modifications (143). Briefly, after protein quantification using the BCA method, 0.85 µg/µL of the different samples were incubated with 0, 5 and 25 µg/mL of Pronase (Roche, cat# 10165921001). The digestion reactions were performed during 1h at 37 °C, before quenching with LDS sample buffer 1X (Life Technologies) and boiling for 5 min at 95 °C. Quenched samples were then added (30 µL) to a 4-20% Criterion TGX stain-free gel (Bio-Rad) and blotted onto a nitrocellulose membrane (Bio-Rad). Blocking was performed during 1h with TBS-T containing 5% non-fat dry milk, before probing with HRPO labelled Tau specific antibodies for 2h at RT. Blots were then detected with West Dura (Thermo Scientific) and image acquisition was performed in Amersham Imager 600 (GE Healthcare Life Sciences).

2.12. Antibody epitopes

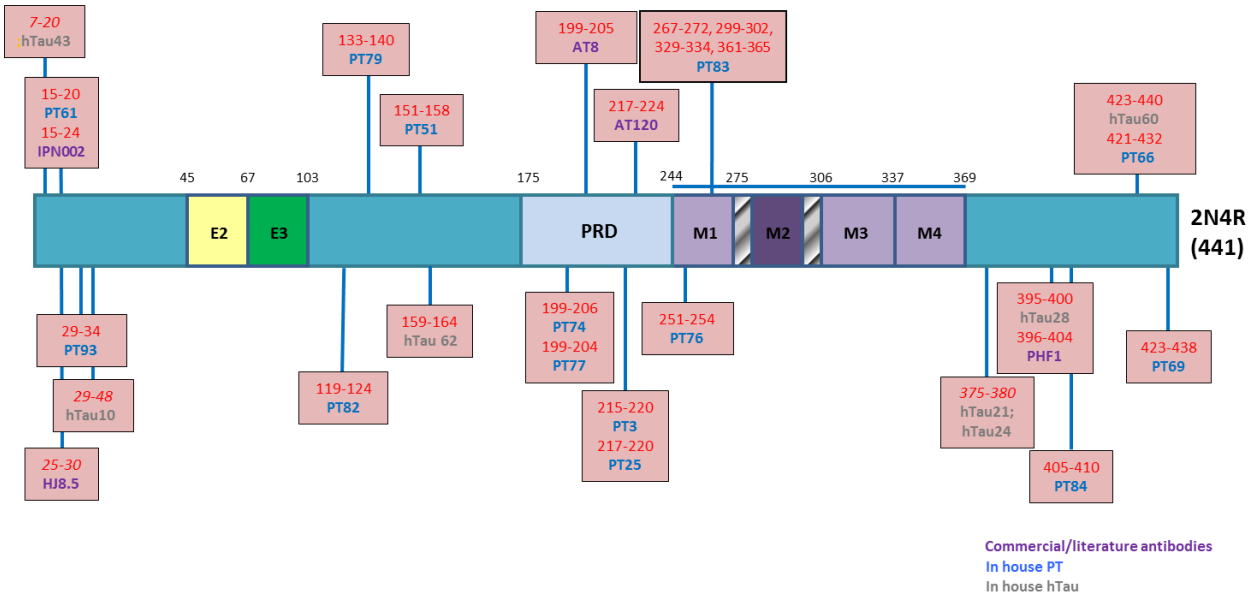

Overview of Janssen collection of anti tau antibodies and some of the competitor lead antibodies (IPN002 (144), HJ8.5 (145) and PHF1 (146)) used in this thesis. PT antibodies have been generated by immunzations with human AD PHFs as antigen while hTau antibodies were raised against recombinant human tau.

3. Results

3.1. Effects of sonication on biochemical and functional properties of K18(P301) fibrils

Several studies demonstrated that tau fibrils, derived from recombinant tau or from *post-mortem* brain tissue, are taken up by cells and recruit intracellular tau into the template tau seed to recapitulate the pathology (114,138). In many cellular and *in vivo* tau seeding procedures, sonication of fibrils is performed (138,147,148) but it is not clear which of the new formed species is responsible for seeding potency. Sonication of tau aggregates fractionates large aggregates into smaller size oligomers (137) and is described to increase aggregation capacity in cells. MYC-tagged K18 P301L, a 4 MTBD tau fragment carrying the P301L mutation (149), can be aggregated *in vitro* and the pellet can be collected by ultracentrifugation. The effect of sonication on the resuspended K18(P301L) pellet was analyzed with a MSD aggregate selective assay and with a HEK293-FRET CFP/YFP cell-based assay, to have a biochemical and a functional readout respectively. Aggregate-selective "self-sandwich" MSD assays use the same antibody for capture and detection. This setup creates epitope competition between capture and detection antibody excluding the detection of monomers but allowing the detection of aggregated forms of the analyte. Accordingly, *in-vitro* aggregated K18 can be analyzed by a "self-sandwich" MSD assay using an antibody with its epitope in the MTBD. Several antibodies are suitable for this and data in Fig. 8a, show that in a PT76 "self-sandwich" MSD assay, aggregate signals of the sonicated K18 dilution curve (red) overlap with the non-sonicated K18 dilution curve (blue) (Fig. 8).

A dilution curve of monomeric K18(P301L), did not reveal a substantial signal in the aggregate-selective assay while a PT76-anti-MYC assay confirmed the presence of monomeric K18-MYC (Fig. S1). Furthermore, the supernatant of the centrifugation after the *in vitro* aggregation showed a modest signal in (Fig. 8a), demonstrating that the centrifugation procedure deposited the majority of the K18 aggregates in the pellet and that sonication of the fibrils did not increase epitope exposure in the aggregates. The cell-based assay uses HEK293-FRET biosensor cells expressing P301S-K18/CFP and -/YFP fusion proteins (142). Upon induction of aggregation by adding tau seeds, both fusion proteins are incorporated in the *de novo* formed aggregates. As a consequence, CFP and YFP labels come in proximity and produce FRET fluorescence, quantified by cell flow

cytometry (142). Tau seeds can be applied to the cells in the presence- or absence of transfection reagent to make the model independent- or dependent on cellular uptake respectively.

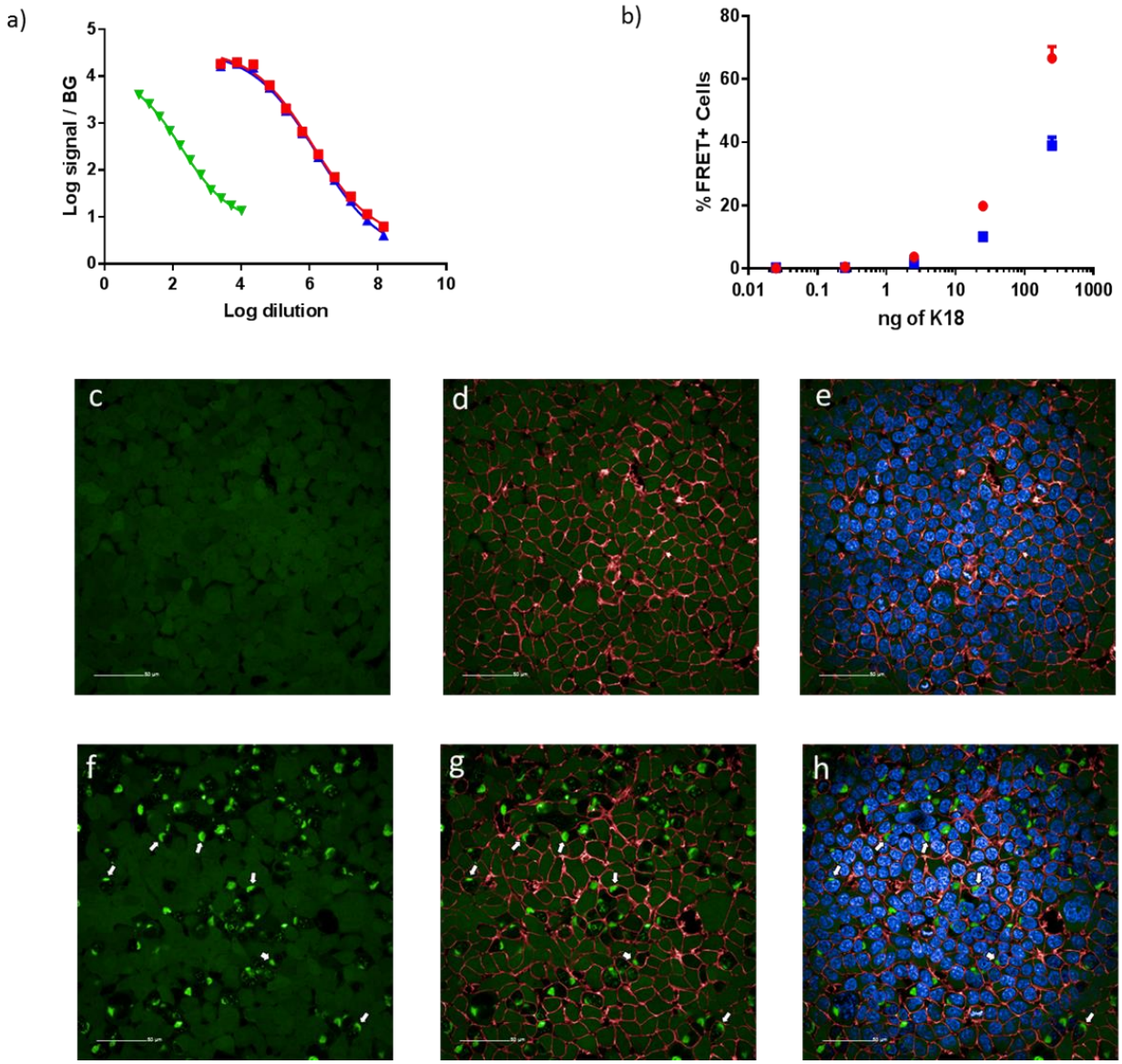

Figure 8 – Sonication effect of aggregated K18 in PT76/PT76 MSD assay and in seeding potency.

***In vitro*-aggregated K18 was collected from the supernatant (green) after high-speed centrifugation and from the resuspended pellet non-sonicated (blue) and sonicated (red), different dilutions of these fractions were analysed with a PT76/PT76 "self-sandwich" MSD assay (a) and with a cell based seeding assay in HEK293-FRET cells (b). HEK293-FRET biosensor cells were plated at the density of 25250 cells/well and not treated (c,d,e) or transfected with 12.5 ng of aggregated and sonicated K18(P301L) (f,g,h). 48h later cells were imaged via confocal microscopy in live-cell imaging. Cells without aggregation show green basal fluorescence of CFP/YFP non-aggregated K18 (c), CellMask™ stained cellular membranes in red (d) and Hoechst 33342 staining the nuclei in blue (d). In the presence of K18 aggregates there is the recruitment and aggregation of the intracellular expressed K18 (d,e,f; white arrows show aggregation). 40x magnification, scale = 50 µm.**

Data in Fig. 8B assay show that in a curve of increasing concentration of K18(P301L) fibrils co-incubated with the cells, the sonicated aggregated K18 curve displayed stronger seeding capacity than the non-sonicated K18 fibrils. The difference became more evident at intermediate fibril concentrations (Fig. 8b) and is less prominent in the presence of transfection reagent (Marreiro et al, manuscript in preparation) suggesting that sonication produces smaller aggregates with enhanced uptake and subsequent seeding in the biosensor cells. Imaging of HEK293-FRET biosensor cells showed a basal CFP/YFP fluorescence signal that displayed a homogeneous distribution in the cells (Fig. 8 c,d,e) but after transfection with 12.5 ng of sonicated K18 aggregates, the cytosolic expressed CFP- and YFP tagged K18 monomers were shown to be recruited and assembled into intracellular aggregates (Fig. 8 f,g,h, white arrows).

As stated above, fragmentation of large tau aggregates into small fibrils by the sonication process is a plausible explanation for the observed increased seeding potency of K18(P301L) fibrils (138,150). To evaluate this hypothesis, these aggregates were separated by size in a discontinuous sucrose gradient ultracentrifugation. Both sonicated and non-sonicated K18(P301L) fibrils and non-aggregated K18(P301L) monomers were loaded on such a gradient from which 19 fractions were collected and the pellet (P) of the ultracentrifugation was resuspended in the same volume as one fraction (500 µL). The collected fractions and the pellet were analysed by MSD aggregate selective assays, cell-based functional seeding assay in HEK293-FRET cells and by native PAGE.

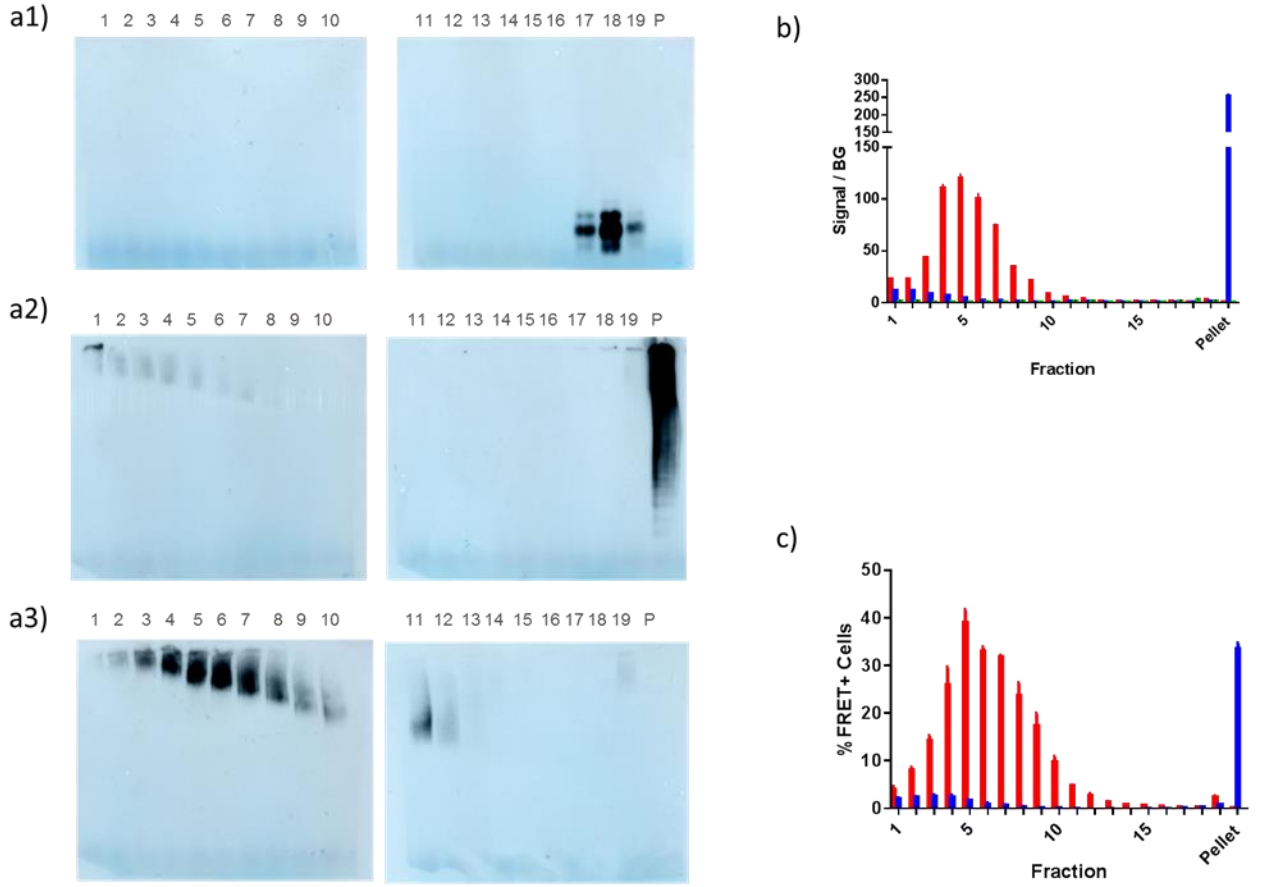

Figure 9 – K18 species separation by sucrose gradient ultracentrifugation

Monomeric and *in vitro* aggregated sonicated and non-sonicated K18 species were separated by sucrose gradient ultracentrifugation. 19 fractions were collected and the pellet of the ultracentrifugation resuspended. Sucrose gradient fractions were analysed in Native PAGE and detected with PT76-HRPO antibody. Representative images of at least two independent experiments show that the non-aggregated K18 species are present in 3 lowest density fractions of the sucrose gradient (a1); Gradient fractions from the non-sonicated K18 fibrils (a2) showed weak signals in the high-density fractions and a strong signal in the resuspended pellet of the ultracentrifugation. Gradient fractions from the sonicated K18 fibrils (a3) showed strong signals in the high to intermediate density fraction (3-12) with the presence of gradually smaller size K18 fibrils. Aggregation signal was detected with PT76 "self-sandwich" MSD assay and data are represented as logarithmic transformation of the mean signal divided by background +/- SD, N=2 (b) and it showed that in gradient fractions of the non-sonicated K18 fibrils (blue) there are modest signals in the high-density fractions and a strong aggregate signal in the pellet. In the gradient fractions of the sonicated K18 fibrils (red) strong aggregate signals were detected in the intermediate-density fractions. In the fractions from the gradient of the non-aggregated K18 (green) no measurable aggregate signals were detected. Functional analysis of the gradient fractions was assessed in HEK293-FRET cell based assay and data are represented as mean % of FRET positive cells that have aggregation +/- SD, N=2 (c). Fraction from the non-aggregated K18 gradient (green) did not show aggregation capacity; Fractions of the gradient with non-sonicated K18 fibrils (blue) showed modest aggregation capacity in high-density fractions of the gradient and strong aggregation capacity in the resuspended pellet; Fractions from the gradient of sonicated K18 fibrils (red) demonstrated strong seeding capacity in the intermediate-density fractions of the gradient.

From the native PAGE immunoblot detected with HRPO-labelled PT76, it is observed that gradient fractions from non-aggregated K18(P301L) only showed signal in the lower-density region (Fig. 9.a1) while the non-sonicated K18(P301L) fibrils showed moderate signals in the higher-density fractions and a very strong signal in the resuspended pellet (Fig. 9.a2). Interestingly, the sonicated

K18(P301L) fibrils displayed strong PT76-HRPO signals distributed in high and intermediate density fractions (2-11) of the gradient, and no signal was detected in the pellet (Fig. 9a.3). These data show that the sonication procedure is indeed affecting the size-distribution of the K18 aggregates from large into smaller fibrillary species. This was also confirmed by analysing the same sucrose gradient fractions with the PT76 "self-sandwich" MSD assay. As expected, in the fractions from the non-aggregated K18(P301L) gradient no aggregation signal was detected. In the fractions of the gradient with non-sonicated K18 fibrils, low aggregate signals were detected in high-density region but a strong signal was displayed in the resuspended pellet. In the gradient with sonicated K18 fibrils, aggregate signals were distributed in a bell-shaped manner between the fractions 1 and 10 (Fig. 9b). Next, we wanted to correlate aggregate signals of the sucrose gradient fractions to their seeding properties in the FRET-biosensor cell-based assay. Data in Fig. 9c show that non-sonicated fibrils have low seeding capacity in the lower fractions of the gradient and a strong seeding capacity of the species present in the pellet while sonicated K18 gradient fibrils show strong seeding capacity in the fractions 1 to 10 and no seeding is observed in the cells treated with the resuspended pellet.

The seeding induced by the pellet fraction from the non-sonicated fibrils was unexpected as we hypothesized that these large MW fibrils are not taken up by the cells. This could be explained by partial fragmentation of the large aggregates by the resuspension into aggregates that can induce FRET positive cells similar to the sonicated fibrils described in Fig. 8B. Altogether, biochemical and functional data suggest that the sonication is breaking large K18(P301L) fibrils into smaller aggregate species with stronger seeding potency, probably because of their improved uptake by the cells.

3.2. Differences between tau seeds derived from Tg-mice and human AD brain

To translate the findings obtained with recombinant tau fibrils to fibrils extracted from mouse and human brain, similar experiments with tau fibrils derived from P301S, P301L tau Tg mice and from *post-mortem* human AD brain were performed. As structural and biochemical studies suggested that some epitopes are differentially exposed in the different types of tau fibrils (140,141,143), it was verified whether this was reflected in the detection of these fibrils by use of aggregate

selective MSD assays using antibodies binding to different tau epitopes. Therefore, tau aggregates in sarkosyl insoluble fractions from P301S and P301L Tg mice and from human AD-brain, were analysed in a PT76 "self-sandwich" MSD assay next to WT and tau KO mouse brain total homogenates to evaluate the specificity on one hand and signal strength of the assay with human and mouse extracts on the other hand.

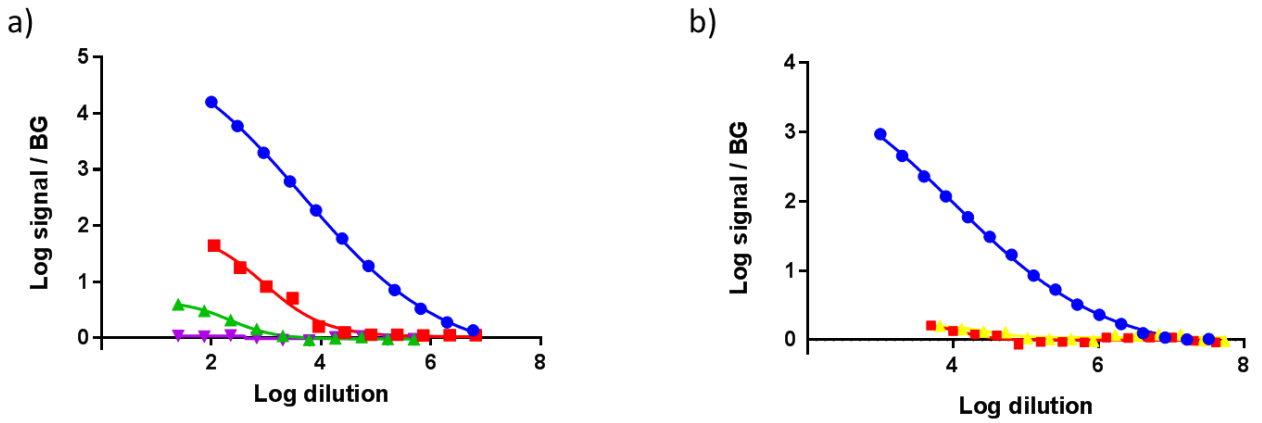

Figure 10 – PT76 "self-sandwich" MSD assay characterization

Dilution curves from human AD-brain PHF (blue), P301S (red) tau Tg mice sarkosyl insoluble fractions, brain homogenates from wild-type mouse (green) and tau knock-out mouse (purple) were loaded in PT76 "self-sandwich" MSD assay. Tg mouse and human AD-brain PHF starting dilution were corrected to the total tau present in the extracts. A stronger detection of human PHF was observed when comparing to Tg mouse seeds (a). Comparison of P301S (red) and P301L (yellow) tau Tg mice aggregates binding in PT76 "self-sandwich" MSD assay shows that aggregates from the 2 Tg models behave the same way in this assay (b). Data are represented as logarithmic transformation of signal divided by background +/- SD and N=2.

Interestingly, in the PT76/PT76 assay, human AD seeds seemed to produce much stronger signals in comparison to P301S tau Tg mice fibrils with a 300-fold difference of the highest signal. WT and tau KO mouse brain total homogenate displayed minor to no binding which confirmed the specificity of this assay to tau aggregates (Fig. 10a). Similar analysis of tau seeds derived from P301L and P301S tau Tg mice showed very low binding in these fibril fractions comparing to human tau PHFs (Fig. 10b). This experiment suggests that tau fibrils derived from P301L and P301S tau Tg mice have a different PT76 epitope exposure compared to human AD derived PHFs, suggesting structural differences between those tau aggregate species.

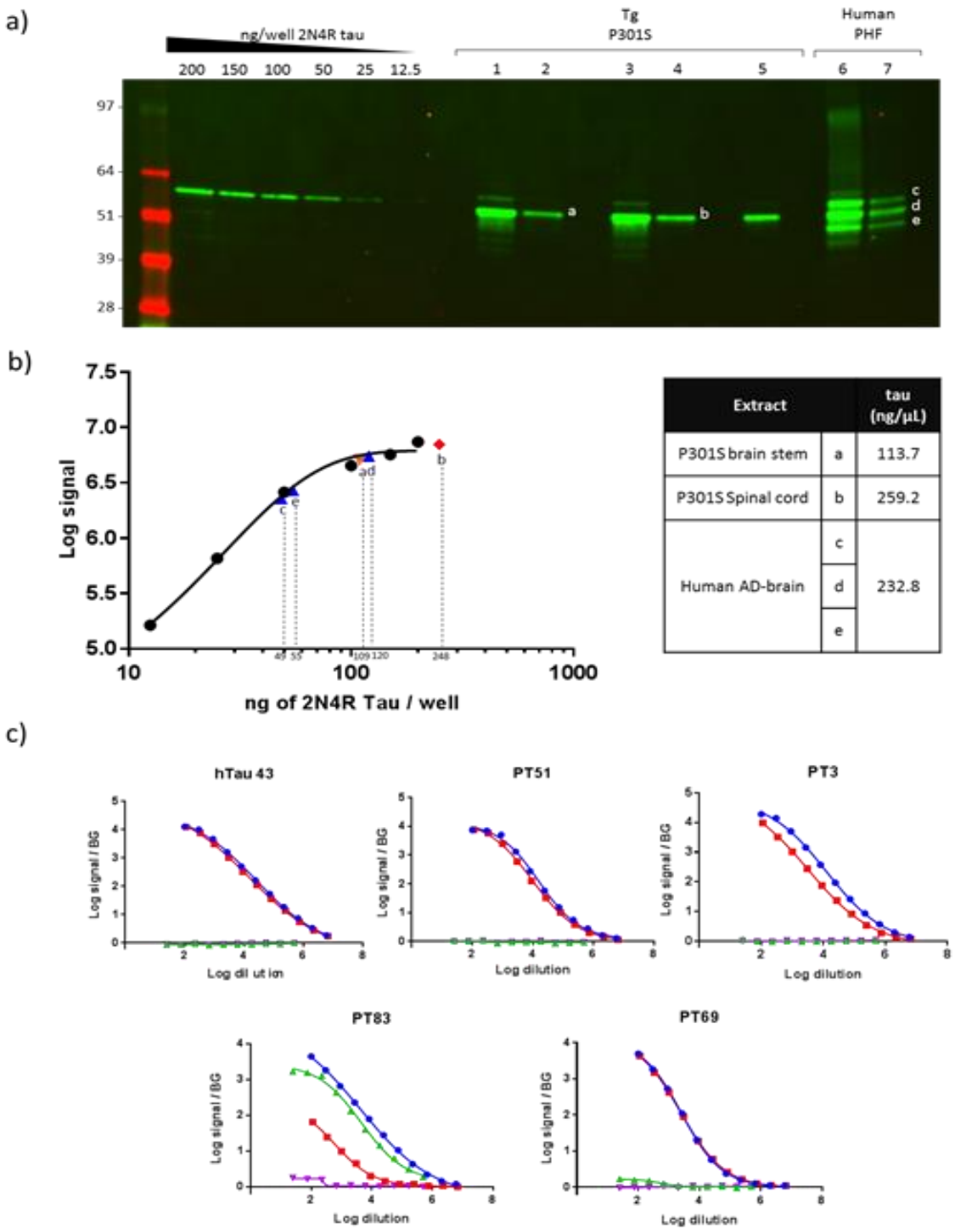

Extract		tau (ng/µL)
P301S brain stem	a	113.7
P301S Spinal cord	b	259.2
Human AD-brain	c	232.8
	d	
	e	

Figure 11 – Comparison of Tg P301S mouse seeds and human AD-brain seeds detection in MSD assays with total tau loading control determined by Western blotting

Fluorescent hTau10 - Alexa 555 (represented with green fluorescence) Western Blot total tau quantification of tau seeds derived from P301S tau Tg mouse brainstem (3.83 µL (1) or 0.96 µL (2)) and spinal cord (3.93 µL (3, 5) or 0.96 µL (4)) or from human AD-brain (3.83 µL (6) or 0.96 µL (7)). Indicated amounts of 2N4R tau are used as calibration curve (a). Extracts 3/4 and 5 are from different pools of spinal cords. Individual bands were quantified using ImageQuant™ as shown in the interpolation curve (b) with the final total tau concentrations of 113.7 ng/µL in P301S Tg mouse brainstem extract, 259.2 ng/µL in P301S Tg mouse spinal cord extract and 232.8 ng/µL in human AD-brain seeds. Detection comparison of human AD-brain seeds (blue), P301S Tg mouse sarkosyl insoluble fraction from spinal cord (red), wild-type mouse (green) and tau KO mouse (purple) total brain homogenates with hTau43 (N-term), PT51 (mid-term), PT3 (PRD), PT83 (MTBD) and PT69 (C-term) antibodies in "self-sandwich" MSD assay allows to detect only aggregate signals and not monomeric tau (c) showing that the binding of human and Tg mouse seeds is similar in N-terminal, mid-term and C-terminal antibodies but stronger to human aggregates in PRD and much stronger in MTBD antibodies. Data are show as logarithmic transformation of signal divided by background +/- SD and N=2.

To confirm that the total tau protein content in P301S and human extracts are the same, both extracts were quantified by Western blot detected with hTau10 (anti-human tau) and secondary anti-mouse Alexa Fluor 555 antibody. Six different concentrations of recombinant 2N4R tau were loaded as calibrants. P301S brain stem and spinal cord sarkosyl insoluble fractions and human PHF were quantified by analysing two different extract volumes. (Fig. 11a). Quantification of the signals in Fig. 11a revealed that the final tau concentration in the extracts was 113.5 ng/µL in the P301S brainstem sarkosyl insoluble fraction, 259.2 ng/µL of tau in the P301S Tg mice spinal cord sarkosyl insoluble fraction and 232.4 ng/µL of tau in the human PHF (Fig. 11b). This quantification allowed to compare the binding of the extracts of P301S Tg mouse spinal cord and human PHF in MSD assays and reassured that any difference in signals was not a consequence of different amounts of tau protein in the tau fibril samples from mouse and human brain. To characterize these tau aggregate species further, "self-sandwich" MSD assays involving tau epitopes outside the MTBD were used to compare the binding of human and mouse aggregates. Data in Fig. 11c show that, in contrast to the PT76/PT76 assay, hTau43 (N-terminal), PT51 (mid-term) and PT69 (C-terminal) antibody assays have similar signals when different dilutions of human and P301S Tg mouse seeds were analysed suggesting a similar exposure of these epitopes in tau fibrils derived from the 2 sources. Interestingly, PT3, a phospho-tau-selective antibody binding in the PRD showed slightly higher signals for human seeds when compared to P301S Tg mouse seeds suggesting that the PT3 epitope is differentially phosphorylated or that the PRD region is somewhat shielded in fibrils from tau Tg mice and more exposed in human AD-derived fibrils. Similar to the PT76/PT76 assay, use of the PT83 "self-sandwich" MSD assay displayed a strong difference between dilution curves of human and P301S seeds suggesting that the epitope of PT83 in the MTBD is also differentially exposed in the two types of seeds. The binding to WT mouse brain homogenates, and to a lesser extent to tau KO mouse homogenates, is explained by sequence homology between the PT83 epitope with the MTBD of other MAPs, (e.g. MAP2 and MAP4) that can also assemble into straight filaments (151).

Overall, the differences in detection of the human and P301S tau Tg mouse-derived fibrils by "self-sandwich" MSD assays using antibodies binding to the MTBD (i.e. PT76 and PT83) and to the PRD (i.e. PT3) suggested that the aggregates from the 2 sources have different structural properties.

3.3. Aggregate structure analysis by limited proteolysis

Due to the differences in the signal of human and mouse seeds that were observed in the MSD assays, it is likely that the aggregates from the 2 sources have different conformations and that some antibody epitopes are differentially exposed by these species. To investigate that further, a limited proteolysis with pronase was performed as described by Sanders et al. 2014 (143). The limited proteolysis technique involves a proteolytic digestion to remove all accessible fragments. In the case of tau aggregates, such an enzymatic reaction is expected to remove the well exposed fuzzy coat and all the antibody epitopes in those fragments while the core of the aggregate is protected and will stay intact. The undigested parts of the aggregate are analysed by Western blot and detected with antibodies binding to different epitopes of the tau protein. This approach allows to determine epitopes protected in the core of the aggregates and epitopes exposed to the outside of the aggregates (140). A similar approach combining limited proteolysis and mass spectrometry revealed substantial differences in the core region of fibrils from different tauopathies (141). To optimize this procedure, untreated human PHF and incubated with 3 pronase concentrations of 5, 25 and 50 µg/mL for a total protein concentration of 0.85 µg/µL were used and after the enzymatic reaction, samples were analysed with Western blotting under non-reducing conditions and detected with antibodies binding to different epitopes in the tau protein. The lower concentration of 5 µg/mL of pronase partially digested the exposed fragments of the aggregates, while in the presence of 25 µg/mL of pronase only the proteolytic-resistant core remained undigested but the 50 µg/mL concentration of pronase digested the entire aggregate species (Fig. S2). These observations experiment allowed to select the optimal pronase concentrations. Human AD-brain PHF and P301S Tg mice spinal cords sarkosyl insoluble fractions were incubated in the absence of enzyme or with 5 and 25 µg/mL of pronase.

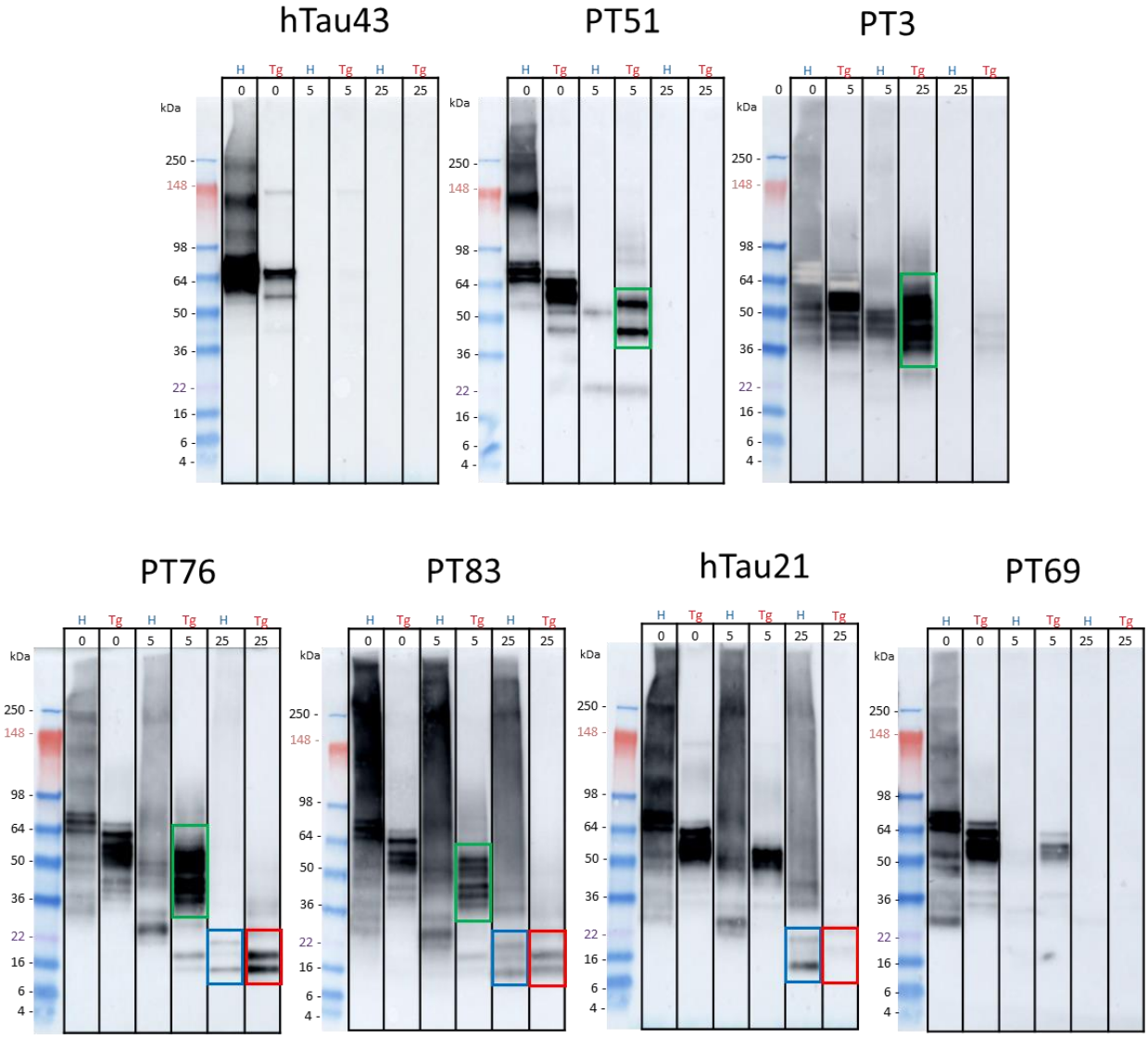

Figure 12 – Antibody epitope exposure analysis in P301S Tg mouse and human AD-brain seeds

Total protein of sarkosyl insoluble extracts from human AD-brains (H) and P301S Tg mouse spinal cord (Tg) were quantified by BSA method (data not shown) and 0.85 µg/µL of total protein was incubated with 0, 5 or 25 µg/mL of pronase. Analysis was performed by Western Blotting under non-reducing conditions, using hTau43 (N-term), PT51 (mid-term), PT3 (PRD), PT76 (MTBD), PT83 (MTBD), hTau21 and PT69 (C-term) antibodies for detection. The intermediate pronase concentration (5 µg/mL) is capable to increase the exposure of some regions of P301S Tg mouse aggregates (green boxes). The higher pronase concentration (25 µg/mL) only leaves the core of the aggregate undigested and identifies what regions are protected in the aggregates (blue and red boxes) being more evident in MTBD with PT76 in Tg mouse aggregates and hTau21 with human derived seeds.

Western blots in Fig. 12 showed that hTau43 (N-terminal) and PT69 (C-terminal) epitopes are easily accessible since the overall signal disappeared already by incubation with 5 µg/mL pronase indicating that N- and C-terminal epitopes are completely hydrolysed under those conditions. Also the PT51 (Mid-term) and the PT3- and PT74 (phospho-epitope in PRD) (Fig. S3) antibody epitopes are removed by 25 µg/mL of pronase but seemed to be still present in P301S tau Tg seeds after

treatment with 5 µg/mL pronase (Green rectangles in Fig. 12). Under the same reaction conditions, PT51, PT3 and PT74 (Fig. S3) epitopes were removed in human seeds suggesting that mid-region and PRD are more exposed in the human AD seeds compared to the Tg mice seeds. A similar observation was made for epitopes of PT76 and PT83, antibodies binding to the MTBD. After digestion with 5 µg/mL of pronase, an increased signal was detected in the Tg mice seeds but not in the human PHF. After treatment with 25 µg/mL of pronase, both antibodies detected 2 low molecular weight (MW) bands ($6 \leq MW \leq 22$) corresponding to the proteolytic-resistant core of the aggregates. This was seen in both human and Tg mice seeds but for the PT76 antibody with a stronger signal in the mice seeds (Fig. 12, blue and red boxes). These observations confirmed that the core of the aggregates is constituted by the MTBD. However, in Tg mice seeds the PT76 epitope, which is situated N-terminal from the MTBD (251-254), is more protected than in the human PHF while the inverse is observed with the hTau21 epitope situated more C-terminal from the MTBD (375-380). The latter hTau21 epitope was digested more efficient in fibrils from tau Tg mice compared to human AD brain-derived PHFs demonstrating that this region belongs to the core of the human PHF but not to the core of the Tg mice seeds. These observations suggest that the N-terminal side of the MTBD is more protected in Tg mice seeds whereas the C-terminal end of the MTBD is more protected in human PHF.

This observed difference in epitope protection of regions adjacent to the MTBD between human AD and tau Tg mice-derived fibrils explains their different binding properties in PT76 and PT83 “self-sandwich” MSD assays. To validate further, a hTau21 “self-sandwich” MSD assay was developed and dilution curves of human PHF, P301S Tg mice sarkosyl insoluble fraction and WT and tau KO mice total brain homogenates were analysed.

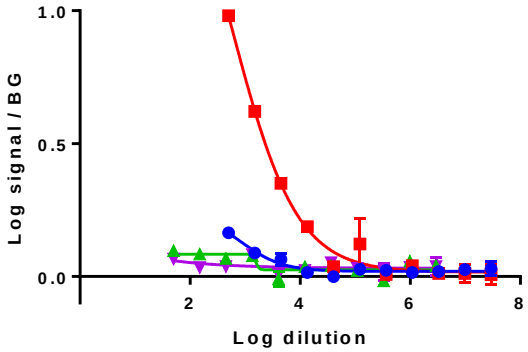

Figure 13 – hTau21 "self-sandwich" MSD assay characterization

Human AD-brain (blue), P301S Tg mouse spinal cord sarkosyl insoluble fraction (red), wild-type mouse (green) and tau knock-out mouse (purple) total brain homogenate dilution curves were loaded in hTau21 "self-sandwich" MSD assay. Data is represented as logarithmic average +/- SD of the signal divided by background, dependent on the dilution of the extract. N=2.

The obtained detection curves showed that the signals in human PHF dilutions (close to background) were lower than the same dilutions of fibrils from tau P301S Tg mice, with 9-fold background intensity, without any signal from WT and tau KO mouse total brain homogenates (Fig. 13). This suggests that the region that comprises the epitope of hTau21, C-terminal to the MTBD, is more protected in the core of human PHFs than in the core from tau Tg mouse fibrils.

3.4. Effect of sonication in human AD-brain and Tg mouse seeds

Since the epitope exposure seems to be dependent on the structure of the aggregate and sonication has been shown to fragmentize large aggregates, it was evaluated how the sonication can have an impact in the size and epitope exposure of tau aggregates from human AD-brain and P301S Tg mouse aggregates. The impact of sonication in the biochemical and functional properties of the aggregates was analysed further by comparing distribution patterns of non-sonicated and sonicated fibrils on a sucrose gradient ultracentrifugation experiment.

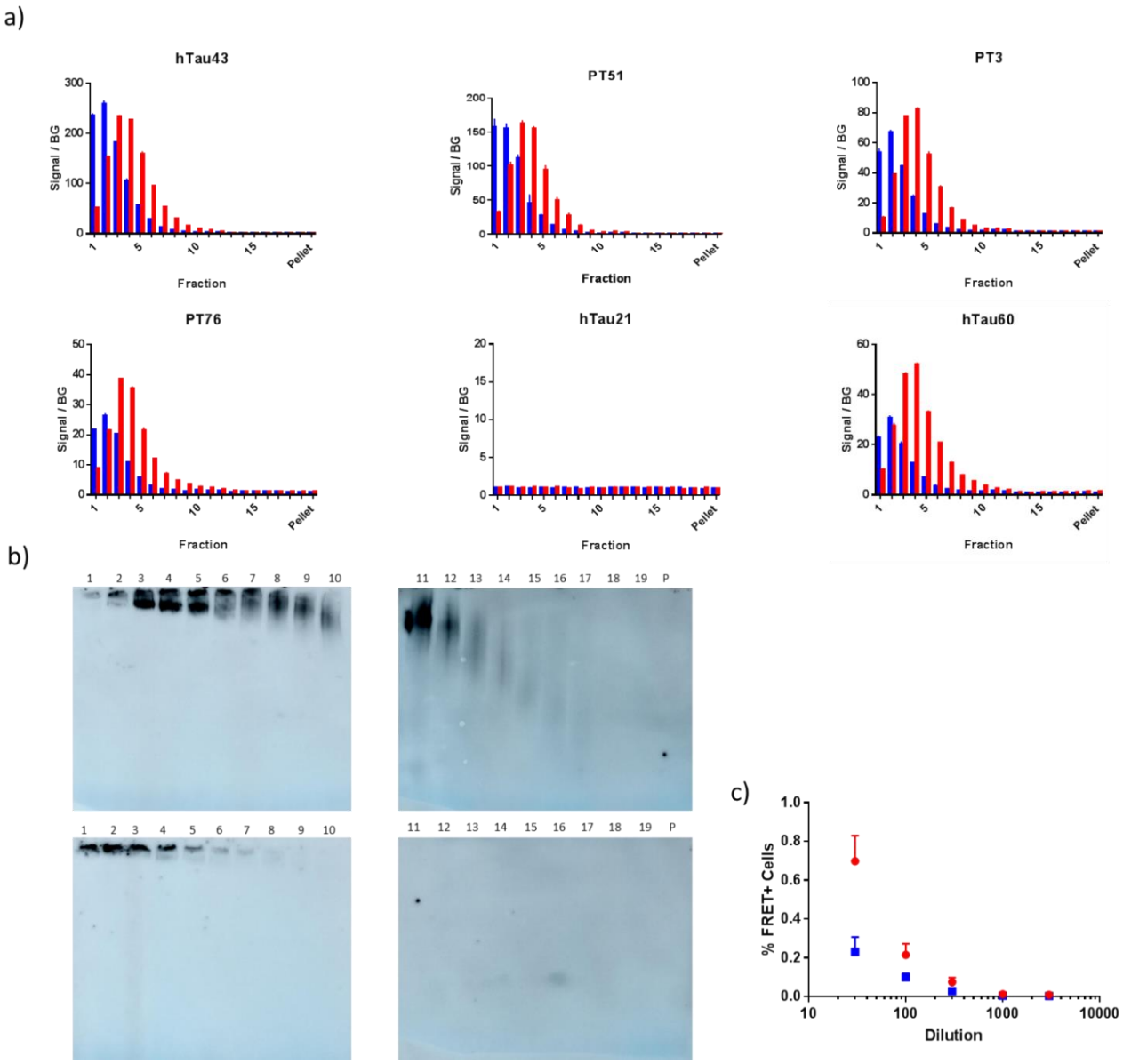

Figure 14 – Effects of sonication in human AD-brain seeds separated by sucrose gradient ultracentrifugation

Sonicated (red) and non-sonicated (blue) tau fibrils from human AD-brain were separated in a sucrose gradient ultracentrifugation experiment as described in the "materials and methods" section. The obtained fractions were analyzed in "self-sandwich" MSD assays with hTau43 (N-terminal), PT51 (mid-term), PT3 (PRD), PT76 (MTBD), hTau21 (C-terminal) and hTau60 (C-terminal) antibodies. Data are representative of at least 2 independent experiments and presented as mean signal divided by background +/- SD (a). Representative images of the Native PAGE analysis of sucrose gradient fractions detected with PT76-HRPO show differences in aggregates weight and distribution in fractions of sonicated (top) and non-sonicated (bottom) human tau aggregates (b). Seeding capacity of dilution curves of sonicated (red) and non-sonicated (blue) human PHF were analyzed in cell-based assay with HEK293-FRET cells, suggesting higher aggregation capacity after sonication. Data are represented as mean percentage of FRET positive cells, who have aggregation, +/- SD, N=4 (c).

Analysis of gradient fractions with MSD aggregation assays using antibodies binding to various epitopes (i.e. hTau43, PT3, PT51, PT76, hTau21 and hTau60), showed that non-sonicated human PHF fractions (blue) display high aggregate signals in the 2 highest-density fractions while the sonicated PHFs signals (red) showed maximal intensity in fractions 3 and 4 (Fig. 14a). This again

suggests that the sonication is affecting the size distribution of the aggregates. In hTau21 assay, there is no detectable tau aggregate signal in both sucrose gradients. This confirms lower sensitivity of this assay due to the protection of this epitope in the human tau aggregate conformation. To confirm that MSD aggregate signals in fractions with a different density indeed correspond to a different MW of the aggregates, all sucrose gradient fractions were analysed by Native PAGE and immunoblot detection with HRPO-labelled PT76. The sonicated PHF gradient has tau multimeric species of gradually lower molecular weight from the fraction 2 towards lower MW fractions (Fig. 14b top panel) while the non-sonicated PHF sucrose gradient only showed higher molecular weight tau species in the five highest-density fractions with the strongest signals in the first two samples (Fig. 14b bottom panel). This confirmed that sonication affects the size distribution of the tau species in the gradient by breaking larger aggregates into smaller fibrils or oligomeric tau species. The functional analysis in biosensor cells was not successful due to low seeding capacity or low concentration of the human PHF present in the fractions. Although, sonicated and non-sonicated PHF concentration curves were analysed and results suggest an increase in aggregation capacity of the PHF after sonication (Fig. 14c), supporting the hypothesis that the sonication is producing smaller aggregates that are more easily taken up by cells to trigger aggregation.

The same experimental setup was used to analyse sonicated and non-sonicated fibrils from P301S Tg mice.

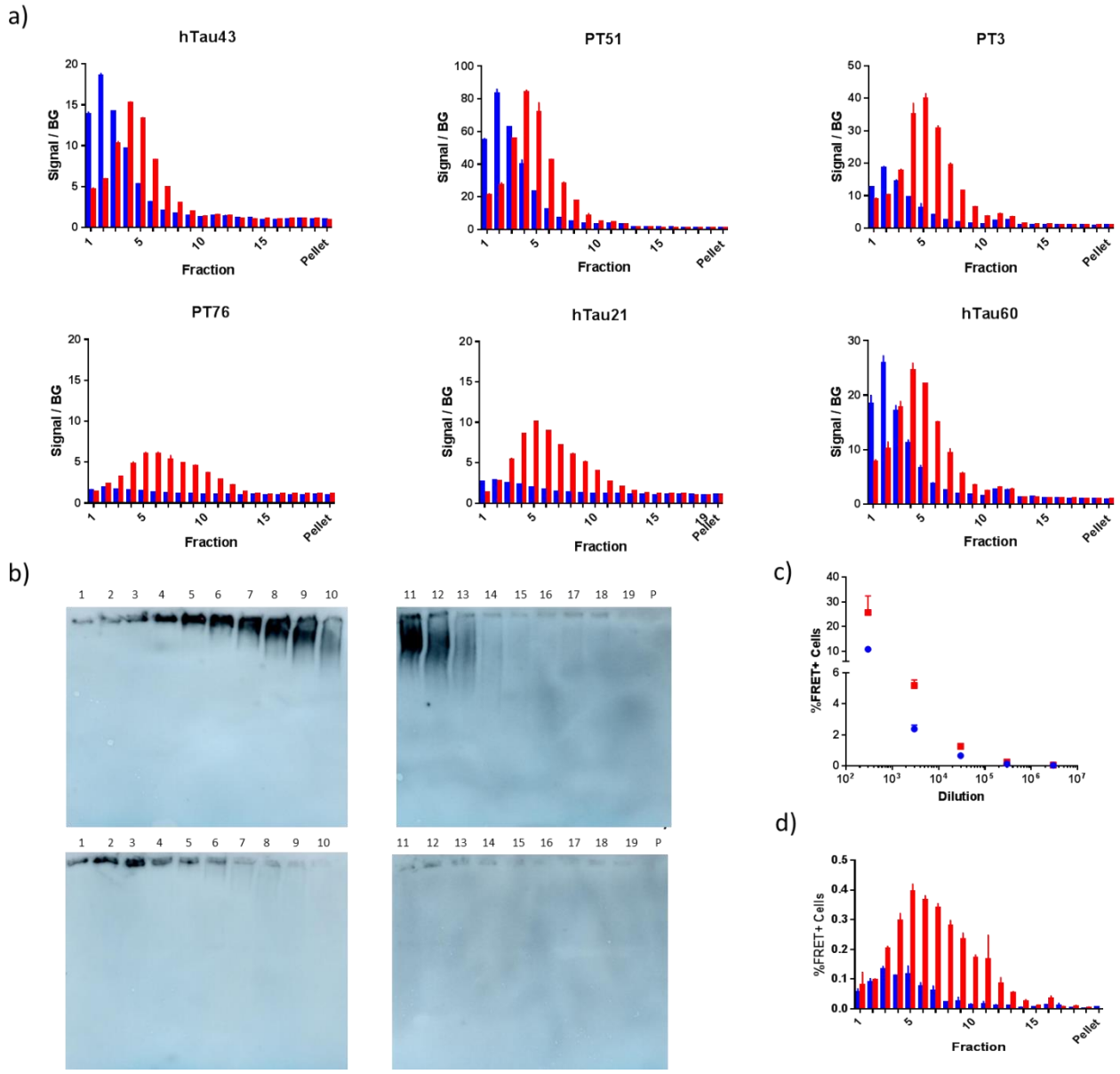

Figure 15 – Effects of Tg P301S mouse tau seeds sonication in sucrose gradient ultracentrifugation

Sonicated (red) and non-sonicated (blue) tau fibrils from P301S tau Tg mouse sarkosyl insoluble fraction were separated in a sucrose gradient ultracentrifugation experiment as described in the "materials and methods" section. Biochemical analyses of the obtained fractions was performed in "self-sandwich" MSD assays with hTau43 (N-terminal), PT51 (mid-term), PT3 (PRD), PT76 (MTBD), hTau21 and hTau60 (C-terminal) antibodies. Data are representative of at least 2 independent experiments and presented as mean signal divided by background +/- SD (a). Representative images of Native PAGE analysis of sucrose gradient fractions detected with PT76-HRPO show differences in aggregate weight and distribution in the fractions of the sonicated (top) and no-sonicated (bottom) Tg mouse seeds (b). Seeding capacity of dilution curves of sonicated (red) and non-sonicated (blue) Tg mouse seeds were analyzed in cell-based assay with HEK293-FRET cells, suggesting higher aggregation capacity after sonication (c). Seeding capacity of the fractions from the gradients with sonicated (red) and non-sonicated (blue) Tg mouse seeds was assessed in the cell-based assay, suggesting higher aggregation capacity in the sonicated seeds gradient fractions (d). Data are represented as mean percentage of FRET positive cells, who have aggregation, +/- SD, N=4 (c, d).

The gradients of sonicated and non-sonicated extract were analysed by MSD with antibodies binding to various epitopes of the tau protein (i.e. hTau43, PT51, PT3, PT76, hTau21 and hTau60).

The biochemical analysis showed that the sonication is affecting the distribution of the aggregates in the fractions of the gradient in hTau43, PT51, PT3 and hTau60 “self-sandwich” MSD assays but also that the signals detected are stronger in PT3 assay after sonication in a 2.5-fold increase of area under curve. Also in PT76 and even stronger in hTau21 assays, the non-sonicated sucrose gradient did not generate detectable signals but the sonicated P301S Tg mouse extract sucrose gradient was detected by this assay (Fig. 15a). These data suggest that sonication is exposing the epitope of PT3 antibody in the PRD and this effect was even more prominent for the PT76 and hTau21 antibody epitopes in the MTBD and C-terminus, respectively. All the factions of the gradients were then analysed by Native PAGE and detected with PT76-HRPO antibody to confirm that the differences in distribution of the aggregates in the biochemical assay were a consequence of the effect of sonication on the size of the aggregates. As expected, the sonicated Tg mouse aggregates showed a gradually decreasing size of the aggregates present in fractions with the stronger signals between fractions 3 and 13 (Fig. 15b top panel) whereas the non-sonicated Tg mouse sucrose gradient only displayed signals in the high-density fractions of the gradient (Fig. 15b bottom panel). Dilution curves of non-separated fibrils from tau Tg mice were also analysed in biosensor cells with (red) and without sonication (blue) (Fig. 15c) and showed higher overall capacity of aggregation after sonication. Next, the seeding potency of sucrose gradient fractions were also analysed in the biosensor cells and data showed higher percentage of FRET-positive cells in the sonicated Tg mouse aggregates sucrose gradient (red) than in the non-sonicated (blue) with a 3.7-fold increase in the area under the curve (Fig. 15d). These data support the hypothesis that sonication produces smaller aggregates present in the intermediate-density fractions of the sucrose gradient that have higher seeding potency.

Data in Fig. 10, 12 and 13 allowed to hypothesize that tau fibrils derived from different sources, have different conformations which on its turn explains why some epitopes are more exposed by others. To assess how the conformation of the aggregates can be dictated by “conformational templating” (115,152), human PHFs were used to trigger aggregation in *in vivo* models such as P301L Tg mice by stereotactic injection (Vandermeeren et al 2018 (153)). The aggregates generated 2 months after the injection of human AD PHF, were extracted and analysed with PT51 and PT76 self-sandwich MSD assays (Fig. 16, orange curves) and compared to the sarkosyl insoluble fraction of aged P301S Tg mice (red curves) along with a curve with human PHF (blue).

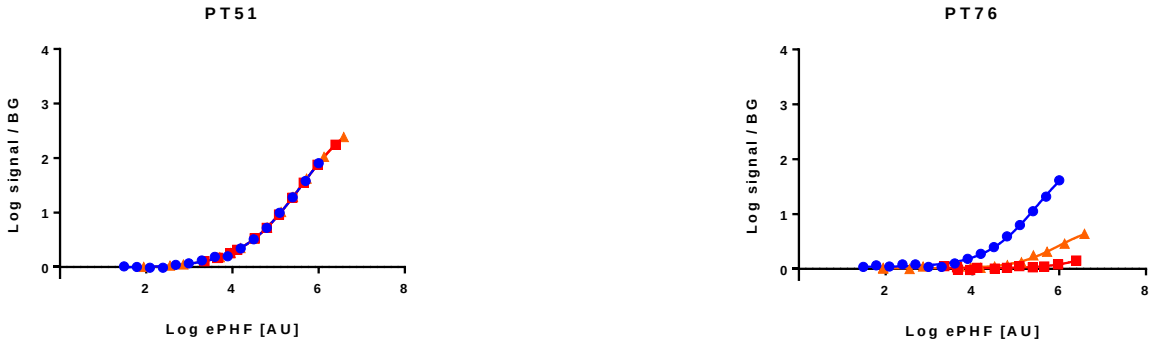

Figure 16 – Effect of human AD-brain seeds injection in P301L Tg mouse seeds binding in PT76 "self-sandwich" MSD assay

Sarkosyl insoluble fractions from P301L Tg mice intracranially injected with human AD-brain seeds or from aged P301S tau Tg mice were diluted as indicated and loaded in PT51 and PT76 "self-sandwich" MSD assays. The concentrations of AD-brain ePHF (blue), P301S Tg mouse seeds (red) and P301L Tg mouse seeds after stereotactic injection of human AD-brain seeds (orange) were normalized to ePHF arbitrary units of concentration and are represented in logarithmic transformation of signal divided by background +/- SD and are representative of at least 2 independent experiments.

As the PT51 self-sandwich assay shows similar detection of human AD and tau Tg mice-derived fibrils (Fig. 11), this assay was used to normalize the signals and confirmed that differential detection of both types of fibrils by the PT76/PT76 assay, are not due to differences in tau aggregate content. The human PHF curve was used to make a relative quantification. In the PT76 "self-sandwich" assay, human AD tau seeds displayed strong binding while corresponding dilutions from the P301S Tg mice fibrils showed very poor binding. Interestingly, the insoluble fraction of the P301L Tg mice injected with human PHF have stronger signals in corresponding dilutions of fibrils derived from aged P301S tau Tg mice (Fig. 16). Comparing with the results from Figure 10.b in which was observed that P301S and P301L fibrils are similarly detected in PT76 MSD assay, it suggests that the fibrils generated in the P301L mice after seeding with human AD PHFs indeed display the biochemical properties of these human tau seeds more than those from the Tg mouse seeds.

The results presented in this thesis suggest that sonication affects biochemical, biophysical and functional properties of tau aggregates from different sources such as *in vitro* aggregated K18, human AD-brain and P301S tau Tg mouse by breaking large aggregates into smaller size fibrils and exposing epitopes that were protected in the aggregates before sonication. It was also observed that human AD-brain PHF and Tg mouse fibrils have differences in structure that influence their detection in biochemical immunoassays. These differences could be overcome by

using human PHF as conformational template in injection models. The importance of these finding will be further discussed in the next section.

4. Discussion

To date, prevention of tau seeding by active- and passive immunotherapy approaches, is one of the most advanced therapeutic approaches for AD and other tauopathies (154). To align with the clinical working hypothesis, pre-clinical evaluation of tau antibodies involves cellular and rodent models of tau seeding. In many of these *in vivo* and *in vitro* studies, sonication is applied to tau aggregates but the effects of this procedure in the biochemical, biophysical and functional characteristics of the fibrils are yet poorly understood. Moreover, there is limited insight in the similarities and differences between the aggregates from different research models and human AD but also between aggregates from different human tauopathies. As a consequence, answering these questions will impact the translational value of preclinical models and will shed light on the applicability of therapeutic antibodies to different tauopathies. Therefore, this project aimed to compare biochemical, functional and structural characteristics of tau aggregates from *in vitro* aggregated K18, *post-mortem* human AD-brain PHF and P301S and P301L tau Tg mice and the effect of sonication in those properties.

By using aggregate-selective PT76/PT76 MSD assays, it was shown that detection of *in vitro* aggregated K18 fragment with the pro-aggregating P301L mutation (155,156) was not affected by sonication (Fig. 8). On the other hand, seeding experiments in FRET-biosensor cells, clearly demonstrated an increased seeding potency of K18 fibrils after sonication. This effect of sonication on the functional capacity of the aggregates suggested that the sonication is facilitating the uptake of those aggregates into the cells and consequent recruitment of the endogenous CFP/YFP tagged K18. It is plausible to assume that the sonication-driven increased uptake of K18 (P301L) fibrils in cells is a consequence of conversion of large aggregates into smaller fibrils. This was investigated further by separating sonicated and non-sonicated K18 (P301L) fibrils by a sucrose gradient ultracentrifugation experiment (Fig. 9) which suggested a profound change in size distribution after sonication of the fibrils. Most striking was the observed shift from the pellet fraction, present in non-sonicated fibrils, into smaller fibrils that are distributed throughout the intermediate density fractions of the gradient. Data is supporting the hypothesis that sonication fragmentizes larger recombinant or human AD tau aggregates into smaller size fibrils with increased seeding potency (157). The same effect was already proposed for α-synuclein fibrils, where in cellular seeding experiments, recombinant protein fibrils were extracted, sonicated and analysed by atomic force microscopy and direct stochastic optical reconstruction microscopy (dSTORM). In these experiments, it was observed that the sonicated fibrils are smaller (158). It was also shown that in

α-synuclein, shorter fibrils (but not oligomers) are the species with stronger aggregation capacity (159).

The observed lack in seeding potential of monomeric K18 (P301L) in the biosensor cells, confirmed that the aggregated conformation of K18 is important for the seeding potency of the aggregates. Small oligomeric species with potent seeding activity, as suggested by other 2 groups (137,148), were not observed which was in accordance with work from Jackson and colleagues (160) who also demonstrated that short fibrils are the seeding-competent tau species that are present in brain homogenates from P301S tau Tg mice.

To translate our findings made with K18 fibrils to *in vivo*-produced tau aggregates from human AD-brains and Tg mouse research models, a number of different "self-sandwich" MSD assays were used for biochemical characterization. For self-sandwich MSD assays using N- and C-terminal antibodies, detection was similar for human AD-brain seeds and Tg mouse seeds. On the other hand, assays using PT76 and PT83 antibodies which epitopes are close or within the MTBD, displayed differences in detection of aggregates from the two sources. In fact, P301S and P301L Tg mouse aggregates are both poorly detected in these assays compared to human PHFs (Fig. 10). Furthermore, PRD antibodies such as PT3, PT25 and AT8 (161) (Fig. S4) showed a weaker detection of fibrils from tau Tg mouse. On the other hand, assays using hTau21 antibody (Fig. 13), binding to a C-terminal epitope, close to the MTBD, showed stronger detection of aggregates from tau Tg mice when compared to human AD fibrils aggregates. These results suggest that human and Tg mouse aggregates have structural differences that do not allow the antibodies to bind equally to both types of aggregates.

Further, in depth, analysis of the aggregates by the use of limited proteolysis, showed that some epitopes are differentially exposed in tau fibrils from human AD and tau Tg mouse brain. Pronase treatment of tau aggregates digests all accessible protein fragments in the aggregate. Consequently, the epitopes of antibodies binding to exposed regions, and the proteolytic resistant cores can be discriminated by Western blotting using tau antibodies with epitopes from N- to C-terminus. In figure 12 it is possible to observe that the PRD and especially MTBD are protected regions that become exposed after the enzymatic digestion. The same experiment in the supplementary figure 5 using 25 different antibodies binding to several regions in the Tau protein, showed that PRD is indeed more protected in Tg mouse aggregates than in human PHF.

Furthermore, it was shown that the MTBD is protected in both types of seeds although the PT76 epitope (N-terminal from MTBD) appeared more protected in Tg mouse seeds while hTau21 epitope (C-terminal from MTBD) is more protected in human PHF. These data support the "self-sandwich" MSD assays results since highly exposed epitopes such as N- and C-termini can be easily detected while the protected PRD and MTBD have lower detection in the biochemical assay. On the other hand, it also supports lower detection of human PHFs by hTau21 since its epitope is more protected in this type of seeds. This means that the structure of the aggregates from the two sources is different, affecting the exposure of protein regions and consequently the binding of antibodies. These findings agree with what is described in the literature. Fitzpatrick and colleagues (140) showed by mass spectrometry that the core of the tau aggregates comprises the MTBD and 10 amino-acids more in the C-terminal direction. This stretch includes the epitopes of PT76, PT83 and hTau21. By electron microscopy it was observed that the anti-4R antibody having its epitope in the same region of PT76, could detect PHF before the pronase treatment but after the digestion the epitope of this antibody was almost completely absent, supporting that in PHF, this epitope is at least more exposed compared to Tg mouse seeds. Together, the mass spectrometry and electron microscopy results support a subtle protection of PT76 epitope in PHF as observed in the experiments in this thesis. In the same publication, Fitzpatrick showed by mass spectrometry that the MN423 antibody epitope (which is close to the hTau21 epitope) is strongly protected in the core of human PHFs. Immuno-electron microscopy detection showed that the MN423 antibody could not bind in untreated PHFs due to the protection of this epitope that becomes exposed after proteolysis with pronase. MN423 and hTau21 antibody epitopes are in close proximity supporting the observations in this thesis that in human PHFs, the hTau21 epitope is strongly protected. Also limited proteolysis experiments using trypsin (141) showed that the hTau21 epitope is part of the trypsin resistant core in human AD PHFs.

These results allow to hypothesise about the differences in epitope protection and as schematized in Fig. 17, from the results in Fig. S5, in P301S tau Tg mouse seeds the Mid-term and PRD are partially shielded while the MTBD is strongly protected. Also, in human AD-brain PHF, the MTBD belongs to the core of the aggregates and also the early region of the C-terminus.

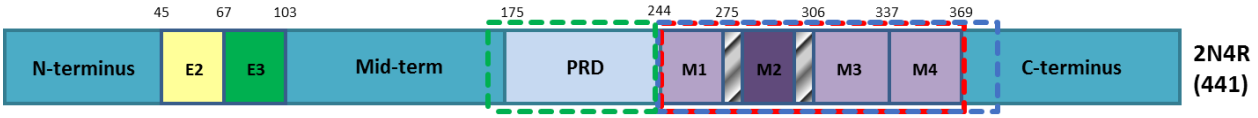

Figure 17 – Epitope protection is different in P301S tau Tg mouse seeds and human AD-brain PHF

From the results obtained with the limited proteolysis experiment, it is observed that in Tg tau mouse seeds the end of the Mid-domain and the PRD are partially shielded (green box) while the core of the aggregate comprises the entire MTBD (red box). In human AD-brain seeds, the core of the aggregate includes the MTBD and the early C-terminus (blue box).

In addition to the differences in epitope exposure between tau fibrils from tau Tg mice and from human AD brain, it was also investigated how this exposure was also altered by sonication, (Fig. 14, 15). Aggregates from sonicated and non-sonicated extracts were separated by sucrose gradient ultracentrifugation where it was observed that the sonication fragmentizes the large aggregates in smaller fibrils with altered size distribution. Native PAGE analysis confirmed that the fibrils produced after sonication are indeed gradually smaller, correlating with the fraction-density within the gradient. Biochemical analysis in "self-sandwich" MSD assays confirmed a shift in the distribution of the aggregates in the sucrose gradient fractions. Antibodies binding to the highly exposed N- and C-termini detected similar signals in the sonicated and non-sonicated gradients. Interestingly, antibodies binding to PRD and MTBD, showed differences in epitope exposure after sonication of human AD-brain PHFs and more pronounced fibrils from in tau Tg mice. Also the early C-terminal antibody hTau21 displayed an increase of signals detected in the self-sandwich assay. This is suggesting that because of the conformation of these aggregates, these antibodies could not bind to their epitopes which are only exposed after sonication. A similar outcome was expected in the assay using hTau21 on human PHF sucrose gradient fractions, but the sensitivity of this assay did not allow to detect the aggregates even after sonication. Increasing the total extract loaded in the sucrose gradient could possibly allow to have a stronger detection of the aggregates present in the fractions. The same limitation was observed for the functional analysis of sucrose gradient fractions from human PHFs where it was not possible to determine the seeding capacity of the species present in the fractions. To overcome this, dilution curves of non-separated sonicated and non-sonicated extracts were analysed and in these samples from both human and Tg mouse tau aggregates, the seeding capacity was enhanced after sonication. Further observations in sucrose gradient fractions from sonicated and non-sonicated fibrils from tau Tg mice showed a 3.7-fold increase of seeding capacity by the sonication procedure. The increased exposure of the epitopes of PT3, PT76 and hTau21 after sonication suggests that also other epitopes might become more

exposed after sonication which could point to additional hypothesis to explain the increased seeding capacity upon sonication. Epitopes of PT76 and hTau21 are close to the MTBD in which the hexapeptide sequences ^{275}VQIINK^{280} and in particular the ^{306}VQIVYK^{311} stretch (162) have been described to have strong propensity for β-Sheet formation and assembly into aggregates (163) and therefore also being considered as a target for the development of tau aggregation inhibitors (164). The increased PT76- and hTau21 epitope exposure after sonication could also increase the exposure of the above described pro-aggregation motifs which can be an additional explanation for the increased seeding potency of sonicated fibrils. A study with sucrose gradient separation of P301S Tg mouse seeds (160) also demonstrated that small fibrils, but not monomeric or small oligomeric tau species, are the most seeding competent species *in vitro* and *in vivo*. In that study, seeding competent species were present in the 40% sucrose gradient, while the fibrils present in the 50% sucrose fraction where no longer seeding competent. This suggests a limit size of the aggregates that allows to be taken up by the cells. Also, Wu and colleagues (85) demonstrated that in cells recombinant tau firstly misfolds into low MW aggregates that further assembly into fibrils. While the low MW aggregates can be taken up by neuronal cells, the long fibrils extracted from human brains were not taken up by the cells. The authors hypothesized that internalization of tau aggregates in cultured neurons is dependent on the conformation and size of the aggregates which is in accordance with the findings described in this thesis and explain the need for the sonication of tau seeds in *in vitro* and *in vivo* studies that are in use to investigate pre-clinical evaluation of tau antibodies.

In that respect, PT76 showed concentration-dependent reduction in K18 (P301L) fibril-induced seeding in HEK293-FRET biosensor cells and demonstrated that it reduces the aggregation capacity (Fig. S6). However, the mechanism of action is yet to be understood both in cells and in Tg tau mouse models. Even so, it was already observed to be also effective with in-house produced antibodies that are in phase 1 clinical trials and also in other studies described in the literature with P301L tau Tg mouse (165), for example IPN002 antibody (144) and HJ8.5 (145). However, the differences in epitope exposure of Tg tau mouse and human AD-brain seeds observed in this thesis can impact the translatability of the results from the pre-clinical models to the clinical trials.

To overcome this challenging issue, injection models using human tauopathy-derived fibrils are used for antibody evaluation *in vivo*. As demonstrated by Clavaguera and colleagues (115), aggregates form *post-mortem* human tauopathy brains recapitulated the tau aggregation upon

intracranial injection in Alz17 mice, suggesting a conformational templating in these research models. To confirm this for the injection models used at Janssen, young P301L tau Tg mice were injected with sonicated human AD-brain PHFs as described in a study from Vandermeeren and colleagues (153). The aggregates generated 2 months after seeding where extracted and characterized by MSD self-sandwich assays showing more signals in the PT76 "self-sandwich" MSD assay which showed almost no signal in samples containing fibrils from aged P301S tau Tg mouse, suggesting that by using human PHF as templates for aggregation, the generated fibrils resemble more the structure of the human AD-brain PHFs. Further structural studies on these aggregates are needed to confirm this hypothesis. Since the P301S tau Tg mouse model only expresses 0N4R human tau protein (166) and P301L tau Tg mouse model only expresses 2N4R human tau protein (103), both with mutations linked to frontotemporal dementia and parkinsonism linked to chromosome 17 (FTDP-17) (167,168), it could be relevant to compare structural properties of fibrils derived from different human tauopathies which are, in a number of cases, composed by 6 isoforms of tau (thus 0N3R, 1N3R, 2N3R, 0N4R, 1N4R, and 2N4R).

This could be further assessed by limited proteolysis of aggregates generated by conformational templating in injection models to verify the exposure of PT76 and hTau21 epitopes in the aggregates. Furthermore, comparing the detection of these aggregates in MSD assays with antibodies binding to other protein regions could help to better understand how the conformational templates are generating AD-brain-like PHF structures.

To summarize, the results presented in this thesis revealed that sonication of tau aggregates is producing smaller size aggregates with stronger seeding capacity but also facilitates exposure of MTBD epitopes that are protected in non-sonicated aggregates. This epitope exposure was also proven to be different in aggregates from *post-mortem* human AD-brains and Tg tau mouse models, which is of high importance for the identification of optimal candidate antibodies for immunotherapy which are not necessarily the same for different tauopathies.

Further studies comparing epitope exposure in aggregates from these tauopathies are needed to shed more light on this, possibly leading to a deeper understanding on tau aggregation process. This knowledge could be invaluable for the development of newer and more personalized medicines.

5. Supplementary data

Figure S1: Sandwich ELISA analysis of K18(P301L) preps.

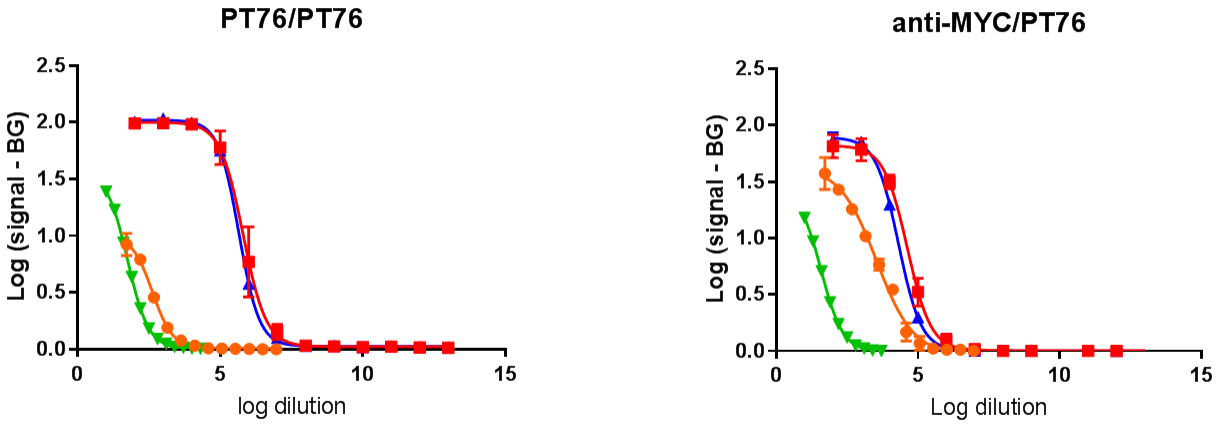

Dilution curves of monomeric (orange), *in vitro* aggregated (red), aggregated and sonicated (blue) K18(P301L) and the supernatant of the centrifugation after the *in vitro* aggregation protocol (green) were loaded in ELISA plates pre-coated with either anti-MYC antibody for a total K18 assay or PT76 for an aggregate selective assay at the concentration of 1 µg/ mL. Detection was performed with PT76-HRPO labelled antibody in both cases. Data is represented as logarithmic transformation of the signal subtracted by the background of the plate, dependent on the dilution of the analytes. Background is the signal correspondent of the wells incubated with blocking buffer instead of sample. Data suggest that PT76/PT76 is an aggregate selective assay with strong similar signals with sonicated and non-sonicated in vitro aggregated K18 whereas monomeric signal is not substantial. Signal in the supernatant of the aggregation protocol is also low suggesting high aggregation and sedimentation efficiency after the centrifugation. On the other hand, anti-MYC/PT76 assay confirms the presence of K18 MYC-tagged in all the analytes and that there is low remaining protein in the supernatant of the aggregation protocol centrifugation.

Figure S2: Evaluation of enzyme concentration for limited proteolysis of human AD-brain PHF.

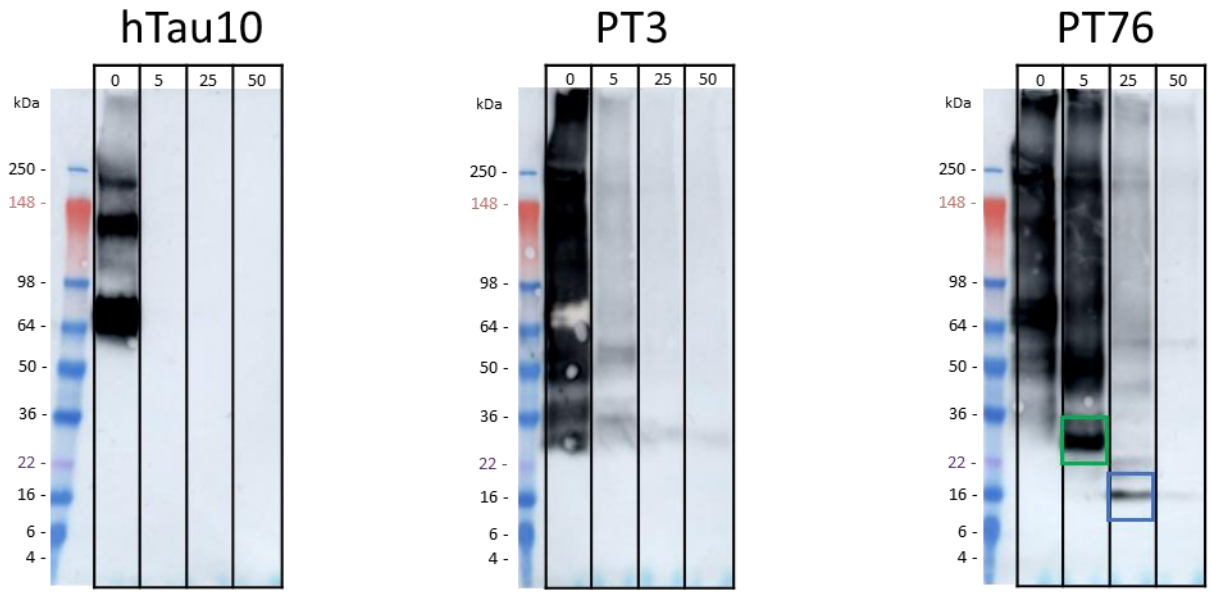

To optimize enzyme concentration for the limited proteolysis assay, human AD-brain PHF was incubated either without or with 5, 25 or 50 µg/mL of pronase (143) and analyzed by Western blot under non-reducing conditions and detected with antibodies for different regions of the Tau protein hTau10 (N-terminal), PT3 (PRD) and PT76 (MTBD). Detection with PT76 showed that 5 µg/mL of enzyme produced an intermediate state with undigested material and a band with the molecular weight between 22 and 36 kDa (green box). Treatment of sample with 25 µg/mL of enzyme generated a band with MW of 16 kDa corresponding to the aggregate core region (blue box). The highest concentration of enzyme (50 µg/mL) seems to be enough to entirely digest the aggregates and only very low signals can be detected.

Figure S3: Limited proteolysis of human AD-brain and P301S Tg mouse seeds

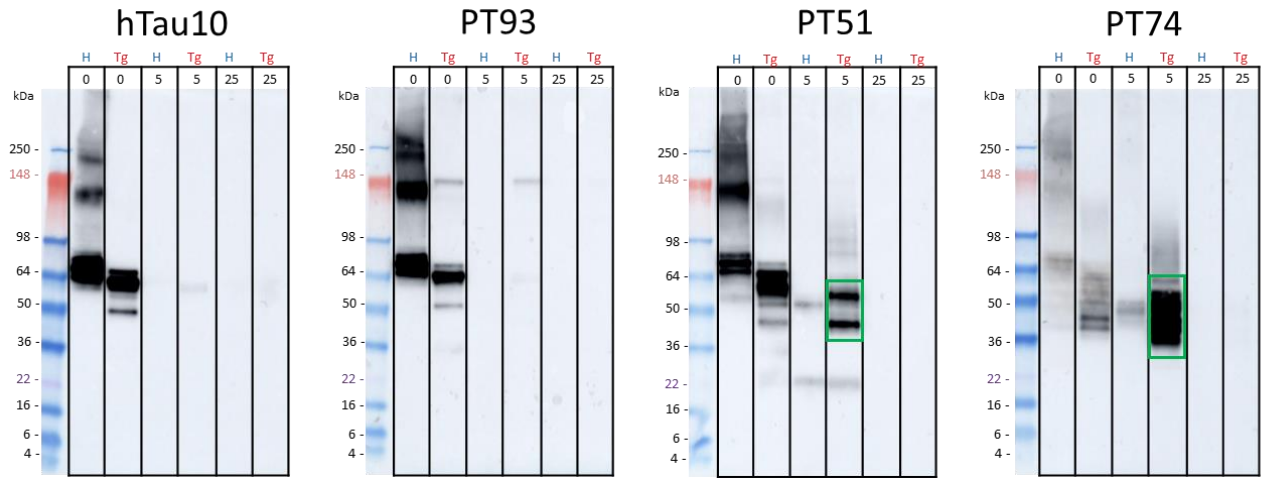

Human AD-brain PHF (H) and P301S Tg mouse sarkosyl insoluble fibrils (Tg) were incubated either without or with 5 or 25 µg/mL of pronase and analyzed by Western blot under non-reducing conditions and detected with antibodies for different regions of the Tau protein. hTau10 and PT93 (N-terminal), PT51 (mid-term), PT74 (PRD, phosphorylation dependent).

It is observed that the N-terminal antibody epitopes were digested with the lower enzyme concentration, suggestion that the epitopes are easily accessible in the fuzzy coat of the aggregates. Mid-term and PRD antibody epitopes were also easily accessible in human PHF. Conversely, in Tg mouse aggregates, epitopes of PT51 and PT74 displayed an increased signal after digestion with 5 µg/mL of Pronase (green boxes), suggesting that those regions are somewhat shielded and become more exposed after the digestion with the lower concentration of enzyme in Tg mouse aggregates. Nevertheless, none of those epitopes are present in the core of the aggregates since they cannot be detected after digestion with the higher concentration of enzyme.

Figure S4: Comparison of detection in MSD aggregate selective assays of human AD-brain PHF and P301S Tg mouse seeds.

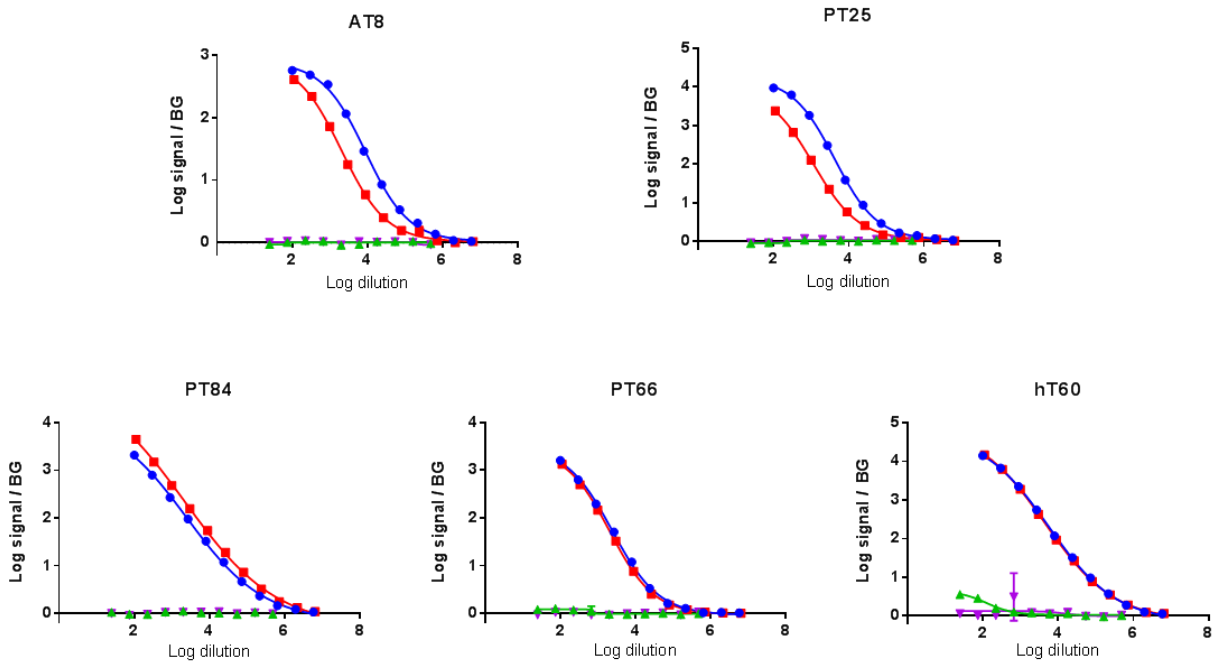

Dilution curves of human AD-brain PHF (blue), P301S Tg mouse seeds (red), wild-type (green) and tau knock-out (purple) mouse total brain homogenate were analyzed by MSD aggregate selective assay with AT8 and PT25 binding to the PRD, PT84, PT66 and hTau60 binding to the C-terminus, where the capture and detection antibody competition for the same epitope allows to only detect aggregates. Dilution curves were adjusted to the same total tau loading to ensure that differences observed are not associated with different total tau content in the samples. Results show stronger detection of human PHF with antibodies for the PRD (AT8 and PT25), slightly stronger detection with PT84 antibody and similar detection with PT66 and hTau60 C-terminal antibodies. Data are show as logarithmic transformation of signal divided by background +/- SD and N=2.

Figure S5: Limited proteolysis of human AD-brain PHF and P301S Tg mouse seeds, analysed by Western blot and detected with tau antibodies from N- to C- termini.

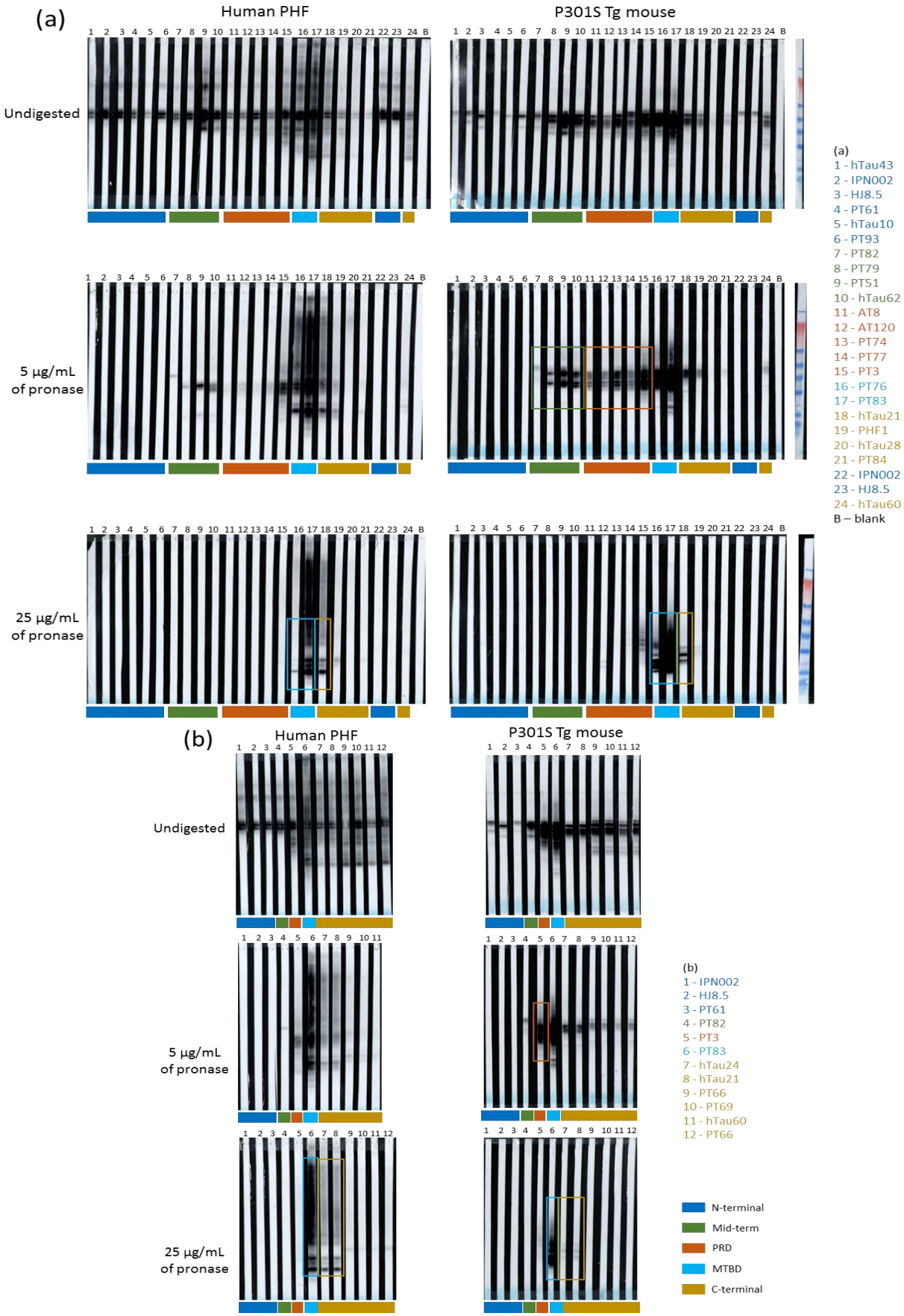

Human AD-brain PHF and P301S Tg mouse seeds were incubated either without pronase or with 5 and 25 µg/mL and the proteolytic resistant fragments were analysed by Western blot and detected with antibodies from N- to C- terminal. It was observed that the mid-term and PRD (orange and golden boxes, respectively) is more protected in the Tg mouse seeds that in human PHF since it can be strongly detected after the incubation with the lower concentration of pronase but not part of the core of the aggregate since they were not detectable with the higher concentration of pronase. On the other hand, MTBD (light blue boxes) seems to be part of the core of both types of aggregates but much strongly protected in Tg mouse aggregates. Interestingly, hTau21 and hTau24 antibodies who share the same epitope (C-terminal close to the MTBD, golden boxes) seems to be protected in both types of aggregates but strongly in human PHF.

Figure S6: PT76 antibody effect in aggregation potency of K18(P301L) sonicated aggregates in HEK293-FRET biosensor cells.

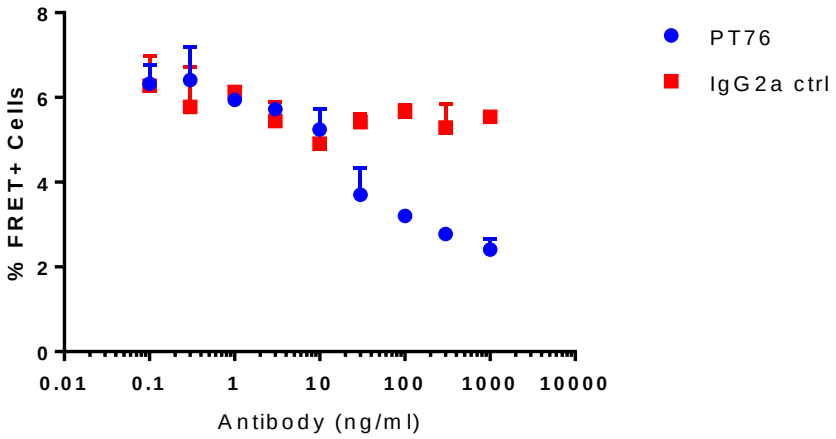

HEK293-FRET biosensor cells were co-incubated with aggregated and sonicated K18(P301L) and either with PT76 or IgG2a (ctrl) antibodies. Dilution curves of the antibodies were taken along with a constant amount of 25 ng of K18/well, starting at a 1:1 Mole ratio at the highest concentration of antibody. Data suggest a 2-fold reduction in the aggregation capacity of K18 aggregates at the highest concentration of PT76 when compared to the control antibody IgG2a. Data is represented as % of FRET-positive cells (with aggregation) +- SD.

6. References

1. Dening, T., and Sandilyan, M. B. (2015) Dementia: definitions and types. *Nursing standard (Royal College of Nursing (Great Britain) : 1987)* **29**, 37-42
2. Stevens, T. I. M., Livingston, G., Kitchen, G., Manela, M., Walker, Z., and Katona, C. (2002) Islington study of dementia subtypes in the community. *The British Journal of Psychiatry* **180**, 270
3. Association, A. s. (2016) *2016 Alzheimer's disease Facts and Figures*,
4. BOARD, E. (2016) *Dementia: report by the Secretariat*, 139th ed., World Health Organization, Geneva
5. Luengo-Fernandez, R., Leal, J., and Gray, A. (2015) UK research spend in 2008 and 2012: comparing stroke, cancer, coronary heart disease and dementia. *BMJ Open* **5**
6. Möller, H.-J., and Graeber, M. B. (1998) The case described by Alois Alzheimer in 1911. *European Archives of Psychiatry and Clinical Neuroscience* **248**, 111-122
7. Alzheimer, A. (1911) Über eigenartige Krankheitsfälle des späteren Alters. *Zeitschrift für die gesamte Neurologie und Psychiatrie* **4**, 356-385
8. Tagarelli, A., Piro, A., Tagarelli, G., Lagonia, P., and Quattrone, A. (2006) Alois Alzheimer: a hundred years after the discovery of the eponymous disorder. *International journal of biomedical science : IJBS* **2**, 196-204
9. Blennow, K., de Leon, M. J., and Zetterberg, H. (2006) Alzheimer's disease. *The Lancet* **368**, 387-403
10. Mayeux, R. (2003) Epidemiology of neurodegeneration. *Annual review of neuroscience* **26**, 81-104
11. Matias-Guiu, J. A., Valles-Salgado, M., Rognoni, T., Hamre-Gil, F., Moreno-Ramos, T., and Matias-Guiu, J. (2017) Comparative Diagnostic Accuracy of the ACE-III, MIS, MMSE, MoCA, and RUDAS for Screening of Alzheimer Disease. *Dementia and geriatric cognitive disorders* **43**, 237-246
12. (!!! INVALID CITATION !!! (12,13)).
13. Braak, H., and Braak, E. (1991) Neuropathological stageing of Alzheimer-related changes. *Acta neuropathologica* **82**, 239-259
14. Braak, H., and Del Tredici, K. (2011) The pathological process underlying Alzheimer's disease in individuals under thirty. *Acta neuropathologica* **121**, 171-181
15. Villemagne, V. L., Fodero-Tavoletti, M. T., Masters, C. L., and Rowe, C. C. (2015) Tau imaging: early progress and future directions. *The Lancet Neurology* **14**, 114-124
16. Duara, R., Lopez-Alberola, R. F., Barker, W. W., Loewenstein, D. A., Zatinsky, M., Eisdorfer, C. E., and Weinberg, G. B. (1993) A comparison of familial and sporadic Alzheimer's disease. *Neurology* **43**, 1377-1384
17. Swearer, J. M., O'Donnell, B. F., Drachman, D. A., and Woodward, B. M. (1992) Neuropsychological features of familial Alzheimer's disease. *Annals of neurology* **32**, 687-694
18. Lista, S., O'Bryant, S. E., Blennow, K., Dubois, B., Hugon, J., Zetterberg, H., and Hampel, H. (2015) Biomarkers in Sporadic and Familial Alzheimer's Disease. *Journal of Alzheimer's disease : JAD* **47**, 291-317
19. Gessel, M. M., Bernstein, S., Kemper, M., Teplow, D. B., and Bowers, M. T. (2012) Familial Alzheimer's disease mutations differentially alter amyloid beta-protein oligomerization. *ACS chemical neuroscience* **3**, 909-918
20. Kimberly, W. T., LaVoie, M. J., Ostaszewski, B. L., Ye, W., Wolfe, M. S., and Selkoe, D. J. (2003) Gamma-secretase is a membrane protein complex comprised of presenilin, nicastrin, Aph-1, and Pen-2. *Proceedings of the National Academy of Sciences of the United States of America* **100**, 6382-6387
21. Cai, Y., An, S. S., and Kim, S. (2015) Mutations in presenilin 2 and its implications in Alzheimer's disease and other dementia-associated disorders. *Clin Interv Aging* **10**, 1163-1172
22. Chow, V. W., Mattson, M. P., Wong, P. C., and Gleichmann, M. (2010) An Overview of APP Processing Enzymes and Products. *Neuromolecular medicine* **12**, 1-12
23. Cole, S. L., and Vassar, R. (2007) The Alzheimer's disease β-secretase enzyme, BACE1. *Molecular Neurodegeneration* **2**, 22
24. Murphy, M. P., and LeVine, H. (2010) Alzheimer's Disease and the β-Amyloid Peptide. *Journal of Alzheimer's disease : JAD* **19**, 311

25. Tang, Y.-P., and Gershon, E. S. (2003) Genetic studies in Alzheimer's disease. *Dialogues in Clinical Neuroscience* **5**, 17-26
26. Lanoiselée, H.-M., Nicolas, G., Wallon, D., Rovelet-Lecrux, A., Lacour, M., Rousseau, S., Richard, A.-C., Pasquier, F., Rollin-Sillaire, A., Martinaud, O., Quillard-Muraine, M., de la Sayette, V., Boutoleau-Bretonniere, C., Etcharry-Bouyx, F., Chauviré, V., Sarazin, M., le Ber, I., Epelbaum, S., Jonveaux, T., Rouaud, O., Ceccaldi, M., Félician, O., Godefroy, O., Formaglio, M., Croisile, B., Auriacombe, S., Chamard, L., Vincent, J.-L., Sauvée, M., Marelli-Tosi, C., Gabelle, A., Ozsancak, C., Pariente, J., Paquet, C., Hannequin, D., Campion, D., and collaborators of the, C. N. R. M. A. J. p. (2017) APP, PSEN1, and PSEN2 mutations in early-onset Alzheimer disease: A genetic screening study of familial and sporadic cases. *PLoS Medicine* **14**, e1002270
27. Kumar-Singh, S., Theuns, J., Van Broeck, B., Pirici, D., Vennekens, K., Corsmit, E., Cruts, M., Dermaut, B., Wang, R., and Van Broeckhoven, C. (2006) Mean age-of-onset of familial alzheimer disease caused by presenilin mutations correlates with both increased Abeta42 and decreased Abeta40. *Human mutation* **27**, 686-695
28. Selkoe, D. J., and Hardy, J. (2016) The amyloid hypothesis of Alzheimer's disease at 25 years. *EMBO Molecular Medicine* **8**, 595-608
29. Bitan, G., Kirkitadze, M. D., Lomakin, A., Vollers, S. S., Benedek, G. B., and Teplow, D. B. (2003) Amyloid beta -protein (Abeta) assembly: Abeta 40 and Abeta 42 oligomerize through distinct pathways. *Proceedings of the National Academy of Sciences of the United States of America* **100**, 330-335
30. Li, S., Hong, S., Shepardson, N. E., Walsh, D. M., Shankar, G. M., and Selkoe, D. (2009) Soluble oligomers of amyloid Beta protein facilitate hippocampal long-term depression by disrupting neuronal glutamate uptake. *Neuron* **62**, 788-801
31. Naj, A. C., Jun, G., Beecham, G. W., Wang, L. S., Vardarajan, B. N., Buros, J., Gallins, P. J., Buxbaum, J. D., Jarvik, G. P., Crane, P. K., Larson, E. B., Bird, T. D., Boeve, B. F., Graff-Radford, N. R., De Jager, P. L., Evans, D., Schneider, J. A., Carrasquillo, M. M., Ertekin-Taner, N., Younkin, S. G., Cruchaga, C., Kauwe, J. S., Nowotny, P., Kramer, P., Hardy, J., Huentelman, M. J., Myers, A. J., Barmada, M. M., Demirci, F. Y., Baldwin, C. T., Green, R. C., Rogaeva, E., St George-Hyslop, P., Arnold, S. E., Barber, R., Beach, T., Bigio, E. H., Bowen, J. D., Boxer, A., Burke, J. R., Cairns, N. J., Carlson, C. S., Carney, R. M., Carroll, S. L., Chui, H. C., Clark, D. G., Corneveaux, J., Cotman, C. W., Cummings, J. L., DeCarli, C., DeKosky, S. T., Diaz-Arrastia, R., Dick, M., Dickson, D. W., Ellis, W. G., Faber, K. M., Fallon, K. B., Farlow, M. R., Ferris, S., Frosch, M. P., Galasko, D. R., Ganguli, M., Gearing, M., Geschwind, D. H., Ghetti, B., Gilbert, J. R., Gilman, S., Giordani, B., Glass, J. D., Growdon, J. H., Hamilton, R. L., Harrell, L. E., Head, E., Honig, L. S., Hulette, C. M., Hyman, B. T., Jicha, G. A., Jin, L. W., Johnson, N., Karlawish, J., Karydas, A., Kaye, J. A., Kim, R., Koo, E. H., Kowall, N. W., Lah, J. J., Levey, A. I., Lieberman, A. P., Lopez, O. L., Mack, W. J., Marson, D. C., Martiniuk, F., Mash, D. C., Masliah, E., McCormick, W. C., McCurry, S. M., McDavid, A. N., McKee, A. C., Mesulam, M., Miller, B. L., Miller, C. A., Miller, J. W., Parisi, J. E., Perl, D. P., Peskind, E., Petersen, R. C., Poon, W. W., Quinn, J. F., Rajbhandary, R. A., Raskind, M., Reisberg, B., Ringman, J. M., Roberson, E. D., Rosenberg, R. N., Sano, M., Schneider, L. S., Seeley, W., Shelanski, M. L., Slifer, M. A., Smith, C. D., Sonnen, J. A., Spina, S., Stern, R. A., Tanzi, R. E., Trojanowski, J. Q., Troncoso, J. C., Van Deerlin, V. M., Vinters, H. V., Vonsattel, J. P., Weintraub, S., Welsh-Bohmer, K. A., Williamson, J., Woltjer, R. L., Cantwell, L. B., Dombroski, B. A., Beekly, D., Lunetta, K. L., Martin, E. R., Kamboh, M. I., Saykin, A. J., Reiman, E. M., Bennett, D. A., Morris, J. C., Montine, T. J., Goate, A. M., Blacker, D., Tsuang, D. W., Hakonarson, H., Kukull, W. A., Foroud, T. M., Haines, J. L., Mayeux, R., Pericak-Vance, M. A., Farrer, L. A., and Schellenberg, G. D. (2011) Common variants at MS4A4/MS4A6E, CD2AP, CD33 and EPHA1 are associated with late-onset Alzheimer's disease. *Nature genetics* **43**, 436-441
32. Hollingworth, P., Harold, D., Sims, R., Gerrish, A., Lambert, J. C., Carrasquillo, M. M., Abraham, R., Hamshere, M. L., Pahwa, J. S., Moskvina, V., Dowzell, K., Jones, N., Stretton, A., Thomas, C., Richards, A., Ivanov, D., Widdowson, C., Chapman, J., Lovestone, S., Powell, J., Proitsi, P., Lupton, M. K., Brayne, C., Rubinsztein, D. C., Gill, M., Lawlor, B., Lynch, A., Brown, K. S., Passmore, P. A., Craig, D., McGuinness, B., Todd, S., Holmes, C., Mann, D., Smith, A. D., Beaumont, H., Warden, D.,

Wilcock, G., Love, S., Kehoe, P. G., Hooper, N. M., Vardy, E. R., Hardy, J., Mead, S., Fox, N. C., Rossor, M., Collinge, J., Maier, W., Jessen, F., Ruther, E., Schurmann, B., Heun, R., Kolsch, H., van den Bussche, H., Heuser, I., Kornhuber, J., Wiltfang, J., Dichgans, M., Frolich, L., Hampel, H., Gallacher, J., Hull, M., Rujescu, D., Giegling, I., Goate, A. M., Kauwe, J. S., Cruchaga, C., Nowotny, P., Morris, J. C., Mayo, K., Sleegers, K., Bettens, K., Engelborghs, S., De Deyn, P. P., Van Broeckhoven, C., Livingston, G., Bass, N. J., Gurling, H., McQuillin, A., Gwilliam, R., Deloukas, P., Al-Chalabi, A., Shaw, C. E., Tsolaki, M., Singleton, A. B., Guerreiro, R., Muhleisen, T. W., Nothen, M. M., Moebus, S., Jockel, K. H., Klopp, N., Wichmann, H. E., Pankratz, V. S., Sando, S. B., Aasly, J. O., Barcikowska, M., Wszolek, Z. K., Dickson, D. W., Graff-Radford, N. R., Petersen, R. C., van Duijn, C. M., Breteler, M. M., Ikram, M. A., DeStefano, A. L., Fitzpatrick, A. L., Lopez, O., Launer, L. J., Seshadri, S., Berr, C., Campion, D., Epelbaum, J., Dartigues, J. F., Tzourio, C., Alperovitch, A., Lathrop, M., Feulner, T. M., Friedrich, P., Riehle, C., Krawczak, M., Schreiber, S., Mayhaus, M., Nicolhaus, S., Wagenpfeil, S., Steinberg, S., Stefansson, H., Stefansson, K., Snaedal, J., Bjornsson, S., Jonsson, P. V., Chouraki, V., Genier-Boley, B., Hiltunen, M., Soininen, H., Combarros, O., Zelenika, D., Delepine, M., Bullido, M. J., Pasquier, F., Mateo, I., Frank-Garcia, A., Porcellini, E., Hanon, O., Coto, E., Alvarez, V., Bosco, P., Siciliano, G., Mancuso, M., Panza, F., Solfrizzi, V., Nacmias, B., Sorbi, S., Bossu, P., Piccardi, P., Arosio, B., Annoni, G., Seripa, D., Pilotto, A., Scarpini, E., Galimberti, D., Brice, A., Hannequin, D., Licastro, F., Jones, L., Holmans, P. A., Jonsson, T., Riemenschneider, M., Morgan, K., Younkin, S. G., Owen, M. J., O'Donovan, M., Amouyel, P., and Williams, J. (2011) Common variants at ABCA7, MS4A6A/MS4A4E, EPHA1, CD33 and CD2AP are associated with Alzheimer's disease. *Nature genetics* **43**, 429-435

33. Bertram, L., and Tanzi, R. E. (2005) The genetic epidemiology of neurodegenerative disease. *Journal of Clinical Investigation* **115**, 1449-1457
34. Bertram, L., McQueen, M. B., Mullin, K., Blacker, D., and Tanzi, R. E. (2007) Systematic meta-analyses of Alzheimer disease genetic association studies: the AlzGene database. *Nature genetics* **39**, 17-23
35. Mahley, R. W., and Rall, S. C., Jr. (2000) Apolipoprotein E: far more than a lipid transport protein. *Annual review of genomics and human genetics* **1**, 507-537
36. Elias-Sonnenschein, L. S., Viechtbauer, W., Ramakers, I. H., Verhey, F. R., and Visser, P. J. (2011) Predictive value of APOE-epsilon4 allele for progression from MCI to AD-type dementia: a meta-analysis. *Journal of neurology, neurosurgery, and psychiatry* **82**, 1149-1156
37. Vassar, R. (2004) BACE1: the beta-secretase enzyme in Alzheimer's disease. *J Mol Neurosci* **23**, 105-114
38. Mullan, M., Crawford, F., Axelman, K., Houlden, H., Lilius, L., Winblad, B., and Lannfelt, L. (1992) A pathogenic mutation for probable Alzheimer's disease in the APP gene at the N-terminus of beta-amyloid. *Nature genetics* **1**, 345-347
39. Jonsson, T., Atwal, J. K., Steinberg, S., Snaedal, J., Jonsson, P. V., Bjornsson, S., Stefansson, H., Sulem, P., Gudbjartsson, D., Maloney, J., Hoyte, K., Gustafson, A., Liu, Y., Lu, Y., Bhangale, T., Graham, R. R., Huttenlocher, J., Bjornsdottir, G., Andreassen, O. A., Jonsson, E. G., Palotie, A., Behrens, T. W., Magnusson, O. T., Kong, A., Thorsteinsdottir, U., Watts, R. J., and Stefansson, K. (2012) A mutation in APP protects against Alzheimer's disease and age-related cognitive decline. *Nature* **488**, 96-99
40. Li, Y. M., Xu, M., Lai, M. T., Huang, Q., Castro, J. L., DiMuzio-Mower, J., Harrison, T., Lellis, C., Nadin, A., Neduvelil, J. G., Register, R. B., Sardana, M. K., Shearman, M. S., Smith, A. L., Shi, X. P., Yin, K. C., Shafer, J. A., and Gardell, S. J. (2000) Photoactivated gamma-secretase inhibitors directed to the active site covalently label presenilin 1. *Nature* **405**, 689-694
41. Scheuner, D., Eckman, C., Jensen, M., Song, X., Citron, M., Suzuki, N., Bird, T. D., Hardy, J., Hutton, M., Kukull, W., Larson, E., Levy-Lahad, E., Viitanen, M., Peskind, E., Poorkaj, P., Schellenberg, G., Tanzi, R., Wasco, W., Lannfelt, L., Selkoe, D., and Younkin, S. (1996) Secreted amyloid beta-protein similar to that in the senile plaques of Alzheimer's disease is increased in vivo by the presenilin 1 and 2 and APP mutations linked to familial Alzheimer's disease. *Nature medicine* **2**, 864-870

42. Citron, M., Westaway, D., Xia, W., Carlson, G., Diehl, T., Levesque, G., Johnson-Wood, K., Lee, M., Seubert, P., Davis, A., Kholodenko, D., Motter, R., Sherrington, R., Perry, B., Yao, H., Strome, R., Lieberburg, I., Rommens, J., Kim, S., Schenk, D., Fraser, P., St George Hyslop, P., and Selkoe, D. J. (1997) Mutant presenilins of Alzheimer's disease increase production of 42-residue amyloid beta-protein in both transfected cells and transgenic mice. *Nature medicine* **3**, 67-72
43. Gravina, S. A., Ho, L., Eckman, C. B., Long, K. E., Otvos, L., Jr., Younkin, L. H., Suzuki, N., and Younkin, S. G. (1995) Amyloid beta protein (A beta) in Alzheimer's disease brain. Biochemical and immunocytochemical analysis with antibodies specific for forms ending at A beta 40 or A beta 42(43). *The Journal of biological chemistry* **270**, 7013-7016
44. Dahlgren, K. N., Manelli, A. M., Stine, W. B., Jr., Baker, L. K., Krafft, G. A., and LaDu, M. J. (2002) Oligomeric and fibrillar species of amyloid-beta peptides differentially affect neuronal viability. *The Journal of biological chemistry* **277**, 32046-32053
45. Klein, W. L., Krafft, G. A., and Finch, C. E. (2001) Targeting small Abeta oligomers: the solution to an Alzheimer's disease conundrum? *Trends in neurosciences* **24**, 219-224
46. Davis, D. G., Schmitt, F. A., Wekstein, D. R., and Markesbery, W. R. (1999) Alzheimer neuropathologic alterations in aged cognitively normal subjects. *Journal of neuropathology and experimental neurology* **58**, 376-388
47. Bateman, R. J., Xiong, C., Benzinger, T. L., Fagan, A. M., Goate, A., Fox, N. C., Marcus, D. S., Cairns, N. J., Xie, X., Blazey, T. M., Holtzman, D. M., Santacruz, A., Buckles, V., Oliver, A., Moulder, K., Aisen, P. S., Ghetti, B., Klunk, W. E., McDade, E., Martins, R. N., Masters, C. L., Mayeux, R., Ringman, J. M., Rossor, M. N., Schofield, P. R., Sperling, R. A., Salloway, S., and Morris, J. C. (2012) Clinical and biomarker changes in dominantly inherited Alzheimer's disease. *The New England journal of medicine* **367**, 795-804
48. Ahn, H. J., Chen, Z. L., Zamolodchikov, D., Norris, E. H., and Strickland, S. (2017) Interactions of beta-amyloid peptide with fibrinogen and coagulation factor XII may contribute to Alzheimer's disease. *Current opinion in hematology*
49. Prusiner, S. B. (2013) Biology and genetics of prions causing neurodegeneration. *Annual review of genetics* **47**, 601-623
50. Beekes, M., Thomzig, A., Schulz-Schaeffer, W. J., and Burger, R. (2014) Is there a risk of prion-like disease transmission by Alzheimer- or Parkinson-associated protein particles? *Acta neuropathologica* **128**, 463-476
51. Watts, J. C., Condello, C., Stohr, J., Oehler, A., Lee, J., DeArmond, S. J., Lannfelt, L., Ingelsson, M., Giles, K., and Prusiner, S. B. (2014) Serial propagation of distinct strains of Abeta prions from Alzheimer's disease patients. *Proceedings of the National Academy of Sciences of the United States of America* **111**, 10323-10328
52. Kovacs, G. G., Lutz, M. I., Ricken, G., Strobel, T., Hoftberger, R., Preusser, M., Regelsberger, G., Honigschnabl, S., Reiner, A., Fischer, P., Budka, H., and Hainfellner, J. A. (2016) Dura mater is a potential source of Abeta seeds. *Acta neuropathologica* **131**, 911-923
53. Ritchie, D. L., Adlard, P., Peden, A. H., Lowrie, S., Le Grice, M., Burns, K., Jackson, R. J., Yull, H., Keogh, M. J., Wei, W., Chinnery, P. F., Head, M. W., and Ironside, J. W. (2017) Amyloid-beta accumulation in the CNS in human growth hormone recipients in the UK. *Acta neuropathologica*
54. Binder, L. I., Frankfurter, A., and Rebhun, L. I. (1985) The distribution of tau in the mammalian central nervous system. *The Journal of cell biology* **101**, 1371-1378
55. Neve, R. L., Harris, P., Kosik, K. S., Kurnit, D. M., and Donlon, T. A. (1986) Identification of cDNA clones for the human microtubule-associated protein tau and chromosomal localization of the genes for tau and microtubule-associated protein 2. *Molecular Brain Research* **1**, 271-280
56. Gu, Y., Oyama, F., and Ihara, Y. (1996) Tau is widely expressed in rat tissues. *J Neurochem* **67**, 1235-1244
57. Huang, D. Y., Weisgraber, K. H., Goedert, M., Saunders, A. M., Roses, A. D., and Strittmatter, W. J. (1995) ApoE3 binding to tau tandem repeat I is abolished by tau serine262 phosphorylation. *Neurosci Lett* **192**, 209-212

58. Reynolds, C. H., Garwood, C. J., Wray, S., Price, C., Kellie, S., Perera, T., Zvelebil, M., Yang, A., Sheppard, P. W., Varndell, I. M., Hanger, D. P., and Anderton, B. H. (2008) Phosphorylation regulates tau interactions with Src homology 3 domains of phosphatidylinositol 3-kinase, phospholipase Cgamma1, Grb2, and Src family kinases. *The Journal of biological chemistry* **283**, 18177-18186
59. Fischer, D., Mukrasch, M. D., Biernat, J., Bibow, S., Blackledge, M., Griesinger, C., Mandelkow, E., and Zweckstetter, M. (2009) Conformational changes specific for pseudophosphorylation at serine 262 selectively impair binding of tau to microtubules. *Biochemistry* **48**, 10047-10055
60. Mandelkow, E. M., Schweers, O., Drewes, G., Biernat, J., Gustke, N., Trinczek, B., and Mandelkow, E. (1996) Structure, microtubule interactions, and phosphorylation of tau protein. *Annals of the New York Academy of Sciences* **777**, 96-106
61. Boluda, S., Iba, M., Zhang, B., Raible, K. M., Lee, V. M., and Trojanowski, J. Q. (2015) Differential induction and spread of tau pathology in young PS19 tau transgenic mice following intracerebral injections of pathological tau from Alzheimer's disease or corticobasal degeneration brains. *Acta neuropathologica* **129**, 221-237
62. Arendt, T., Stieler, J. T., and Holzer, M. (2016) Tau and tauopathies. *Brain Research Bulletin* **126, Part 3**, 238-292
63. Ayers, J. I., Giasson, B. I., and Borchelt, D. R. (2017) Prion-like Spreading in Tauopathies. *Biological psychiatry*
64. Goedert, M., and Jakes, R. (1990) Expression of separate isoforms of human tau protein: correlation with the tau pattern in brain and effects on tubulin polymerization. *The EMBO journal* **9**, 4225-4230
65. Takuma, H., Arawaka, S., and Mori, H. (2003) Isoforms changes of tau protein during development in various species. *Brain research. Developmental brain research* **142**, 121-127
66. Kosik, K. S., Orecchio, L. D., Bakalis, S., and Neve, R. L. (1989) Developmentally regulated expression of specific tau sequences. *Neuron* **2**, 1389-1397
67. Wolfe, M. S. (2009) Tau mutations in neurodegenerative diseases. *The Journal of biological chemistry* **284**, 6021-6025
68. Trinczek, B., Biernat, J., Baumann, K., Mandelkow, E. M., and Mandelkow, E. (1995) Domains of tau protein, differential phosphorylation, and dynamic instability of microtubules. *Molecular Biology of the Cell* **6**, 1887-1902
69. St-Cyr Giguere, F., Attiori Essis, S., Chagniel, L., Germain, M., Cyr, M., and Massicotte, G. (2017) The sphingosine-1-phosphate receptor 1 agonist SEW2871 reduces Tau-Ser262 phosphorylation in rat hippocampal slices. *Brain research* **1658**, 51-59
70. Luna-Muñoz, J., Harrington, C. R., Wischik, C. M., Flores-Rodríguez, P., Avila, J. s., Zamudio, S. R., Cruz, F. D. l., Mena, R. l., Meraz-Ríos, M. A., and Floran-Garduño, B. (2013) Phosphorylation of Tau Protein Associated as a Protective Mechanism in the Presence of Toxic, C-Terminally Truncated Tau in Alzheimer's Disease. in *Understanding Alzheimer's Disease* (Zerr, I. ed.), InTech, Rijeka. pp Ch. 05
71. Martin, L., Latypova, X., and Terro, F. (2011) Post-translational modifications of tau protein: implications for Alzheimer's disease. *Neurochemistry international* **58**, 458-471
72. Martin, L., Latypova, X., Wilson, C. M., Magnaudeix, A., Perrin, M.-L., Yardin, C., and Terro, F. (2013) Tau protein kinases: Involvement in Alzheimer's disease. *Ageing Research Reviews* **12**, 289-309
73. Braithwaite, S. P., Stock, J. B., Lombroso, P. J., and Nairn, A. C. (2012) Protein phosphatases and Alzheimer's disease. *Progress in molecular biology and translational science* **106**, 343-379
74. Lee, S., and Shea, T. B. (2013) Regulation of tau proteolysis by phosphatases. *Brain research* **1495**, 30-36
75. Matsuo, E. S., Shin, R. W., Billingsley, M. L., Van deVoorde, A., O'Connor, M., Trojanowski, J. Q., and Lee, V. M. (1994) Biopsy-derived adult human brain tau is phosphorylated at many of the same sites as Alzheimer's disease paired helical filament tau. *Neuron* **13**, 989-1002

76. Marklund, N., Blennow, K., Zetterberg, H., Ronne-Engstrom, E., Enblad, P., and Hillered, L. (2009) Monitoring of brain interstitial total tau and beta amyloid proteins by microdialysis in patients with traumatic brain injury. *Journal of neurosurgery* **110**, 1227-1237
77. Saman, S., Kim, W., Raya, M., Visnick, Y., Miro, S., Saman, S., Jackson, B., McKee, A. C., Alvarez, V. E., Lee, N. C., and Hall, G. F. (2012) Exosome-associated tau is secreted in tauopathy models and is selectively phosphorylated in cerebrospinal fluid in early Alzheimer disease. *The Journal of biological chemistry* **287**, 3842-3849
78. Chai, X., Dage, J. L., and Citron, M. (2012) Constitutive secretion of tau protein by an unconventional mechanism. *Neurobiol Dis* **48**, 356-366
79. Simon, D., Garcia-Garcia, E., Gomez-Ramos, A., Falcon-Perez, J. M., Diaz-Hernandez, M., Hernandez, F., and Avila, J. (2012) Tau overexpression results in its secretion via membrane vesicles. *Neuro-degenerative diseases* **10**, 73-75
80. Pooler, A. M., Phillips, E. C., Lau, D. H., Noble, W., and Hanger, D. P. (2013) Physiological release of endogenous tau is stimulated by neuronal activity. *EMBO Rep* **14**, 389-394
81. Holmes, B. B., DeVos, S. L., Kfoury, N., Li, M., Jacks, R., Yanamandra, K., Ouidja, M. O., Brodsky, F. M., Marasa, J., Bagchi, D. P., Kotzbauer, P. T., Miller, T. M., Papy-Garcia, D., and Diamond, M. I. (2013) Heparan sulfate proteoglycans mediate internalization and propagation of specific proteopathic seeds. *Proceedings of the National Academy of Sciences of the United States of America* **110**, E3138-3147
82. Jack, C. R., Jr., Knopman, D. S., Weigand, S. D., Wiste, H. J., Vemuri, P., Lowe, V., Kantarci, K., Gunter, J. L., Senjem, M. L., Ivnik, R. J., Roberts, R. O., Rocca, W. A., Boeve, B. F., and Petersen, R. C. (2012) An operational approach to National Institute on Aging-Alzheimer's Association criteria for preclinical Alzheimer disease. *Annals of neurology* **71**, 765-775
83. Blomberg, M., Jensen, M., Basun, H., Lannfelt, L., and Wahlund, L. O. (2001) Cerebrospinal fluid tau levels increase with age in healthy individuals. *Dementia and geriatric cognitive disorders* **12**, 127-132
84. Gomez-Ramos, A., Diaz-Hernandez, M., Rubio, A., Diaz-Hernandez, J. I., Miras-Portugal, M. T., and Avila, J. (2009) Characteristics and consequences of muscarinic receptor activation by tau protein. *European neuropsychopharmacology : the journal of the European College of Neuropsychopharmacology* **19**, 708-717
85. Wu, J. W., Herman, M., Liu, L., Simoes, S., Acker, C. M., Figueroa, H., Steinberg, J. I., Margittai, M., Kayed, R., Zurzolo, C., Di Paolo, G., and Duff, K. E. (2013) Small misfolded Tau species are internalized via bulk endocytosis and anterogradely and retrogradely transported in neurons. *The Journal of biological chemistry* **288**, 1856-1870
86. Morris, M., Maeda, S., Vossel, K., and Mucke, L. (2011) The Many Faces of Tau. *Neuron* **70**, 410-426
87. Gratuze, M., Cisbani, G., Cicchetti, F., and Planel, E. (2016) Is Huntington's disease a tauopathy? *Brain : a journal of neurology* **139**, 1014-1025
88. Wilson, D. M., and Binder, L. I. (1995) Polymerization of microtubule-associated protein tau under near-physiological conditions. *The Journal of biological chemistry* **270**, 24306-24314
89. Mandelkow, E.-M., and Mandelkow, E. (2012) Biochemistry and Cell Biology of Tau Protein in Neurofibrillary Degeneration. *Cold Spring Harbor Perspectives in Medicine* **2**, a006247
90. Wang, Y., and Mandelkow, E. (2016) Tau in physiology and pathology. *Nat Rev Neurosci* **17**, 22-35
91. Cowan, C. M., and Mudher, A. (2013) Are Tau Aggregates Toxic or Protective in Tauopathies? *Frontiers in neurology* **4**, 114
92. Ward, S. M., Himmelstein, D. S., Lancia, J. K., and Binder, L. I. (2012) Tau oligomers and tau toxicity in neurodegenerative disease. *Biochemical Society transactions* **40**, 667-671
93. Kopeikina, K. J., Hyman, B. T., and Spires-Jones, T. L. (2012) Soluble forms of tau are toxic in Alzheimer's disease. *Translational neuroscience* **3**, 223-233
94. Spires-Jones, T. L., Stoothoff, W. H., de Calignon, A., Jones, P. B., and Hyman, B. T. (2009) Tau pathophysiology in neurodegeneration: a tangled issue. *Trends in neurosciences* **32**, 150-159

95. Fox, L. M., William, C. M., Adamowicz, D. H., Pitstick, R., Carlson, G. A., Spires-Jones, T. L., and Hyman, B. T. (2011) Soluble tau species, not neurofibrillary aggregates, disrupt neural system integration in a tau transgenic model. *Journal of neuropathology and experimental neurology* **70**, 588-595
96. Alonso Adel, C., Li, B., Grundke-Iqbal, I., and Iqbal, K. (2006) Polymerization of hyperphosphorylated tau into filaments eliminates its inhibitory activity. *Proceedings of the National Academy of Sciences of the United States of America* **103**, 8864-8869
97. Ali, Y. O., Ruan, K., and Zhai, R. G. (2012) NMNAT suppresses tau-induced neurodegeneration by promoting clearance of hyperphosphorylated tau oligomers in a Drosophila model of tauopathy. *Hum Mol Genet* **21**, 237-250
98. Gomez-Ramos, A., Diaz-Hernandez, M., Rubio, A., Miras-Portugal, M. T., and Avila, J. (2008) Extracellular tau promotes intracellular calcium increase through M1 and M3 muscarinic receptors in neuronal cells. *Mol Cell Neurosci* **37**, 673-681
99. Kopeikina, K. J., Carlson, G. A., Pitstick, R., Ludvigson, A. E., Peters, A., Luebke, J. I., Koffie, R. M., Frosch, M. P., Hyman, B. T., and Spires-Jones, T. L. (2011) Tau accumulation causes mitochondrial distribution deficits in neurons in a mouse model of tauopathy and in human Alzheimer's disease brain. *Am J Pathol* **179**, 2071-2082
100. Lasagna-Reeves, C. A., Castillo-Carranza, D. L., Guerrero-Muoz, M. J., Jackson, G. R., and Kayed, R. (2010) Preparation and characterization of neurotoxic tau oligomers. *Biochemistry* **49**, 10039-10041
101. Lasagna-Reeves, C. A., Castillo-Carranza, D. L., Sengupta, U., Clos, A. L., Jackson, G. R., and Kayed, R. (2011) Tau oligomers impair memory and induce synaptic and mitochondrial dysfunction in wild-type mice. *Mol Neurodegener* **6**, 39
102. Sydow, A., Van der Jeugd, A., Zheng, F., Ahmed, T., Balschun, D., Petrova, O., Drexler, D., Zhou, L., Rune, G., Mandelkow, E., D'Hooge, R., Alzheimer, C., and Mandelkow, E. M. (2011) Tau-induced defects in synaptic plasticity, learning, and memory are reversible in transgenic mice after switching off the toxic Tau mutant. *J Neurosci* **31**, 2511-2525
103. Terwel, D., Lasrado, R., Snauwaert, J., Vandeweert, E., Van Haesendonck, C., Borghgraef, P., and Van Leuven, F. (2005) Changed conformation of mutant Tau-P301L underlies the moribund tauopathy, absent in progressive, nonlethal axonopathy of Tau-4R/2N transgenic mice. *The Journal of biological chemistry* **280**, 3963-3973
104. Crespo-Biel, N., Theunis, C., Borghgraef, P., Lechat, B., Devijver, H., Maurin, H., and Van Leuven, F. (2014) Phosphorylation of protein Tau by GSK3β prolongs survival of bigenic Tau.P301L × GSK3β mice by delaying brainstem tauopathy. *Neurobiology of Disease* **67**, 119-132
105. Schneider, A., Biernat, J., von Bergen, M., Mandelkow, E., and Mandelkow, E. M. (1999) Phosphorylation that Detaches Tau Protein from Microtubules (Ser262, Ser214) Also Protects It against Aggregation into Alzheimer Paired Helical Filaments. *Biochemistry* **38**, 3549-3558
106. Guo, J. L., Narasimhan, S., Changolkar, L., He, Z., Stieber, A., Zhang, B., Gathagan, R. J., Iba, M., McBride, J. D., Trojanowski, J. Q., and Lee, V. M. Y. (2016) Unique pathological tau conformers from Alzheimer's brains transmit tau pathology in nontransgenic mice. *The Journal of Experimental Medicine* **213**, 2635-2654
107. Wischik, C. M., Harrington, C. R., and Storey, J. M. (2014) Tau-aggregation inhibitor therapy for Alzheimer's disease. *Biochemical pharmacology* **88**, 529-539
108. Braak, H., and Braak, E. (1995) Staging of Alzheimer's disease-related neurofibrillary changes. *Neurobiology of aging* **16**, 271-278; discussion 278-284
109. Wischik, C. M., Edwards, P. C., Lai, R. Y., Roth, M., and Harrington, C. R. (1996) Selective inhibition of Alzheimer disease-like tau aggregation by phenothiazines. *Proceedings of the National Academy of Sciences of the United States of America* **93**, 11213-11218
110. Mocanu, M. M., Nissen, A., Eckermann, K., Khlistunova, I., Biernat, J., Drexler, D., Petrova, O., Schonig, K., Bujard, H., Mandelkow, E., Zhou, L., Rune, G., and Mandelkow, E. M. (2008) The potential for beta-structure in the repeat domain of tau protein determines aggregation, synaptic

decay, neuronal loss, and coassembly with endogenous Tau in inducible mouse models of tauopathy. *J Neurosci* **28**, 737-748
111. Ahmed, Z., Cooper, J., Murray, T. K., Garn, K., McNaughton, E., Clarke, H., Parhizkar, S., Ward, M. A., Cavallini, A., Jackson, S., Bose, S., Clavaguera, F., Tolnay, M., Lavenir, I., Goedert, M., Hutton, M. L., and O'Neill, M. J. (2014) A novel in vivo model of tau propagation with rapid and progressive neurofibrillary tangle pathology: the pattern of spread is determined by connectivity, not proximity. *Acta neuropathologica* **127**, 667-683
112. Holmes, B. B., Furman, J. L., Mahan, T. E., Yamasaki, T. R., Mirbaha, H., Eades, W. C., Belaygorod, L., Cairns, N. J., Holtzman, D. M., and Diamond, M. I. (2014) Proteopathic tau seeding predicts tauopathy in vivo. *Proceedings of the National Academy of Sciences of the United States of America* **111**, E4376-4385
113. Gerson, J. E., and Kayed, R. (2013) Formation and propagation of tau oligomeric seeds. *Frontiers in neurology* **4**, 93
114. Clavaguera, F., Bolmont, T., Crowther, R. A., Abramowski, D., Frank, S., Probst, A., Fraser, G., Stalder, A. K., Beibel, M., Staufenbiel, M., Jucker, M., Goedert, M., and Tolnay, M. (2009) Transmission and spreading of tauopathy in transgenic mouse brain. *Nature cell biology* **11**, 909-913
115. Clavaguera, F., Akatsu, H., Fraser, G., Crowther, R. A., Frank, S., Hench, J., Probst, A., Winkler, D. T., Reichwald, J., Staufenbiel, M., Ghetti, B., Goedert, M., and Tolnay, M. (2013) Brain homogenates from human tauopathies induce tau inclusions in mouse brain. *Proceedings of the National Academy of Sciences of the United States of America* **110**, 9535-9540
116. Scholl, M., Lockhart, S. N., Schonhaut, D. R., O'Neil, J. P., Janabi, M., Ossenkoppele, R., Baker, S. L., Vogel, J. W., Faria, J., Schwimmer, H. D., Rabinovici, G. D., and Jagust, W. J. (2016) PET Imaging of Tau Deposition in the Aging Human Brain. *Neuron* **89**, 971-982
117. Thal, D. R., Attems, J., and Ewers, M. (2014) Spreading of amyloid, tau, and microvascular pathology in Alzheimer's disease: findings from neuropathological and neuroimaging studies. *Journal of Alzheimer's disease : JAD* **42 Suppl 4**, S421-429
118. Cho, H., Choi, J. Y., Hwang, M. S., Kim, Y. J., Lee, H. M., Lee, H. S., Lee, J. H., Ryu, Y. H., Lee, M. S., and Lyoo, C. H. (2016) In vivo cortical spreading pattern of tau and amyloid in the Alzheimer disease spectrum. *Annals of neurology* **80**, 247-258
119. Vitali, A., Piccini, A., Borghi, R., Fornaro, P., Siedlak, S. L., Smith, M. A., Gambetti, P., Ghetti, B., and Tabaton, M. (2004) Soluble amyloid beta-protein is increased in frontotemporal dementia with tau gene mutations. *Journal of Alzheimer's disease : JAD* **6**, 45-51
120. Nisbet, R. M., Polanco, J.-C., Ittner, L. M., and Götz, J. (2015) Tau aggregation and its interplay with amyloid-β. *Acta neuropathologica* **129**, 207-220
121. Clinton, L. K., Blurton-Jones, M., Myczek, K., Trojanowski, J. Q., and LaFerla, F. M. (2010) Synergistic Interactions between Abeta, tau, and alpha-synuclein: acceleration of neuropathology and cognitive decline. *J Neurosci* **30**, 7281-7289
122. Lewis, J., Dickson, D. W., Lin, W. L., Chisholm, L., Corral, A., Jones, G., Yen, S. H., Sahara, N., Skipper, L., Yager, D., Eckman, C., Hardy, J., Hutton, M., and McGowan, E. (2001) Enhanced neurofibrillary degeneration in transgenic mice expressing mutant tau and APP. *Science (New York, N.Y.)* **293**, 1487-1491
123. Reitz, C. (2012) Alzheimer's Disease and the Amyloid Cascade Hypothesis: A Critical Review. *International Journal of Alzheimer's Disease* **2012**, 369808
124. Chabrier, M. A., Cheng, D., Castello, N. A., Green, K. N., and LaFerla, F. M. (2014) Synergistic effects of amyloid-beta and wild-type human tau on dendritic spine loss in a floxed double transgenic model of Alzheimer's disease. *Neurobiol Dis* **64**, 107-117
125. Roberson, E. D., Scearce-Levie, K., Palop, J. J., Yan, F., Cheng, I. H., Wu, T., Gerstein, H., Yu, G. Q., and Mucke, L. (2007) Reducing endogenous tau ameliorates amyloid beta-induced deficits in an Alzheimer's disease mouse model. *Science (New York, N.Y.)* **316**, 750-754
126. Ferrer, I. (2004) Stress kinases involved in tau phosphorylation in Alzheimer's disease, tauopathies and APP transgenic mice. *Neurotoxicity research* **6**, 469-475

127. Vasconcelos, B., Stancu, I.-C., Buist, A., Bird, M., Wang, P., Vanoosthuyse, A., Van Kolen, K., Verheyen, A., Kienlen-Campard, P., Octave, J.-N., Baatsen, P., Moechars, D., and Dewachter, I. (2016) Heterotypic seeding of Tau fibrillization by pre-aggregated Abeta provides potent seeds for prion-like seeding and propagation of Tau-pathology in vivo. *Acta neuropathologica* **131**, 549-569
128. Rapoport, M., Dawson, H. N., Binder, L. I., Vitek, M. P., and Ferreira, A. (2002) Tau is essential to β-amyloid-induced neurotoxicity. *Proceedings of the National Academy of Sciences of the United States of America* **99**, 6364-6369
129. Bloom, G. S. (2014) Amyloid-beta and tau: the trigger and bullet in Alzheimer disease pathogenesis. *JAMA neurology* **71**, 505-508
130. Higuchi, M. (2009) Visualization of brain amyloid and microglial activation in mouse models of Alzheimer's disease. *Curr Alzheimer Res* **6**, 137-143
131. Sturchler-Pierrat, C., and Staufenbiel, M. (2000) Pathogenic mechanisms of Alzheimer's disease analyzed in the APP23 transgenic mouse model. *Annals of the New York Academy of Sciences* **920**, 134-139
132. Gotz, J., Chen, F., van Dorpe, J., and Nitsch, R. M. (2001) Formation of neurofibrillary tangles in P301l tau transgenic mice induced by Abeta 42 fibrils. *Science (New York, N.Y.)* **293**, 1491-1495
133. Stancu, I.-C., Vasconcelos, B., Terwel, D., and Dewachter, I. (2014) Models of β-amyloid induced Tau-pathology: the long and "folded" road to understand the mechanism. *Molecular Neurodegeneration* **9**, 51
134. de Calignon, A., Polydoro, M., Suarez-Calvet, M., William, C., Adamowicz, D. H., Kopeikina, K. J., Pitstick, R., Sahara, N., Ashe, K. H., Carlson, G. A., Spires-Jones, T. L., and Hyman, B. T. (2012) Propagation of tau pathology in a model of early Alzheimer's disease. *Neuron* **73**, 685-697
135. Liu, L., Drouet, V., Wu, J. W., Witter, M. P., Small, S. A., Clelland, C., and Duff, K. (2012) Trans-Synaptic Spread of Tau Pathology In Vivo. *PLOS ONE* **7**, e31302
136. Hochgrafe, K., Sydow, A., and Mandelkow, E. M. (2013) Regulatable transgenic mouse models of Alzheimer disease: onset, reversibility and spreading of Tau pathology. *The FEBS journal* **280**, 4371-4381
137. Gerson, J. E., and Kayed, R. (2013) Formation and Propagation of Tau Oligomeric Seeds. *Frontiers in Neurology* **4**, 93
138. Peeraer, E., Bottelbergs, A., Van Kolen, K., Stancu, I.-C., Vasconcelos, B., Mahieu, M., Duytschaever, H., Ver Donck, L., Torremans, A., Sluydts, E., Van Acker, N., Kemp, J. A., Mercken, M., Brunden, K. R., Trojanowski, J. Q., Dewachter, I., Lee, V. M. Y., and Moechars, D. (2015) Intracerebral injection of preformed synthetic tau fibrils initiates widespread tauopathy and neuronal loss in the brains of tau transgenic mice. *Neurobiology of disease* **73**, 83-95
139. Greenberg, S. G., and Davies, P. (1990) A preparation of Alzheimer paired helical filaments that displays distinct tau proteins by polyacrylamide gel electrophoresis. *Proc Natl Acad Sci U S A* **87**, 5827-5831
140. Fitzpatrick, A. W. P., Falcon, B., He, S., Murzin, A. G., Murshudov, G., Garringer, H. J., Crowther, R. A., Ghetti, B., Goedert, M., and Scheres, S. H. W. (2017) Cryo-EM structures of tau filaments from Alzheimer's disease. *Nature* **547**, 185-190
141. Taniguchi-Watanabe, S., Arai, T., Kametani, F., Nonaka, T., Masuda-Suzukake, M., Tarutani, A., Murayama, S., Saito, Y., Arima, K., Yoshida, M., Akiyama, H., Robinson, A., Mann, D. M. A., Iwatsubo, T., and Hasegawa, M. (2016) Biochemical classification of tauopathies by immunoblot, protein sequence and mass spectrometric analyses of sarkosyl-insoluble and trypsin-resistant tau. *Acta neuropathologica* **131**, 267-280
142. Holmes, B. B., Furman, J. L., Mahan, T. E., Yamasaki, T. R., Mirbaha, H., Eades, W. C., Belaygorod, L., Cairns, N. J., Holtzman, D. M., and Diamond, M. I. (2014) Proteopathic tau seeding predicts tauopathy in vivo. *Proceedings of the National Academy of Sciences* **111**, E4376-E4385
143. Sanders, D. W., Kaufman, S. K., DeVos, S. L., Sharma, A. M., Mirbaha, H., Li, A., Barker, S. J., Foley, A., Thorpe, J. R., Serpell, L. C., Miller, T. M., Grinberg, L. T., Seeley, W. W., and Diamond, M. I. (2014) Distinct tau prion strains propagate in cells and mice and define different tauopathies. *Neuron* **82**, 1271-1288

144. Bright, J., Hussain, S., Dang, V., Wright, S., Cooper, B., Byun, T., Ramos, C., Singh, A., Parry, G., Stagliano, N., and Griswold-Prenner, I. (2014) *Human secreted tau increases amyloid-beta production*,
145. Yanamandra, K., Kfoury, N., Jiang, H., Mahan, Thomas E., Ma, S., Maloney, Susan E., Wozniak, David F., Diamond, Marc I., and Holtzman, David M. (2013) Anti-Tau Antibodies that Block Tau Aggregate Seeding In Vitro Markedly Decrease Pathology and Improve Cognition In Vivo. *Neuron* **80**, 402-414
146. L., O., L., F., E., L., I., S. G., M., G., and M-Y., L. V. (1994) Monoclonal antibody PHF-1 recognizes tau protein phosphorylated at serine residues 396 and 404. *Journal of Neuroscience Research* **39**, 669-673
147. Kaufman, S. K., Del Tredici, K., Thomas, T. L., Braak, H., and Diamond, M. I. (2018) Tau seeding activity begins in the transentorhinal/entorhinal regions and anticipates phospho-tau pathology in Alzheimer's disease and PART. *Acta neuropathologica*
148. Mirbaha, H., Holmes, B. B., Sanders, D. W., Bieschke, J., and Diamond, M. I. (2015) Tau Trimers Are the Minimal Propagation Unit Spontaneously Internalized to Seed Intracellular Aggregation. *The Journal of biological chemistry* **290**, 14893-14903
149. Shammas, S. L., Garcia, G. A., Kumar, S., Kjaergaard, M., Horrocks, M. H., Shivji, N., Mandelkow, E., Knowles, T. P. J., Mandelkow, E., and Klenerman, D. (2015) A mechanistic model of tau amyloid aggregation based on direct observation of oligomers. *Nature Communications* **6**, 7025
150. Chakrabarty, P., Hudson, V. J., Sacino, A. N., Brooks, M. M. T., D'Alton, S., Lewis, J., Golde, T. E., and Giasson, B. I. (2015) Inefficient induction and spread of seeded tau pathology in P301L mouse model of tauopathy suggests inherent physiological barriers to transmission. *Acta neuropathologica* **130**, 303-305
151. DeTure, M. A., Di Noto, L., and Purich, D. L. (2002) In vitro assembly of Alzheimer-like filaments. How a small cluster of charged residues in Tau and MAP2 controls filament morphology. *The Journal of biological chemistry* **277**, 34755-34759
152. Morozova, O. A., March, Z. M., Robinson, A. S., and Colby, D. W. (2013) Conformational features of tau fibrils from Alzheimer's disease brain are faithfully propagated by unmodified recombinant protein. *Biochemistry* **52**, 6960-6967
153. Vandermeeren, M., Borgers, M., Van Kolen, K., Theunis, C., Vasconcelos, B., Bottelbergs, A., Wintmolders, C., Daneels, G., Willems, R., Dockx, K., Delbroek, L., Marreiro, A., Ver Donck, L., Sousa, C., Nanjunda, R., Lacy, E., Van De Casteele, T., Van Dam, D., Paul De Deyn, P., Kemp, J., Malia, T. J., and Mercken, M. H. (2018) Anti-tau monoclonal antibodies derived from soluble and filamentous tau show diverse functional properties *in vitro* and *in vivo*. *Journal of Alzheimer's disease : JAD*, *Accepted manuscript*
154. Hung, S.-Y., and Fu, W.-M. (2017) Drug candidates in clinical trials for Alzheimer's disease. *Journal of Biomedical Science* **24**, 47
155. DeTure, M., Ko, L.-w., Yen, S., Nacharaju, P., Easson, C., Lewis, J., van Slegtenhorst, M., Hutton, M., and Yen, S.-H. (2000) Missense tau mutations identified in FTDP-17 have a small effect on tau–microtubule interactions. *Brain Research* **853**, 5-14
156. Maeda, S., Sato, Y., and Takashima, A. (2018) Frontotemporal dementia with Parkinsonism linked to chromosome-17 mutations enhance tau oligomer formation. *Neurobiology of Aging* **69**, 26-32
157. Meyer, V., Dinkel, P. D., Rickman Hager, E., and Margittai, M. (2014) Amplification of Tau Fibrils from Minute Quantities of Seeds. *Biochemistry* **53**, 5804-5809
158. Apetri, M. M., Harkes, R., Subramaniam, V., Canters, G. W., Schmidt, T., and Aartsma, T. J. (2016) Direct Observation of α-Synuclein Amyloid Aggregates in Endocytic Vesicles of Neuroblastoma Cells. *PLoS ONE* **11**, e0153020
159. Volpicelli-Daley, L. A., Luk, K. C., Patel, T. P., Tanik, S. A., Riddle, D. M., Stieber, A., Meaney, D. F., Trojanowski, J. Q., and Lee, V. M. (2011) Exogenous alpha-synuclein fibrils induce Lewy body pathology leading to synaptic dysfunction and neuron death. *Neuron* **72**, 57-71
160. Jackson, S. J., Kerridge, C., Cooper, J., Cavallini, A., Falcon, B., Cella, C. V., Landi, A., Szekeres, P. G., Murray, T. K., Ahmed, Z., Goedert, M., Hutton, M., O'Neill, M. J., and Bose, S. (2016) Short Fibrils

Constitute the Major Species of Seed-Competent Tau in the Brains of Mice Transgenic for Human P301S Tau. *The Journal of Neuroscience* **36**, 762-772

161. Mercken, M., Vandermeeren, M., Lubke, U., Six, J., Boons, J., Van de Voorde, A., Martin, J. J., and Gheuens, J. (1992) Monoclonal antibodies with selective specificity for Alzheimer Tau are directed against phosphatase-sensitive epitopes. *Acta neuropathologica* **84**, 265-272
162. von Bergen, M., Barghorn, S., Li, L., Marx, A., Biernat, J., Mandelkow, E. M., and Mandelkow, E. (2001) Mutations of tau protein in frontotemporal dementia promote aggregation of paired helical filaments by enhancing local beta-structure. *The Journal of biological chemistry* **276**, 48165-48174
163. Plumley, J. A., and Dannenberg, J. J. (2010) The Importance of Hydrogen Bonding between the Glutamine Side Chains to the Formation of Amyloid VQIVYK Parallel β-Sheets: An ONIOM DFT/AM1 Study. *Journal of the American Chemical Society* **132**, 1758-1759
164. Haj, E., Losev, Y., Guru KrishnaKumar, V., Pichinuk, E., Engel, H., Raveh, A., Gazit, E., and Segal, D. (2018) Integrating in vitro and in silico approaches to evaluate the "dual functionality" of palmatine chloride in inhibiting and disassembling Tau-derived VQIVYK peptide fibrils. *Biochimica et Biophysica Acta (BBA) - General Subjects* **1862**, 1565-1575
165. d'Abramo, C., Acker, C. M., Jimenez, H. T., and Davies, P. (2013) Tau Passive Immunotherapy in Mutant P301L Mice: Antibody Affinity versus Specificity. *PLOS ONE* **8**, e62402
166. Allen, B., Ingram, E., Takao, M., Smith, M. J., Jakes, R., Virdee, K., Yoshida, H., Holzer, M., Craxton, M., Emson, P. C., Atzori, C., Migheli, A., Crowther, R. A., Ghetti, B., Spillantini, M. G., and Goedert, M. (2002) Abundant tau filaments and nonapoptotic neurodegeneration in transgenic mice expressing human P301S tau protein. *J Neurosci* **22**, 9340-9351
167. Mirra, S. S., Murrell, J. R., Gearing, M., Spillantini, M. G., Goedert, M., Crowther, R. A., Levey, A. I., Jones, R., Green, J., Shoffner, J. M., Wainer, B. H., Schmidt, M. L., Trojanowski, J. Q., and Ghetti, B. (1999) Tau Pathology in a Family with Dementia and a P301L Mutation in Tau. *Journal of Neuropathology & Experimental Neurology* **58**, 335-345
168. Bugiani, O., Murrell, J. R., Giaccone, G., Hasegawa, M., Ghigo, G., Tabaton, M., Morbin, M., Primavera, A., Carella, F., Solaro, C., Grisoli, M., Savoiardo, M., Spillantini, M. G., Tagliavini, F., Goedert, M., and Ghetti, B. (1999) Frontotemporal Dementia and Corticobasal Degeneration in a Family with a P301S Mutation in Tau. *Journal of Neuropathology & Experimental Neurology* **58**, 667-677